8-2018

Hybrid perovskite characterization and device applications.

Kasun Fernando
University of Louisville

HYBRID PEROVSKITE CHARACTERIZATION AND DEVICE APPLICATIONS

By

Kasun Fernando
B.Sc., University of Sri Jayewardenepura, Sri Lanka, 2006
M.Sc., University of Louisville, USA 2011

A Dissertation
Submitted to the Faculty of the
J.B. Speed School of Engineering of the University of Louisville
in Partial Fulfillment of the Requirements
for the Degree of

Doctor of Philosophy
in
Electrical Engineering

Department of Electrical & Computer Engineering
University of Louisville
Louisville, KY 40292

August 2018

HYBRID PEROVSKITE CHARACTERIZATION AND DEVICE APPLICATIONS

By

Kasun Fernando
B.Sc., University of Sri Jayewardenepura, Sri Lanka, 2006
M.Sc., University of Louisville, USA 2011

A Dissertation Approved on
July 24, 2018
by the following Dissertation Committee:

_____
Dr. Bruce W. Alphenaar, Dissertation Director

_____
Dr. Aditya Mohite

_____
Dr. Kevin M. Walsh

_____
Dr. Cindy K. Harnett

_____
Dr. Gamini U. Sumanasekera

DEDICATION

“යේ ධම්මා හේතුප්පභවා

තේසං හේතුං තථාගතෝ ආහ

තේසඤ්ච යෝ නිරෝධෝ

ඒවං වාදී මහාසමණෝ ” - අරහත් අස්සජි ථේර.

As a universal truth, it has been understood that any experiences of things which we observe through our five senses (eye, ear, nose, tongue and body) in spiritual world are all mental phenomena and are not based on the actual objects themselves. Spiritually, in a deep understanding level, even time and space become illusions of mind. Simply the world we believe to exist, and which we think we are interacting with is relative to our own mind. There won’t be any single world shared by two different persons.

When an average mind processes an objective reality, and the feeling it undergoes could be considered as an illusion processed through its mind, linking the current experience of the senses to an experience from the past. Therefore, the reality it latches becomes relative.

It is such a state of mind that would be able to experience the origin and science behind this phenomenon. “It’ll be the effect which arises from a cause, and the value of it ceases when the cause is no longer present”. Thathagatha went on to understand that it is related to the nature of experiences (karma). By understanding this, a mind could attain a state that it can no longer produce causes to latch on to in its next exitances. I dedicate this thesis to such Noble state of mind(Buddha), the mental phenomena it latches(Dhamma) and followers who’s practicing (Sangha).

ACKNOWLEDGEMENTS

First and foremost, I would like to convey my sincere gratitude to my PhD supervisor Prof .Bruce Alphenaar for mentoring me, supporting me with my research and providing me with great opportunities in the field of research throughout my eight years of research work. It has been a great honor to work under a supervisor with such an immense knowledge of science, experimental work and ability of interpreting that deep understanding of science.

Secondly, it was an honor to work with Light to Energy team at LANL under the supervision of Dr.Aditya Mohite. I would like to thank Dr.Mohite for giving me the opportunity and guidance to achieve the best out of me. I would like to thank Dr.Wanyi Nie for her guidance and showing me the way to achieve great scientific achievements specially by doing that extra bit of work that most of us miss, which eventually results in greater findings.

Also, I would like to thank Prof.Mahendra Sunkara for supporting me in my initial three years through the Conn Center for renewable energy at UofL. My sincere gratitude also goes to Prof.Gamini Sumanasekara for recruiting me as an MS student in the Department of Physics of UofL, where under his supervision I started my initial research work in US. Also, I'm grateful to him, his wife Dr.Wasana Sumanasekara and his family who considered me and every student from Sri Lanka who came to Louisville as member of their own family and supported us in every aspect of our lives. Also my gratitude also goes to Dr.Zamborini, Dr.Jinjun Liu, his former post-doc Dr.Bill Pandith and his student Abed for the support they provided me during the collaborative work conducted at UofL and also to the rest of my thesis committee members Prof.Kevin Walsh and Dr.Cindy Harnett for spending their valuable time and providing me with their valuable ideas. Human relations in and out of working place could be identified as an important factor that helps to overcome challenges and achieve the best in life. I consider myself as the luckiest because, since

arriving in US I have been able to work with and live around great personalities who showed immense perspectives of life to achieve greater good. Former and current lab mates at UofL, Ruwantha, Hemanth, Kiran, Buddhika , Sowmya, Austin, Tulashi, Pom, Pranoy, George, Tereza, Jack and all others who have given me great support while making environment in the lab enjoyable. Then I would like to thank Arun, JC, Fangze, Akhilesh, Hisato, Sehmus, Dave, Ismail, Daniel and specially Noelia for the support they gave me while I was working at LANL. I would like to thank Harsha, Primal, Ruwini and all the others of the Sri Lankan community in NM for treating me as one of their family members at a time I missed my own family in Louisville.

We Sri Lankan students have been living in Louisville as one family unit supporting one another while understanding each other's needs. Families of Buddika, Ruwantha, Dilan, Ruchira, Chathura, Saliya, Ashan, Akila, Manthila and all other Sri Lankan families gave me and my family whatever we needed. So, I'm grateful to them for everything.

Finally, I would like to convey my gratitude to my parents for their support and counseling from my birth. I'm grateful to my father who went through every word and sentence in this thesis and suggested ways of making myself better understood. I thank Keaton Price at UofL writing center for double checking small grammatical mistakes in the thesis and also Courtney Kerr from graduate school for going through it few times for formatting errors.. My gratitude goes to my brother and his family who convinced and brought me to US for graduate studies, my mother-in-law for all the help she gave us in bringing up our son while I was at LANL and finally my wife Udika and our son Kemith for baring all discomforts and giving unconditional support in life so that I could complete this work.

ABSTRACT

HYBRID PEROVSKITE CHARACTERIZATION AND DEVICE APPLICATIONS

Kasun Fernando

July 24, 2018

Hybrid perovskites are a group of materials that has shown a great impact in the field of scientific research in the past decade. It is mainly due to the efficiency gained by hybrid perovskite solar cells, which came close to that of those produced with silicon. One method of fabricating high-quality hybrid perovskite thin film solar cells is the hot casting technique. It has been reported that this technique can produce highly efficient and stable solar cells. The following thesis describes successful attempts made in finding a few new alternative device options from solar cells using thin films of hybrid perovskites. Strategies for synthesizing, testing and optimizing performances are discussed.

After going through a brief history of the group of material perovskite, we discuss basic characteristics which have been known in the field of conventional and hybrid perovskites. A brief description of solar cell applications which use hybrid perovskites as their active material has been discussed.

As a background study, three main device structures were discussed. First device structure used to understand various characteristics of the thin film is Field Effect Transistor (FET). Then, novel device concept of memristor is introduced as one of the device options using hybrid perovskite thin films. Gas sensing ability of semiconductors using the photo adsorption is also presented in the later part of the introduction.

Detailed explanation of the steps we followed to fabricate the high-quality crystal films are presented. Characterizing techniques that we used to understand the quality of the films and theories behind them are addressed.

In the results section, our discussion starts with two terminal device structure using top contacts. Impressive behavior of the film under dark condition, where a sudden increase in its conductivity after reaching a certain electric field was observed. When reversing the field, it was able to hold that increased conductivity until the field reaches zero. This was the main observation which prompted us to look for the memristive behavior of the film. More experiments were done to understand the effect and compare it with common memristor effect of semiconductor devices. This unique unipolar memristor ability was discussed in several ways. Work done towards finding better performance in the devices were also presented. Finally, based on the experimental results a model is hypothesized using the concepts of inbuilt potential, ion motion and carrier generation in the film.

Initial results of three terminal devices are presented referring to the work done with the aim of understanding the basic characteristics of the film using Field Effect Transistors (FETs). Initial results from the scans showed the N-type behavior in the presence of light

condition and ambipolar behavior under dark condition. Various wave lengths of light suggested that with the introduction of photo generated charges the average dopant behavior through electrical measurement altered significantly for different energy levels of photons incidental on the devices.

In the final section of results, gas sensing ability of the film is discussed. With the introduction of reactive gases over the hybrid perovskites film, AC photo current scans demonstrated a sudden increase in the current followed by a permanent decrease compared to the initial level. Yet, introduction of non-reactive gases such as noble gases didn't produce such change in electrical current. However, exposure to extra sun with monochromatic light showed that even non-reactive gas environments can produce an increase in current values. This current increase returns to its original values simply by removing the extra sun and keeping the device under darkness. The effect of various inert gases with different atomic weights were tested. It was found out that argon gas combined with light makes the biggest reversible effect of increased surface conductivity under inert gas environments.

This work could be considered as an alternative route in understanding some of the characteristics of hybrid perovskite devices, which could lead to getting better performances in the device applications as well as to understand overall behavior of the film it-self.

TABLE OF CONTENTS

DEDICATION iii

ACKNOWLEDGEMENT iv

ABSTRACT vi

1. INTRODUCTION 1

1.1 Origin of perovskite 1

1.2 What is perovskite 2

1.3 Types of perovskite 5

1.3.1 Conventional perovskites 5

1.3.2 Hybrid Perovskite 7

1.3.3 Applications of Hybrid Perovskites 15

2. FABRICATION AND CHARACTERIZATION 38

2.1 Fabrication techniques 38

2.1.1 FETs, Memristors, Gas sensors 38

2.1.2 Mother materials 39

2.1.3 Substrates 40

2.1.4 Solvents 41

2.1.5 Deposition technique 42

2.1.6 Electrode deposition 43

2.1.7 Characterization techniques 43

3. ELECTRICAL CHARACTERIZING RESULTS 51

3.1 Two probes results 51

3.1.1 Various parameters compared with standard devices 51

3.2 Study on the memristive behavior of hot casted films. 56
3.2.1 Testing three finger prints of memristor 57
3.2.2 AC photocurrent experiment with DC bias 60
3.2.3 Temperature dependence on device characteristics 61
3.2.4 Charge holding ability of the memristor 64
3.2.5 Improving the properties of memristor device 65
3.2.6 Improvements possible 67
3.2.7 Mix cation in memristor 68
3.3 Three probe results (FETs) 69
3.3.1 Electrical measurements 69
4. PHOTO CONDUCTIVITY RESULTS 77
4.1 Gas sensor result 77
4.2 Exposure to different gases 78
4.2 Extended exposure of air & light 79
4.3 Analysis of gas exposure 82
4.4 Photo conductivity of degraded sample 85
4.5 Exposure to inert environment 86
4.6 Analysis of inert gas exposure 88
4.7 QCM results on inert gas exposure 92
5. CONCLUSION 94
REFERENCES 97
CURRICULUM VITAE 103

LIST OF FIGURES

Figure1-01.(a)Vintage specimens chlorite-calcite[2].(b) Gustav Rose [3](c) Count Lev A.Perovskiy[4] 1
Figure 1-02 (a) primitive cell of perovskite and it noted form. (b)Molecular formula with material specifics. 2
Figure 1-03-Ionic packing in an ideal cubic perovskite structures[8] 4
Figure 1-04-Principle of operation and energy level scheme of DSSC[20] 9
Figure 1-05-absorbance spectra of $MAPbX_3$ [21] 9
Figure 1-06-Calculated total and partial DOS of MA,Pb and I[24] 11
Figure 1-07 -PL measurements and fits to diffusion model.[26] 12
Figure 1-08-Multidomain ferroelectric tin film[28] 13
Figure 1-09 -Light soaking effects on PV performance for standard perovskite device.[31] 14
Figure 1-10-Efficiency chart from NREL 15
Figure 1-11-Working principle of DSSC. 17
Figure 1-12-(a) Possible charge transfer to TiO2 from Perovskite as a dye(b) Unit cell of material of initial work 18
Figure 1-13- Possible crystalline structures of CH_3NH_3SnBr/Cl 18
Figure 1-14-Working principle of OSC. 20
Figure 1-15-Band structure of OSC. 20
Figure 1-16-Resistivity change with temperature, crystal structure and absorbance change with band tuning. 21
Figure 1-17- (a) Julius Edgar Lilienfeld (b) William Shockley 22
Figure 1-18- Schematic representative of top and bottom contact FETs 23
Figure 1-19- Characteristics curves from FETs. 23
Figure 1-20- Polycrystalline state of hybrid perovskite that has been used in FETs by Mitzi et.al[5]. 25
Figure 1-21- Basic electrical systems possible 26
Figure 1-22- Field dependence of TiO_2 memristor. 27
Figure 1-23- Frequency dependence of TiO_2 memristor. 27
Figure 1-24- Extreme frequency dependence of potassium ion channel memristor. 28
Figure 1-25- Unipolar and bi polar behavior of a memristor. 29
Figure 1-26- Bardeen's circuit diagram on measurement of adsorption. 30
Figure 1-27- Optical image of large grained perovskite. 33
Figure 1-28- (a)Planar device configuration for the study(b) JV curves with grain size. 33
Figure 1-29- Hole and electron spin density distribution of charged CsPbI3 35
Figure 1-30-Possible self-healing process of Hybrid Perovskites. 36
Figure 2-01- Combination of materials used in film fabrication. 39
Figure 2-02- Combination of materials to include Cs in to the lattice 39
Figure 2-03-(a) Si wafer with 100nm of SiO_2 layer for FET fab(b) Glass substrate used in Memristor fab. 40

Figure 2-04- Chemical structure of solvent DMF. 41
Figure 2-05- Chemical structure of solvent DMSO. 41
Figure 2-06- Fabrication of small and large grain devices. 42
Figure 2-07- Basic diffraction pattern from two planes in crystal structure. 44
Figure 2-08- Typical diffraction pattern of hot casted perovskite film on glass.[68] 44
Figure 2-09- XRD spectrums of Large and Small grain devices we used in our measurements. 45
Figure 2-10- Absorbance spectrum of Large grain film. 46
Figure 2-11-(a) Device view (b)Top view of Large and Small grain devices. 46
Figure 2-12-Comparison of IPCE of Large and Small grain devices with DC bias. 47
Figure 2-13- DC voltage scan on positive bias with repeating. 49
Figure 2-14-(a)Initial status of the Quartz crystal (b)After applying the AC voltage on the crystal 49
Figure 3-01- Optical images of different channel length with small and large grain devices 51
Figure 3-02- Initial current voltage comparison of devices on glass. 52
Figure 3-03- Normalized area under the curve Vs applied bias under dark. 53
Figure 3-04- Cycled Ids Vs Vds scans under dark for various temperatures. 53
Figure 3-05- Activation energy calculated for large grain device. 54
Figure 3-06-(a) Devices of various # of grain boundaries (b) Ids Vs Vds curves under dark of shown devices. 54
Figure 3-07- Dependence of different electric field under dark condition of 3 channel lengths. 55
Figure 3-08-(a) Device structure inside one grain boundary (b) Cyclic Ids Vs Vds curve for such device 56
Figure 3-09-Cyclic J_{ds} Vs E_{ds} curve for different ranges. Inset showed R_{off}/R_{on} ratio with max E field. 57
Figure 3-10-(a) Frequency dependence of a device (b) Summary of Area under curve with frequency. 58
Figure 3-11-Poling effect of cyclic J_{sd} Vs E_{sd} curve. 59
Figure 3-12-(a) Poling effect of various fields (b) Summary of poling effect. 59
Figure 3-13- AC photo current setup with DC bias. 60
Figure 3-14- Shift of the minimums due to poling. 61
Figure 3-15 -(a) Temperature dependence of a device (b) Summary of activation energy calculated with temperature (c)Summary of R_{off}/R_{on} ratio with temperature. 61
Figure 3-16 -Current density dependence with the calculated (1/kT) values 62
Figure 3-17 -Proposed model for the memristive behavior of hybrid perovskite 63
Figure 3-18-(a) Repeatability of poling and probing (b) Summary of time constants for poling and probing. (c)Summary of poling with temperature. 64
Figure 3-19-Cyclic J Vs V curve for sandwiched device. 65
Figure 3-20-(a) Probing from 2V in sandwiched structure (b) Time constant change calculated. 66
Figure 3-21-Cystal orientation of mixed cation devices. 67
Figure 3-22-Cyclic J_{sd} Vs E_{sd} curve for sandwiched mixed cation device. 68
Figure 3-23- Cross sectional SEM images of perovskite device on glass. 69

Figure 3-24- (a) J_{sd} Vs E_{sd} scan under dark with different gate voltages. (b) zoomed view 71
Figure 3-25- Extracted data of J_{sd} Vs E_g from J_{sd} Vs E_{sd} curve. 72
Figure 3-26-(a) Optical image of interdigitated device. (b) I_{sd} Vs V_{sd} scan under dark. .. 73
Figure 3-27- Extracted data from I_{sd} Vs V_{sd} curves under dark. 73
Figure 3-28- (a)I_{ds} Vs V_{ds} scan under light condition. (b) zoomed view 74
Figure 3-29- Ids Vs Vg scan under light condition. 75
Figure 3-30- I_{ds} Vs V_g scan under different wavelengths of light. 75
Figure 4-01- Optical view and device structure of the interdigitated finger pattern. 77
Figure 4-02- IPCE of AC photo current with different environments. (a)Vacuum (b)Nitrogen (c)Argon (d)Oxygen (e)Air 78
Figure 4-03- IPCE of AC photo current with different environments with extra Sun after 100mins (a)Vacuum (b)Nitrogen (c)Argon (d)Oxygen (e)Air 79
Figure 4-04- Time dependence of IPCE of AC photo current under air. (a)Initial (b)With extra light (c)After recovery 80
Figure 4-05- Recovery of AC photo current under air with time. (a) Initial (b) with extra light (c) Recover overnight. 81
figure 4-09. (a)Photo current response under various environments. Inset shows the device configuration. (b)Possible band diagrams under Vacuum (c) Under Air. 82
Figure 4-06-Recovery of AC photocurrent after initial light exposure with variation of time. Top graph shows the variation of 650nm value. 85
Figure 4-07- Comparison of IPCE of AC photo current with different environments. (a)Argon (b)Vacuum (c)He 86
Figure 4-08- Comparison of IPCE of AC photo current with different environments. (a)Argon (b)Krypton (c)Xenon 87
Figure 4-10. Normalized photo current curves under systematic exposure of various environments. 88
Figure 4-11 (a)Time constants values of the current saturation with extra light and gas. (b) Possible mechanism improves surface conductivity under dark and (c) extra light illumination. 90
Figure 4-12Resonance frequency measurement in MHz with (a)He (b) Ar environment in dark. 92
Figure 4-13 Resonance frequency with light and dark under (a)He (b) Ar with 1.5e-1torr pressure. 93

LIST OF TABLES

Table 1-01 commonly used materials in perovskites..... 7
Table 1-02-Calculated Diffusion constants(D) and lengths(L_D)[26]..... 12
Table 1-03-Certified Cell efficiencies [34-38] 15

1. INTRODUCTION

1.1 Origin of perovskite

It was in 1839 that German mineralogist Gustav Rose[1] discovered mineral perovskites. The first prediction of its characteristics was done by analyzing a sample sent by Russian mineral collector August Alexander Kammerer. The name perovskite was given to this mineral in honor of Napoleonic war veteran Count Lev A.Perovskiy. Initially there were some differences of opinion regarding two of its characteristics namely, the isometric morphology of the crystal and its biaxial optical properties. In 1957 it was resolved by using the X-ray diffraction technique.

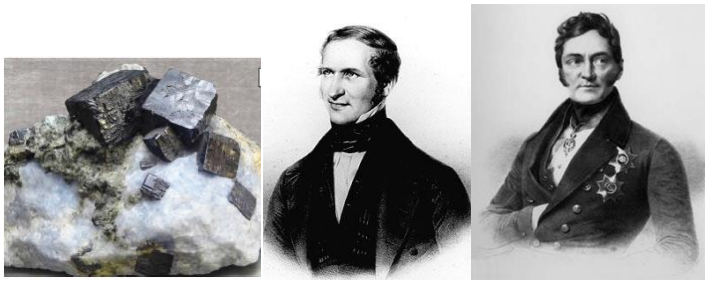

Figure1-01.(a)Vintage specimens chlorite-calcite[2].(b) Gustav Rose [3](c) Count Lev A.Perovskiy[4]

At the outset $CaTiO_3$ was the material explored for the specific crystallographic properties. In the 1940s $BaTiO_3$ came in to the picture due to its high dielectric constant with important ferroelectric properties which we will discuss later. Even today this material is being widely used in the production of thermal switches, mainly due to its piezoelectric properties.

1.2 What is perovskite

As described before main signature of the perovskite is the crystal structure. The primitive cell of the crystal structure has ABX_3 formula (X=oxygen, halogen). The larger A cation occupies a cubo-octahedral site shared with twelve X anions while the smaller B cation is stabilized in an octahedral site shared with six X anions[5]as in Fig 1-02.Mostly it has been discussed with oxides, carbides, nitrides, hydrides or halides, which also have been known to exist with this structure.

Ideal perovskite structure is cubic with the space group Pm_3m-O_h. This is also known to have a super structure with ReO_3 type frame work.[6]

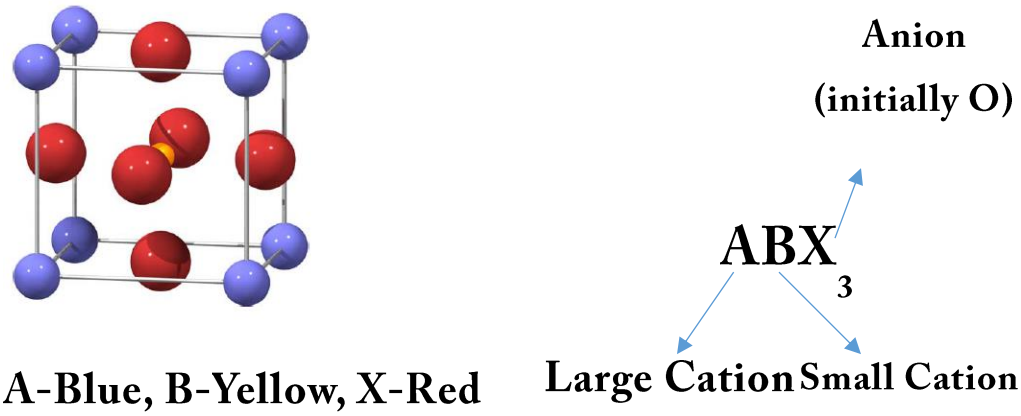

Figure 1-02 (a) primitive cell of perovskite and it noted form. (b)Molecular formula with material specifics.

Perovskites generally have the ABX_3 structure. Normally in an ideal cubic structure there are 5 atoms in a cell. Under ideal conditions, the standard requirement for the structure to be stable can be achieved by equation 1.1,

$$t = \frac{\{R_A + R_X\}}{\left\{\sqrt{2(R_B + R_X)}\right\}} \qquad (1.1)$$

where t value can be identified as the ideality factor and R is the ionic radii of the given atom. If the t value becomes lower than 1 the structure would be disordered. To have a stable structure it is necessary to have a larger A cation compared to B cation. Or else it is possible to form phases like β phase(tetragonal), γ phase (Orthorhombic) rather than the α phase(cubic). The standard is that the factor has to be between 0.89 and 1 to become a cubic structure[7].

As the largest atom known in the group I is Cs (Cesium), $CsPbI_3$ could be identified as less stable compared to the $CH_3NH_3PbI_3$.This is due to the ionic radii of CH_3NH_3(MA ion) being larger than the Cs atom by itself.

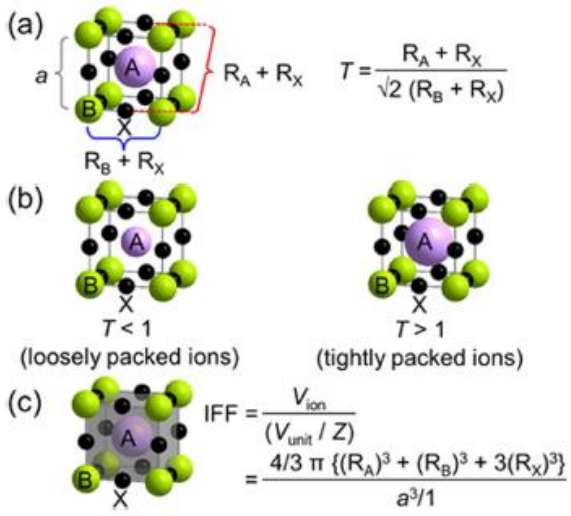

Figure 1-03-Ionic packing in an ideal cubic perovskite structures[8]

Fig 1-03 shows some of the possible ionic packaging options calculated on this perovskite structure. Effective ionic radii calculated by R.D.Shannon et al[9] showed that the calculated t value satisfies the condition to have a stable atomic structure in $MAPbX_3$. A MA cation has an ionic radius of $1.8A^0$ and that allows it to form a stable structure.

Out of most of the metals found naturally, it has been found that perovskite structure-based metals are mostly stable. Ceramics such as $CaTiO_3$ or $BaTiO_3$ were some of the initial perovskite materials that showed ferroelectric properties naturally. Other various technologies such as high temperature superconductors, fuel cells, magneto resistors. etc. were developed using the crystal structure from natural resources or synthesized materials originating from naturally available structures.

1.3 Types of perovskite

Based on the material composition of the ABX_3 crystal structure which introduced before, we can separate the group of perovskites in to two main categories. One structure as conventional perovskites where the composition of material structure just consists of inorganic cations where hybrid perovskites has a mixture of inorganic and organic cations in the crystal structure.

Since the conventional perovskites has been known for a sometime the properties of the materials are well understood. Also because of this it has been used in various current day to day applications. Since the crystal structure is the same as the hybrid perovskites it is possible that in understanding the properties of conventional that could useful in understanding the characteristics. Following section present some of important properties and how they become significant in examples that have known in the field of conventional perovskites.

1.3.1 Conventional perovskites

1.3.1.1 Ferroelectric/magnetic property

$BaTiO_3$ was well recognized as a material that showed ferroelectric property and $SrRuO_3$ of ferromagnetic property. Also, $LaCO_3$ had been used in industries because it showed large thermal conductivity and it continues to be used as a common material in thermistor applications in the present day.

Out of these properties, magnetic properties are said to arise from B^{3+} cations. In the lattice, one O^{2-} is supposed to be shared by two B^{3+} ions. For an ideal case, this O-B-O is supposed to have 180^0 angle. It has been proved that it is the favorable setup for super exchange interaction between two B^{3+} cations. This exchange would have resulted in

antiparallel coupling of the nearest neighboring atoms. The magnetic moment induced by this phenomenon resulted in possible applications of the material which used the magnetic property [10].

1.3.1.2 Superconducting property

It was the discovery of superconductivity at higher temperature (40K) of cuprates, which started the interest in electrical property of conventional perovskites[11].These cuprates were considered as hole superconductors while Ce doped Nd_2CuO_4 showed T_c at 25K where the contribution for the superconductivity comes from electrons.

1.3.1.3 Optical property

Also, optical properties of conventional perovskites have been explored. These have been identified as model systems for spectroscopic studies in visible, IR and ultraviolet regions. The difference between the ordering temperatures of two ions resulted in centered or broadened effects in absorption spectra. It has been found that emission spectra can be tuned in such a way that it can be visibly recognized by the actual color of the materials. This can be optically visualized in the compositions themselves[12].

1.3.1.4 Electrical conducting property

These conventional perovskites also show some mixed conducting properties. As we have two types of ions available in the crystal structure, we could discuss it in both ways. Generally, it has been known that oxygen vacancies in the crystal support the ionic conductivity. By looking at the potential energy surfaces, it has been well documented that the defect energy levels were calculated based on the diffusion paths available [13] in

the material. The effect of oxygen vacancies has been determined by adding excessive amounts of oxygen and observing the changes.

Compared to oxygen supported transport, less amount of work has been done for the cation supported transport. Only a few studies have been done on proton supported transport systems such as $SrCeO_3$[14] and $BaCeO_3$[15] . Yet it has been determined that the effect of cations was much less when compared to the effect of anions.

In the field of perovskites, above mentioned properties are mostly investigated and used with inorganic cations occupying in the basic crystal structure of perovskite. Recently the interest in the scientific research field of perovskites has been shifted towards hybrid perovskites. As described before in the structure of perovskite, some of the inorganic cations were replaced by the organic cations. Following Table 01 summarizes the materials that are being used as perovskites.

	A	**B**	**X**
Conventional	**La^{3+},Cd^{3+},Nd^{3+},Eu^{3+}**	**Al^{3+},Cr^{3+},Fe^{3+},In^{3+}**	**O^{2-}**
Hybrid	**$(CH3NH3)^{1+}$**	**Pb^{2+}, Sn^{2+}**	**X^{-1}**

Table 1-01 commonly used materials in perovskites

1.3.2 Hybrid Perovskite

Hybrid Perovskites had been little discussed until recently. In 1978 the cubic structure of $CH_3NH_3PbX_3$ (X=Cl, Br, I) has been addressed in scientific journal by Weber et.al[16] . He went on to describe the unusual properties such as the color intensifying from each halide. Also charge transfer characteristics of Pb-X bonds and possibility photo conduction was addressed back then. An thorough study on the crystallography using

XRD was done by Knop et al[17] in 1989.Yet the interest on the photo conversion was initiated by Miyasaka et al in 2009.

1.3.2.1 History

In 2009, Miyasaka et al[18]reported the first use of hybrid perovskite in DSSC , as a dye which absorbs light in the photo conversion device . He also went on to report the self-organizing ability of the perovskite nanocrystals on TiO2 nanoparticles. In DSSC structure light sensitizing dye is used by covering up the TiO_2 nanoparticles to form the photo electrode. It was $MAPbI_3$ and $MAPbBr_3$ are the two materials he reported. Photo conversion efficiency of 3.8% from the fabricated cells from iodide based cell and 0.96V photovoltage for bromide based cell was reported. Nevertheless, photo conversion efficiency was lower compared to the DCCS with standard dye at that time, it was considered as the starting point of hybrid perovskite research up-to-date.

1.3.2.2 Mechanism of first use.

In dye sensitized solar cells, the main purpose of the dye is to absorb the photons coming from solar light. As shown in Fig1-04 it generates electron and hole pairs which are transported to the electrodes through electron and hole transporting mediums. It is known that various novel dyes were explored to maximize the conversion efficiency of DSSCs[19].

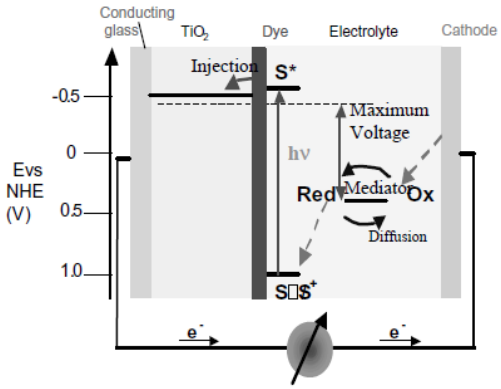

Figure 1-04-Principle of operation and energy level scheme of DSSC[20]

1.3.2.3 Absorbance of the material

When the TiO_2 layer of nano particles is coated with a specific thickness of hybrid perovskite, it has been found that it gives sufficient photo conductive efficiency and also that the absorbance covered by such combination of the materials supports the absorbance of the energies coming from the visible region in solar light.

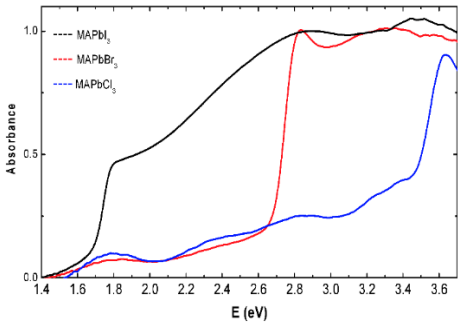

Figure 1-05-absorbance spectra of $MAPbX_3$ [21]

Since, for a 550nm wave length light, absorption coefficient has been estimated to be 1.5 X 10^4 cm^{-1} and for 700nm wave length light absorption coefficient estimated to be 0.5 X 10^4 cm^{-1}, it can be calculated that a 2-micron thin film would be sufficient enough to collect the entire spectrum.

When femtosecond transient absorbance spectrum was conducted on films with and without mesoporous layer of TiO_2 photo voltaic devices, they could still achieve something similar in value to an injection process. By replacing the mesoporous layer and introducing a scaffold layer of Al_2O_3 researchers showed that the device of hybrid perovskite could achieve PCE of 10.9%[22] which provides evidence of feasibility in application of solar cells on their own .Fig 1-05 shows the absorbance of different halide as anion.

1.3.2.4 Comparison with DFT calculations.

From theoretical calculations, hybrid perovskite thin film showed some superior electronic properties which made it a good candidate in photovoltaics. Superior optical absorption properties which contributed to low non-radiative recombination, combined with small effective masses (due to strong s-p bonding) led to the possibility of its use in efficient solar cell applications.[23].It has been shown that the absorption process is also superior in Hybrid perovskites according to calculations. This quality is mainly predicted by using strong direct transitions from p orbitals in halides to metal.

Proper understanding of possible states gives us the ability to compare and improve the quality of the fabricated film. This prediction was done by altering the composition in crystal lattice of the DFT-PBE calculations (density functionalized Theory found by Perdew, Burke and Ernzerhof) as shown in Fig 1-06. Possible Density of Sates (DOS) of $MAPbI_3$ was calculated using the above mentioned DFT calculations. By understanding possible DOS it could determine the contribution made by each molecule. It has been shown that the organic molecule plays a significantly smaller role in conduction while its larger contribution is for the stability of the structure of hybrid perovskite.

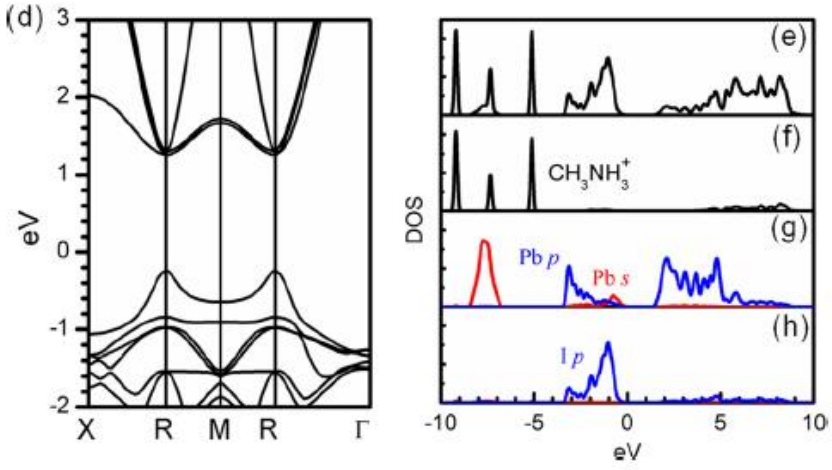

Figure 1-06-Calculated total and partial DOS of MA,Pb and I[24]

Similarly, band structures were calculated for the 3 possible phases in hybrid perovskite structure. It [23]has been shown that important parameters in fabrication process should be carefully controlled .If not that process can produce secondary phases such as δ phase that tend to have deep defect states which could deviate overall performances of the film from the standard structure or β and α phases .

Also by the DFT calculation it has been shown that the effective masses of electrons and holes in conduction could be contributed to the prediction of that the material should perform as an ambipolar type electronically[25].

1.3.2.5 Charge Transport properties

Another important characteristic in hybrid perovskite is the charge transport. This property is calculated using transient spectroscopy measurements. Here photo luminescent(PL) transient was observed after hitting with 507nm source with 30nJcm^{-2} fluence as shown in Fig 1-07. Measuring the peak emission at 770nm.

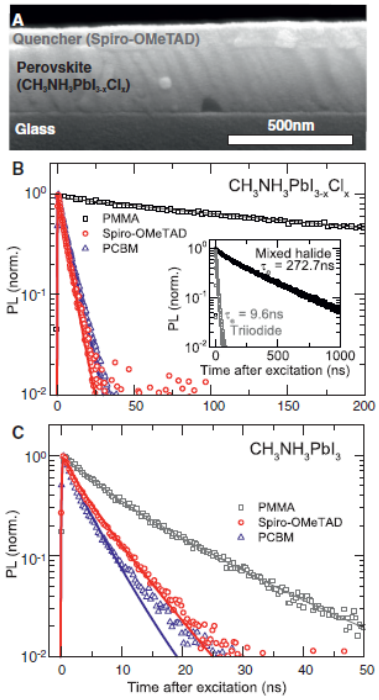

Figure 1-07 -PL measurements and fits to diffusion model.[26]

Perovskite	Species	D (cm^2 s^{-1})	L_D (nm)
$CH_3NH_3PbI_{3-x}Cl_x$	Electrons	0.042 ± 0.016	1069 ± 204
	Holes	0.054 ± 0.022	1213 ± 243
$CH_3NH_3PbI_3$	Electrons	0.017 ± 0.011	129 ± 41
	Holes	0.011 ± 0.007	105 ± 32

Table 1-02-Calculated Diffusion constants(D) and lengths(L_D)[26]

As it is shown in the table1-02, it has been proved that the hybrid perovskite film with mixed halides shows larger diffusion length compared to the pure iodide version of it.

1.3.2.6 Ferro electric properties

Ferro electric properties of hybrid perovskite crystal is another area that has been used to explain some of the unusual behavior of hybrid perovskites in practical applications. To explain the effects such as hysteresis in IV curves, sweep rate dependences this phenomenon had been proposed. By density functional theory calculations of the primitive cell of $MAPbI_2$ based on the molecular orientation including structural

optimization and static dielectric responses it has been simulated domain structure and polarization fields. Fig 1-08 shows a cartoon that helping the transportation by alignment of ion domains. By these calculations it has been simulated this is coming from either the alignment of organic cation or intrinsic lattice distortion. Either way it has been proposed that this could enhance the transport properties of the film itself[27].

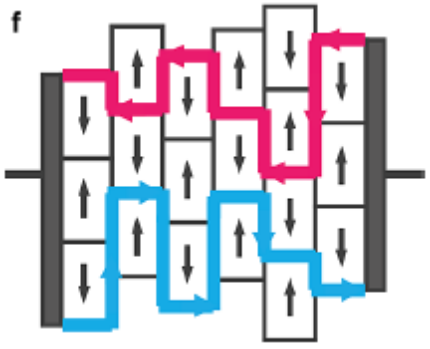

Figure 1-08-Multidomain ferroelectric tin film[28]

1.3.2.7 Drawbacks discussed

Surface and interface traps are two of the potential drawbacks discussed in using hybrid perovskite for photovoltaics. It has been proven by using PL studies that, the continuous light illumination can reduce the density of charged bulk defects within the hybrid perovskite layer though charge trapping effect by temporary filling them. Chemical methods such as doping, or deposition techniques are developed to avoid or to reduce this effect[29, 30]. It has also been suggested that the effect of light soaking could reduce this effect temporarily. Effect on IV curves with light soaking showed in Fig 1-09.

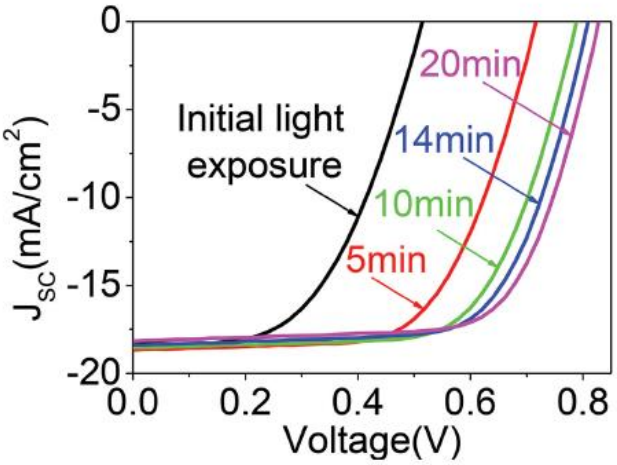

Figure 1-09 -Light soaking effects on PV performance for standard perovskite device.[31]

Instability under high relative humidity is another drawback discussed in the field. A few groups have already taken some steps towards figuring out the ways to overcome this issue. Noh et al.[32] has shown that inclusion of Br in to the crystal improves the stability under relatively higher humidity levels.

To avoid well known hazardous health effects introduced by the material lead (Pb) , alternatives such as Cs have been found recently which could easily be incorporated with the rest of the material [33].

1.3.3 Applications of Hybrid Perovskites

1.3.3.1 Solar cells

As the demand for energy grows with ever gaining new technologies in our day to day life it is necessary to find cheap resources for generating the energy requirement. Solar cells are one source that can generate clean energy at comparatively low costs. Hybrid perovskite has been identified as one material that has the potential to become a cheap source of electricity generation at low production costs in the future.

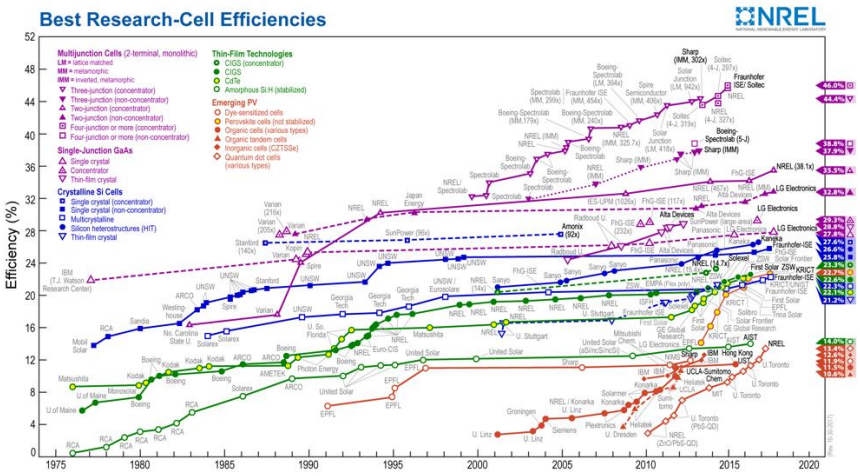

Figure 1-10-Efficiency chart from NREL

	2010 Jan	2015 Jan	2016 Jan	2017 Jan	2018 Jan
Si Crystalline	25	25.6	25.6	26.3	26.7
III-V Cell	26.1	28.8	28.8	28.8	28.8
DSSC	10.4	11.9	11.9	11.9	11.9
Organic	5.15	11	11	11.2	11.2
Perovskite	3.8		15.6	19.7	20.9

Table 1-03-Certified Cell efficiencies [34-38]

Efficiency values extracted from certified solar cells in Fig 1-10, in Table 1-03 shows that hybrid perovskite technology has overtaken some of the conventional research areas

such as organic and dye sensitized technologies. Rapid increase in efficiency has been observed within a small period of time. But it needs to be mentioned that this hybrid type of solar cell fabrication is mostly based on those two types of cell technologies. So, some of its drawbacks in application level that are not represented in the graph could be avoided or reduced by making use of the knowledge incorporated in the above-mentioned technologies. Basic theories of applications which have been discussed in the field of hybrid perovskites are described below.

1.3.3.1.1 Dye Sensitized Solar Cells (DSSC)

This was the initial type of solar cell which is reported have used hybrid perovskite in experimental level.

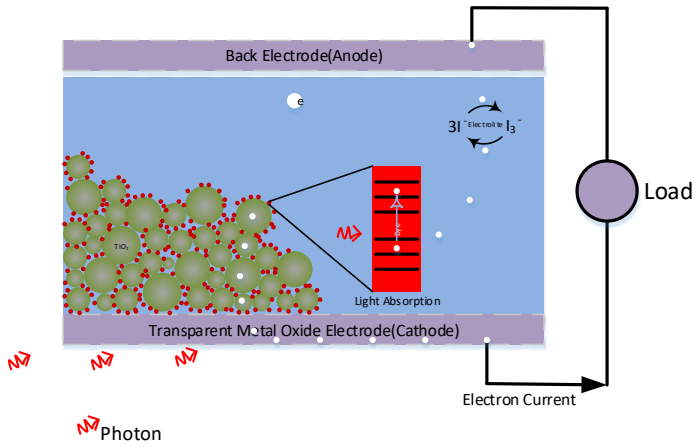

Figure 1-11-Working principle of DSSC.

Here the dye is considered the main absorbing material. As shown in Fig 1-11 device has been constructed in a way that the area of dye coverage is maximized covering the TiO_2 nano-particles and following equations describe the mechanisms that support the conversion,

$$\text{Anode:} \quad S + h\nu \rightarrow S^{*}(\text{Absorption})$$

$$S^{*} \rightarrow S^{+} + e^{-}(TiO_2)(\text{Electron Injection})$$

$$2S^{+} + 3I^{-} \rightarrow 2S + I_3^{-}(\text{Regeneration})$$

$$\text{Cathode:}\ I_3^{-} + 2\,e^{-}(Pt) \rightarrow 3I^{-}$$

$$\text{Cell:} \quad e^{-}(Pt) + h\nu \rightarrow e^{-}(TiO_2)$$

As described before, initial successful attempt in using hybrid perovskite in PV application was done in 2009 Kojima at the University of Tokyo. They reported 3.81% efficiency by using the hybrid perovskite as a dye in the solar cell. Possible mechanism of charge transfer is shown in Fig1-12.

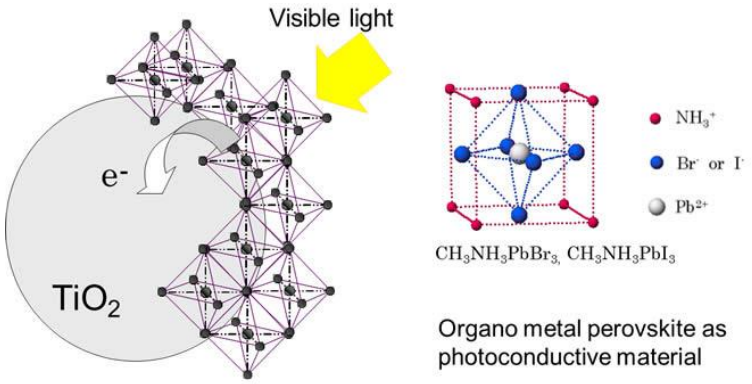

Figure 1-12-(a) Possible charge transfer to TiO2 from Perovskite as a dye(b) Unit cell of material of initial work

To improve the efficiencies various techniques were used in the DSSC research Chiarella et al predicted in 2008 that Sn based halide perovskite could be a good replacement according to their theoretical calculations[39]. It has been also predicted by the calculations $CsSnI_3$ as a direct band gap material with a band gap of 1.3eV in room temperature.

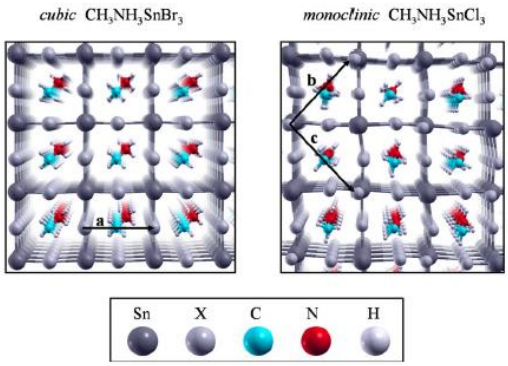

Figure 1-13- Possible crystalline structures of CH_3NH_3SnBr/Cl

Inclusion of Sn was reported in experimental hybrid perovskite solar cells by Ching et.al. where they used the $CsSnI_3$ in DSSC as hole transporting medium (HTM)[40]and possible crystal structures are shown in Fig1-13. Their device configuration used TiO_2 nano-particles as electron transporting medium (ETM) which is adapted from DSSC, whereas some of the other groups used the basics from organic solar cell structure in the application of hybrid perovskites.

1.3.3.1.2 Organic Solar Cells(OSC)

Initially, the structure of OSC was based on the material of doped polymer polyacetylene with halogens sandwiched between two electrodes that have different work functions. Then the second type of solar cell was introduced which consists of two types of doped polymer layers namely donor type and the acceptor type materials. Acceptor material is considered as the main contributor in separating the singlet exciton from bonded exciton pair. The third type of solar cell consists of multi junction boundaries, compared to the previous cells consisting of one junction between the two sandwiched layers. In the Bulk Hetro Junction (BHJ) devices, donor and acceptor materials are mixed together in order to have more interface area to separate the excitons and then collected by the contacts as shown in Fig 1-14.

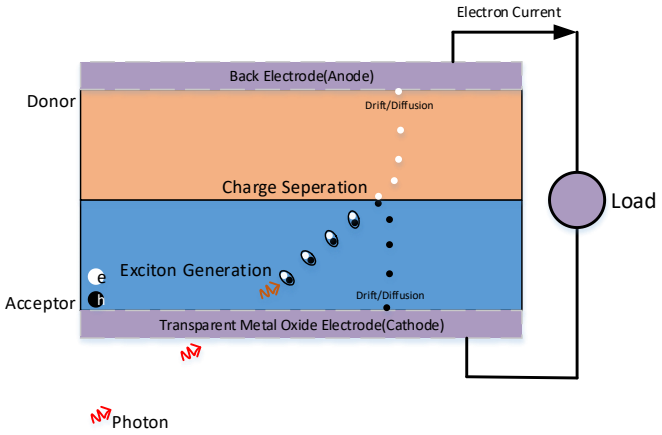

Figure 1-14-Working principle of OSC.

Fig 1-15 describes the standard band diagram used in such solar cells.

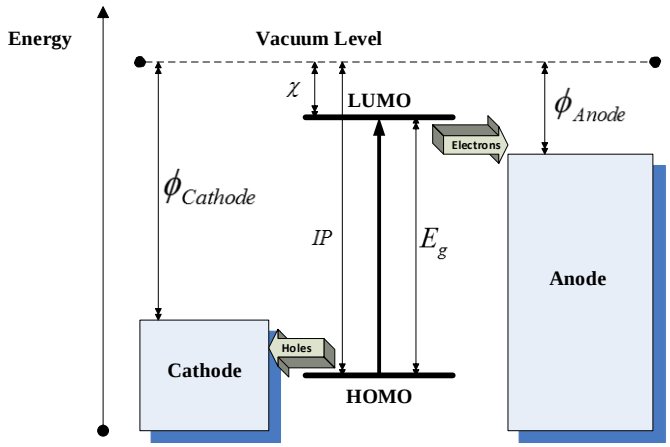

Figure 1-15-Band structure of OSC.

There has been experimental and theoretical exploration[41, 42] conducted by many groups based on the OSC device structure on hybrid perovskite solar cells.

As similar to DSSC work in OSC structure many techniques were tested to improve the efficiency of the solar cells. To improve the performances and reduce the defects, some other experimental groups have been exploring novel chemical techniques and materials too.

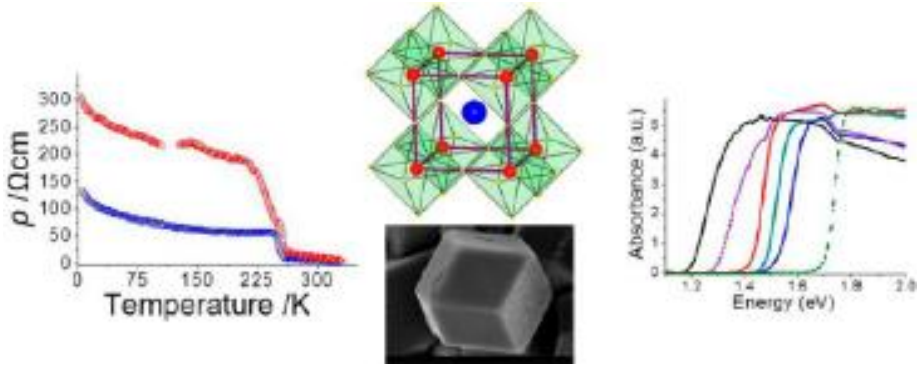

Figure 1-16-Resistivity change with temperature, crystal structure and absorbance change with band tuning.

It has been known with the band tuning concept for this material, LED is an option of application in hybrid perovskites[43].Fig 1-16 shows possible band tuning concept based on the absorbance spectrums. They also explored that halide perovskite could act as a hole transporting media.

Hybrid perovskite solar cells exclusively fabricated with Sn were reported in the basis of OSC structure[44]. Like DSSC structure, lead-based devices from OSC structure based cells are said to be unstable under ambient air, Sn based solar cells are said to be showing better performance compared to standard cells under inert conditions[45].

1.3.3.2 Field Effect Transistors

To understand basic characteristics of semiconducting devices (specially which is fabricated using thin films) Field Effect Transistor(FET) is a device that has been used regularly. Following describe some of the basic concepts and history of FETs which was the initial objective assigned to me using halide perovskites. FETs had been proposed in 1930 by Jewish physicist named Julius Edgar Lilienfeld(Fig1-17). It was in 1926 that he got the patent for FET which was based on amplified effect of the conductivity using a device fabricated with copper sulfide material.

[46] 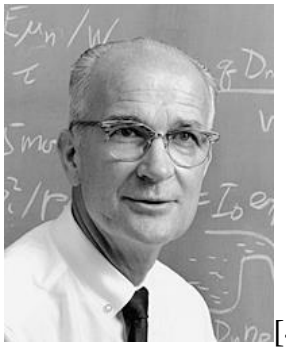
[47]

Figure 1-17- (a) Julius Edgar Lilienfeld (b) William Shockley

It was William Shockley's use of the concept in practical device structure in the 1950's that has been the starting point in various current day applications such as microprocessors and memory devices. The Metal Oxide Semiconductor FET(MOSFET) has been the main structure which surpasses the rest in importance in understanding their various material properties. A gate separated by an insulated material provides the opportunity of controlling the current flow between Source(S) and Drain(D) and gives the opportunity to understand the electrical properties of the material connecting them. Getting to know specially about the value of the mobility of electrons or holes opens a vast area for applications using the given material.

Thin Film transistor (TFT) is the most applicable area in organic or hybrid types of semiconducting films available or yet to come. It could be identified as a subgroup in the field of FETs. Depending on the technique of deposition and structure it can be divided into two categories, namely top gated and bottom gated.[48]

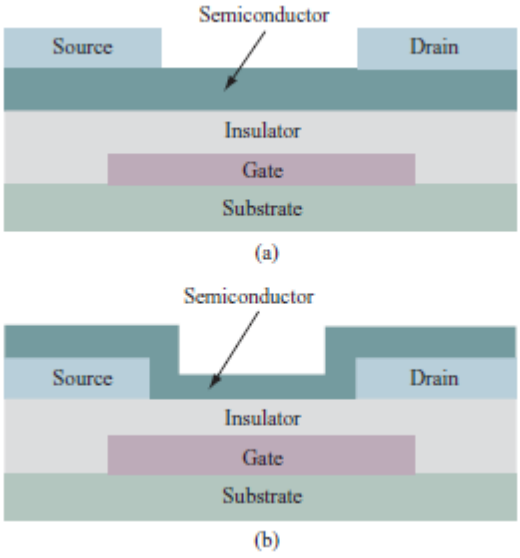

[48]

Figure 1-18- Schematic representative of top and bottom contact FETs

By using either of the Fig1-18 shown device structures, important information about the device itself and about the material could be easily extracted. Example,

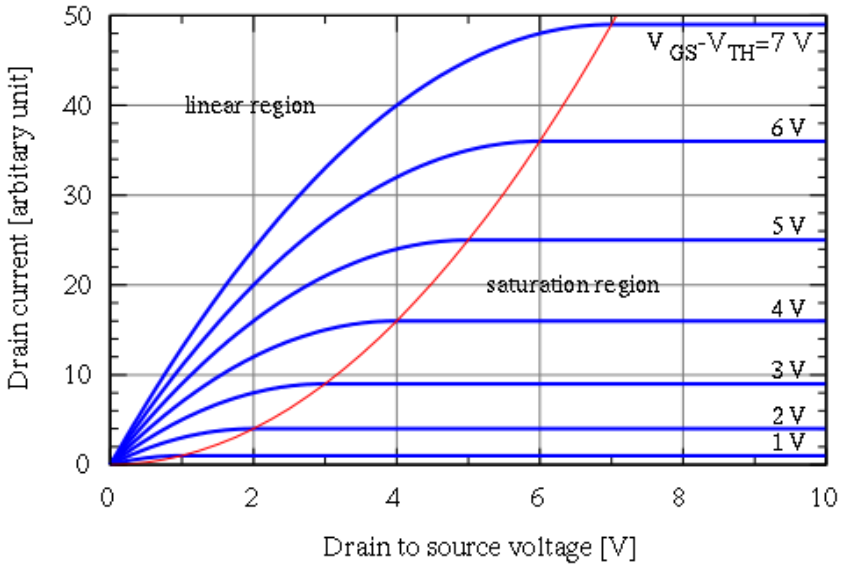

[49]

Figure 1-19- Characteristics curves from FETs.

Once we do the Id Vs Vg for given no leaking device we would be able to get curves as shown in Fig 1-19.By getting Id Vs Vg curves for a given thickness of the film, we could extract the mobility of the film or the device by solving the following equations.

For the linear region,

$$I_{DS} = \frac{W}{L} C_i \mu (V_G - V_T) V_D \; for \; V_D < V_G - V_T \quad (1.2)$$

And for the saturated region,

$$I_{DS} = \frac{W}{2L} C_i \mu (V_G - V_T)^2 \; for \; V_D > V_G - V_T \quad (1.3)$$

Where,

I_{DS} is the current between source and drain and V_D is the voltage applied between those two.V_G is the voltage applied to the gate.V_T is given as the threshold voltage. As it is given in the above figure, C_i is defined as the capacitance of the gate dielectric. W is the width of the conducting channel and L is the length of the channel.

It has been found that mobility calculated from these can undergo alterations due to some other factors not considered in the equations. Structural defects, interface defects and contact resistance could affect the calculated mobility and it could be used to understand the effect of such defects too. Also, there are some measurement techniques that can help to avoid such effects. Four probe measurement is a method which can be used to avoid the contact resistance effect[50].

Mobility in the saturation region can be altered from the density of charge carriers of the material inside the channel. Near the source contact, this is the largest, and near the drain, it becomes totally zero. Edge effect could be considered as another way of affecting the actual value calculated.

Not much exploration was done by FETs in halide perovskite field since it has been showing non-stable currents with applied biases.[51]

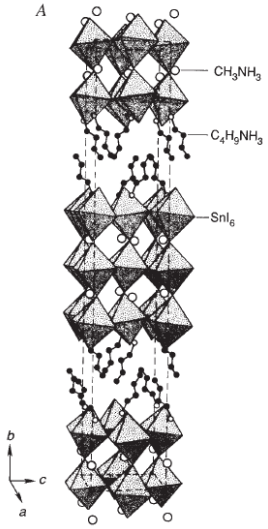

Figure 1-20- Polycrystalline state of hybrid perovskite that has been used in FETs by Mitzi et.al[5].

David Mitzi et.al. reported the hybrid perovskite FET device in a poly crystalline state in early as 2001[52]. As shown in Fig 1-20, Sn version of the hybrid perovskite was used in the scans. Mobilities calculated for m=4,2 were reported in the range of 0.2~0.6$cm^2V^{-1}s^{-1}$ for m-fluorophenethylammonium-based $(C_6H_4FC_2H_4NH_3)_2SnI_4$ perovskites. In theory it has been predicted the mobilities at 400K can take a value high as 3000 $cm^2V^{-1}s^{-1}$ for electrons and 1500 $cm^2V^{-1}s^{-1}$ for holes[53].Yet in experimentally at 200K only 66 $cm^2V^{-1}s^{-1}$ has been reported[54].Not much have stable FETs were reported near room temperature yet due to unstable signal and hysteresis effect accompanied with hybrid perovskites at room temperature.

1.3.3.3 Memristors

In 1971 L.O. Chua proposed the idea of Memristor[55]. It was considered as the missing class of dynamical device structure in electrical circuit theory.

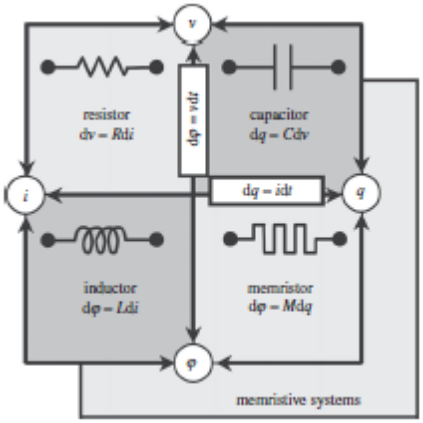

[56]

Figure 1-21- Basic electrical systems possible

In two terminal device systems, 3 basic electrical elements could be used to explain the electrical conduction. This is well known as LRC components of electrical systems.

A new concept called memristive element came into the picture to complete the missing component to describe the relationship between the electrical charge and electrical flux of a system as shown in Fig 1-21.

He defined a time invariant memristance as a state dependent variable which could satisfy Ohm's law regarding the memristor voltage v and memristive current i. A voltage controlled memristance is defined by,

$$i = W(x_1, x_2, \dots x_n,)v \qquad (1.4)$$

$$dx_k/_{dt} = f_k(x_1, x_1, \dots x_1), k = 1,2, \dots, n \qquad (1.5)$$

where W is a continuous function of $(x_1, x_1, \dots x_n)$,called memductance.[55]

Moreover based on the state function defined as memristance he extracted a few unique characteristics which he went on to name as basic fingerprints of a memristor.

1.3.3.3.1 Pinched Hysteresis Loop

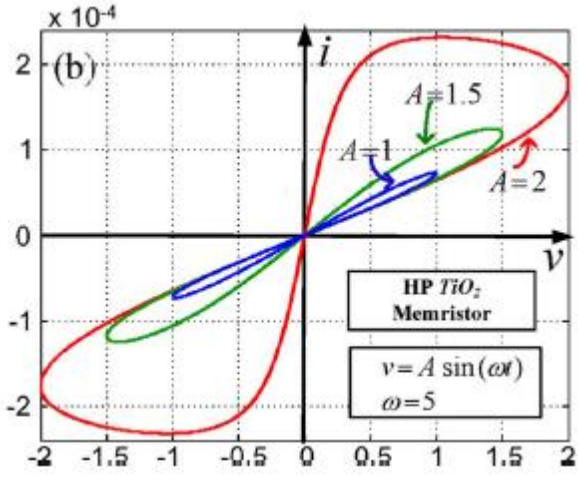

[57]

Figure 1-22- Field dependence of TiO_2 memristor.

As shown in the Fig 1-22, the 1st important characteristic is defined as the hysteresis loop which necessarily goes through the origin. For any amplitude level of the signal or any initial condition of the looped electrical bias, we should observe the pinched hysteresis loop to define the system as a possible memristive system.

1.3.3.3.2 Hysteresis Lobe area decreases with increase in frequency.

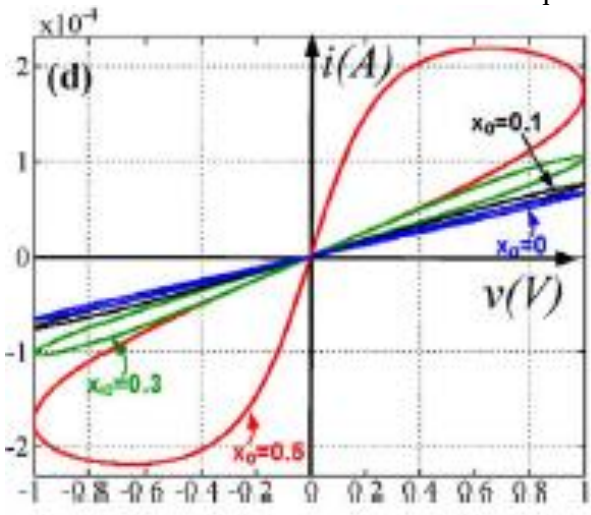

[57]

Figure 1-23- Frequency dependence of TiO_2 memristor.

As shown in Fig1-23 the 2nd fingerprint is defined as the behavior of the lobe area with the scanning speed or the frequency. In such a dynamic system showing the pinched hysteresis loop, the behavior of a dependent variable (current) should follow a condition where, with an increase in frequency of the controlling variable (voltage) the dependent variable makes less hysteresis compared to the initial. This is considered as a unique characteristic of a two-terminal memory based resistive device.

1.3.3.3.3 Pinched hysteresis loop becomes a single value function at infinite frequency.

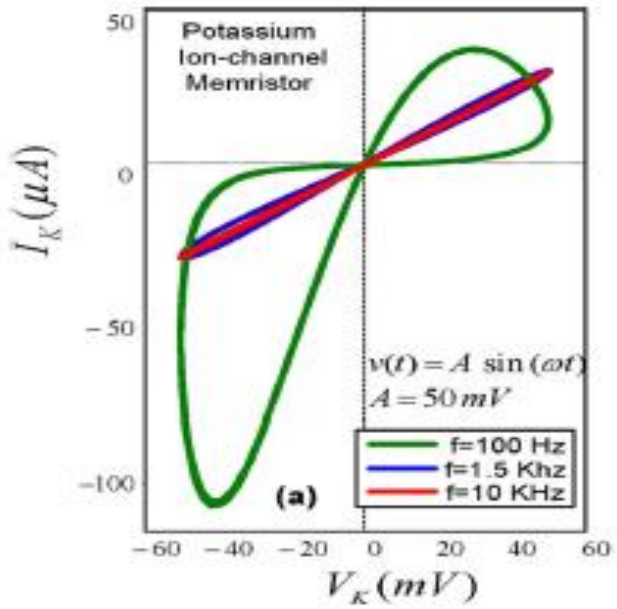

[57]

Figure 1-24- Extreme frequency dependence of potassium ion channel memristor.

The last characteristic of the 3 fingerprint is the uniqueness of the behavior of the system when it is driven at infinite frequency. As it shows in Fig 1-24 at a comparatively higher frequency level it must become a single function of the variable. Overall it should become a single value resistance at higher frequencies where it can be considered as infinity frequency relative to initial frequencies.

Based on the assumption if a device shows the basic characteristics of a memristive device, it is necessary to understand the basic operations of such a device. For a memory device it should have two states (0 and 1 in logic states) that operate while being able to switch between them with a user controllable variable. For electrical systems in general, the voltage is the 1st option as a user controllable variable. With a conductive or resistive change happening due to a given variable alteration, the change of state could be achieved in a useful manner in device operations.

1.3.3.3.4 Unipolar or bipolar

Switching between high resistive state (OFF in switch mode=logic 0) and low resistive state (ON in switch mode=logic 1) can be considered as the two states of operation in memory logic devices. If we consider the polarity change in the applied bias that we have to use in switching the device either OFF or ON , such devices could be categorized into either unipolar and bipolar devices as shown in Fig 1-25.

Most common out of those two is the bipolar devices where unipolar is unique to its non-polarity behavior in a switching mechanism.

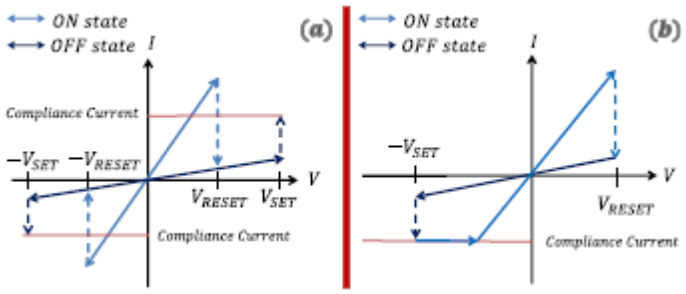

[58]

Figure 1-25- Unipolar and bi polar behavior of a memristor.

Interested people have proposed different mechanisms to explain the phenomenon of memristive behavior (in thermal, electronic or ionic wise) in systems. According to these explanations it is clear that it is not a purposely fabricated device functionality but an

explanation of a natural occurrence. The task ahead is to examine ways and means of using it in memory-based devices. Due to leakage currents and the fact that the maximum possible speed that could be achieved by transistor-based devices has been reached, the motivation to seek for nonvolatile memory devices has increased in recent years.

Bi-polar memristive devices are more common today due to lower voltages that have been used by them[59].

Hybrid perovskite memristors have been reported to show bi-polar behavior with potential of non-volatile random access memory[60]. Ability to deposited on flexible substrates made hybrid perovskite a potential candidate in flexible electronics[61].

1.3.3.4 Gas sensors

In 1953 Bardeen et al discovered[62] gas adsorption of semiconductors, which gives rise to a change in conductance of that material.

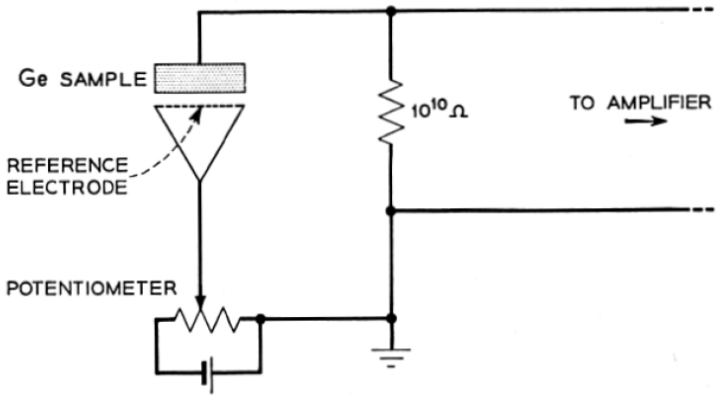

[62]

Figure 1-26- Bardeen's circuit diagram on measurement of adsorption.

This could be identified as the initiating work conducted on gas detection using devices fabricated from semiconducting materials.

Adsorption could be identified as an effect that changes the surface characteristics of a semiconductor by interacting with some gaseous medium. Possible circuit that can be

used for such detection is shown in Fig1-26. This alteration could be an instantaneous process, or it might take some time to show the property change.

This change could indirectly result in changes in bulk too.

As early as 1916, Langmuir proposed a theory on this adsorption effect[63].He predicted that the adsorption centers(or states) on the semiconductor surface had something to do with the effect. Here the molecule on the surface interacted with the gas molecules passing through. He also went on to calculate the Kinetics of adsorption that took place and to calculate the effect as a function of surface area.

By changing the exposed gas, it has been observed that changes which occur on the surface differ significantly from one another. Also, it has been shown that this effect has some dependence on the temperature and pressure of the environment. This phenomenon could easily be used in the detection of gases or pressure. Also, if the change happens on the surface it has a relatively fast response time and it means that flow sensing is also possible by using such material.

It has been well established that the effect of adsorption could be altered by some external conditions. One such condition is the Illumination of light. In scientific terms it's called the photoadsorption effect.

It has been confirmed that the illumination effect associated with adsorption could result in an enhanced, reduced or non-affected change in the kinetics or equilibrium states.

The enhanced effect was defined as the positive photoadsorption effect where negative photoadsorption shows the reduced effect of adsorption. As mentioned before, it is known that this process is time sensitive where sometimes the time of response in overall kinetics would have some delay.

This type of effect was considered as some “memory” effect in the device study. When the device shows some light activated effect in a gaseous environment, the process of removal of light and returning to its initial state would take some time and such material could be considered as a good candidate in photo-controlled memory effect using adsorption.

Since it has been known that hybrid perovskites show some hysteresis effect and its potential in memory application would open a new area of study in light activated and controlled memory devices.

1.3.3.5 Overview of the thesis work

Like other popular materials which have emerged in the field of scientific research many groups are examining hybrid perovskite material for possibilities of alternative applications. From semiconducting materials with such possibilities, it has been found that some of them can be used to understand the properties in the material itself.

Many groups strived to achieve the maximum efficiencies and modifications that could result in better performance. Lead free devices, larger band gap materials, better hole and electron transporting mediums and a few defects at crystal level are some of the challenges faced by the community. By understanding the characteristics it’s possible that some of the above-mentioned challenges can be simplified to overcome them.

The goal assigned initially at Light to Energy team from Los Alamos National Lab(LANL) was to understand the film characteristics by fabricating FETs using the hot casted technique. Major part of the following thesis is based on the work that has been conducted at LANL and later sections at the University of Louisville (UofL).

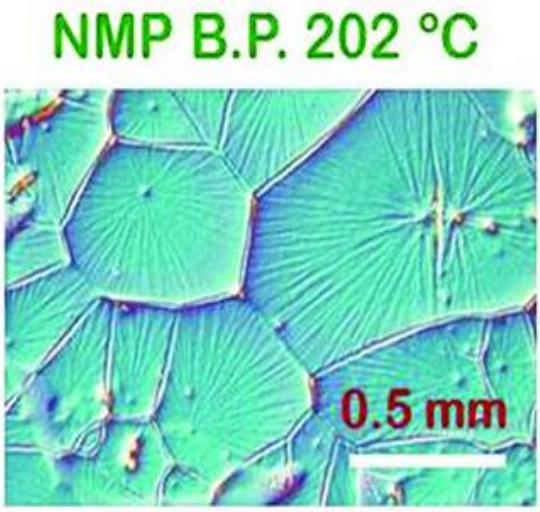

Figure 1-27- Optical image of large grained perovskite.

In 2015 Wanyi et at[64] reported a new and innovative technique called hot casting to fabricate hybrid perovskite films. They were able to get large crystal structures as millimeter sized grains as shown in Fig 1-27.As mentioned before initial assignment at LANL was to use the hot casting technique to fabricate the FETs and use the film to conduct electrical scans to characterize the film.

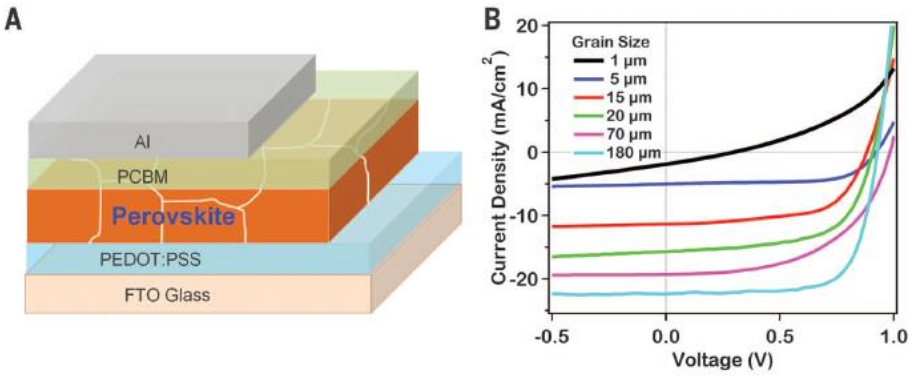

Figure 1-28- (a)Planar device configuration for the study(b) JV curves with grain size.

As it was reported hot casted thin films of hybrid perovskites has been achieving almost 18% efficiency constantly [64] in the solar cell structure. Depending on the grain size

optically they were able to get higher efficiencies as shown in Fig1-28 .Optical characterizations were conducted on the films fabricated using hot casting and conventional technique to compare the qualities of the films with standard film in literature. Being able to get larger grain devices made us unique opportunity to understand the grain boundary effect.

Two terminal electrical measurements (top contact) were done to understand the grain boundary effect. Best performing devices were produced using the lateral devices with both contacts lying inside a single grain boundary. In dark condition IV scans were conducted and proven to have a threshold voltage that current value suddenly starts to increase from almost none. Over that threshold value significant improvement of the conductivity was observed. With the hysteresis effect observed on the devices while sweeping the voltage suggested us to consider the ability of holding its conductivity. This is the memory based resistive behavior we describe in the results section. Various measurements were conducted to prove the memristive behavior of the film rather than just a simple resistive behavior. Three fingerprints of the memristors were tested and proven the feasibility of large grain hybrid perovskite film in memristive device fabrication. Various parameters that could be used as controllers (Temperature, poling…) were also tested. After understanding the basics of the memristive behavior attempts were made to improve the properties we observed.

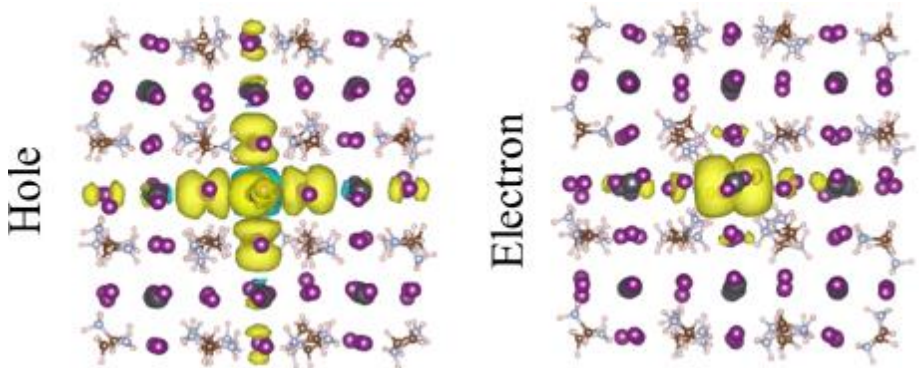

Figure 1-29- Hole and electron spin density distribution of charged CsPbI3

It has been proven that improvement of the hybrid perovskite film could be achieved by introducing formaldehyde(FA) and cesium(Cs) in to the crystal[65]. Based on the calculations possible electron and hole cloud that could be possible is shown in Fig 1-29. In our study, we were successful in applying that theory to fabricate devices with the improvement expected by the introducing Cs in to the crystal lattice. This addition was done by the optimized conditions mentioned above literature using chemical techniques. For the lateral devices the voltage we need to apply to see the conductive state was about 15-20V.By constructing the sandwiched structured device, to get the same field we have proved that the turn on voltage could be reduced to less than 1V. Various characterizations done on that structure and are also discussed in the results section. Some of the initial work on the main idea of understanding the basics by using three terminal device structures was presented. Cross sectional SEM was also conducted to understand the film structure below the top surface to see the effect of the grain boundary continuation to the substrate surface. Initial FET studies proven that under dark condition hot casted films showed bipolar behavior. Under illumination it tends to show photo biasing with overall n-type behavior. Also, it is presented that by illuminating same power of light in lower wave lengths produce larger n-type behavior compared to the

longer wavelengths. Yet I_d Vs V_g curve showed some instability which could related the poling effect we observed in the memristor study.

Second stage of the thesis work is based on the work conducted at UofL. To improve the current magnitude and observe magnified effect a finger pattern was fabricated as two terminal device structures. After confirming the quality of the films using XRD spectra various gases were introduced and observed the effective change of the AC phot conductivity. For the initial scans significant improvement was observed with reactive gases of hybrid perovskite where more exposure resulted in permanent damage to the film. For inert gases no change was observed. Nevertheless, by the introduction of secondary DC light made the conductivity improved significantly. After significant time in dark made the film recovered back to original. This recovery process is similar to the what Wanyi et al reported and shown in Fig 1-30 in self-healing ability of such films.[66]

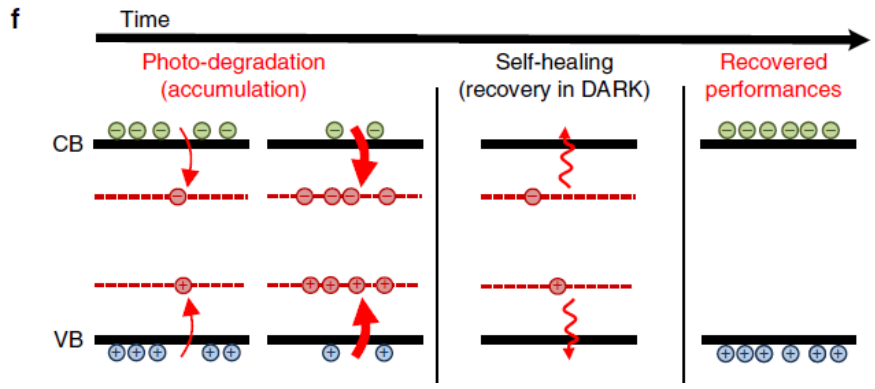

Figure 1-30-Possible self-healing process of Hybrid Perovskites.

By understanding the basic solar cell characterizing techniques they went on to explain possible traps generated during the light soaking process[66]. In our work these results prompted us to look at the gas sensing ability of hybrid perovskite, we extended the

discussion of the light exposure for lateral device structure. We used the light exposing mechanism to increase the current level to detect the gas sensing ability of the film. Exploration of mass change in the film was conducted using Quartz Crystal Microbalance(QCM). QCM was also used to understand the possible adsorption effect with gas exposure and when extra light exposure happens with non-reacting gases. The results presented below suggest it could be effect of lattice expansion as Hsinihan Tsai et al. reported in the expansion of lattice of thin films of hybrid perovskites. In their study they went on to mention that this process could be resulted in better performing photovoltaics [67]. In our scans we observe significant enhancement of currents with the exposure of some gases with large molecules with extra DC light amplification.

More interesting science is being continued in the all the three sections (FETs, memristors and gas sensors) mentioned before. It has been found out that more stability was shown in the 2D material in hybrid perovskites. Work is already underway to understand the possibilities in applying the 2D structure in the above-mentioned device areas.

2. FABRICATION AND CHARACTERIZATION

To understand the performances of each device (field effect transistor/memristor/gas sensor) fabrication techniques and characterization techniques plays a major role in getting repeatable results. Following section describes the detailed information about the materials that has been used in fabrication and basics of the characterization techniques that we used to characterize the devices.

2.1 Fabrication techniques

All fabrications were done under an inert gas environment (Argon filled glovebox) and processed samples were directly transferred to the electron beam/thermal chamber for deposition of gold contacts. Then the samples were transferred to a high vacuum environment for characterizations

In the fabrication process the first and the most important step was to identify the required materials and their correct molar proportionalities. It is necessary to have optimized recipe to get the best results in the characterization and device processes. Such optimized conditions used are described below.

2.1.1 FETs, Memristors, Gas sensors

Since the interest of the study was on the thin film of hybrid perovskites, material wise variation of the material selection could be identified to be in minimal level in the study. Another advantage was that the study was based on a film that had been optimized for photo voltaic studies of the group at LANL and the initial work was done at the same conditions at LANL.

2.1.2 Mother materials

As shown in Fig 2-01 Methylammonium chloride (MACl) and lead iodide (PbI_2) were used as the mother materials in fabrication of Halide perovskites with 1:1 molar ratio for large grain devices. For smaller grain devices methylammonium iodide and lead iodide were used.

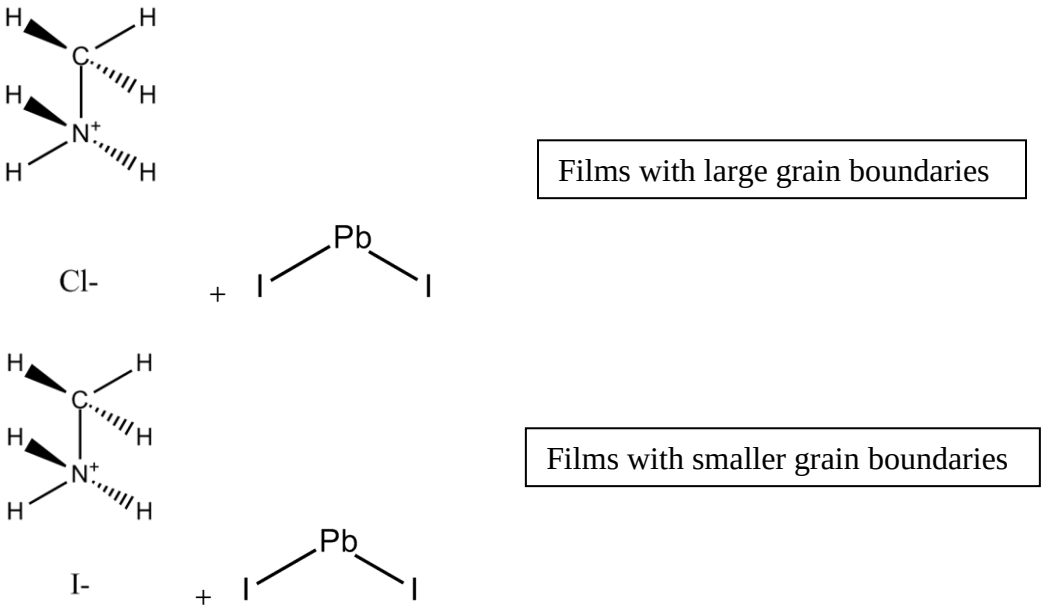

Figure 2-01- Combination of materials used in film fabrication.

To increase the current levels in memristors, 5% Cesium Iodide was used(Fig 2-02).

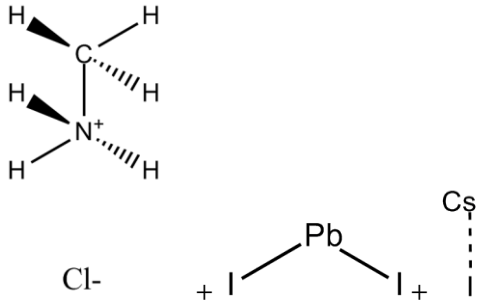

Figure 2-02- Combination of materials to include Cs in to the lattice.

For MACl, purification was done before mixing and other materials were bought from commercially available sources (Sigma-Aldrich).

2.1.3 Substrates

For the memristors' fabrication, glass substrates were used and for Field Effect Transistors, doped Silicon wafers with a thin layer of SiO_2 were used.(Fig 2-03) In both instances after dicing into required dimensions, they were thoroughly cleaned by chemical techniques and Oxygen plasma treatment to remove any organic and any other residuals lying on the surface. Then they were transferred to the glovebox for the fabrication process.

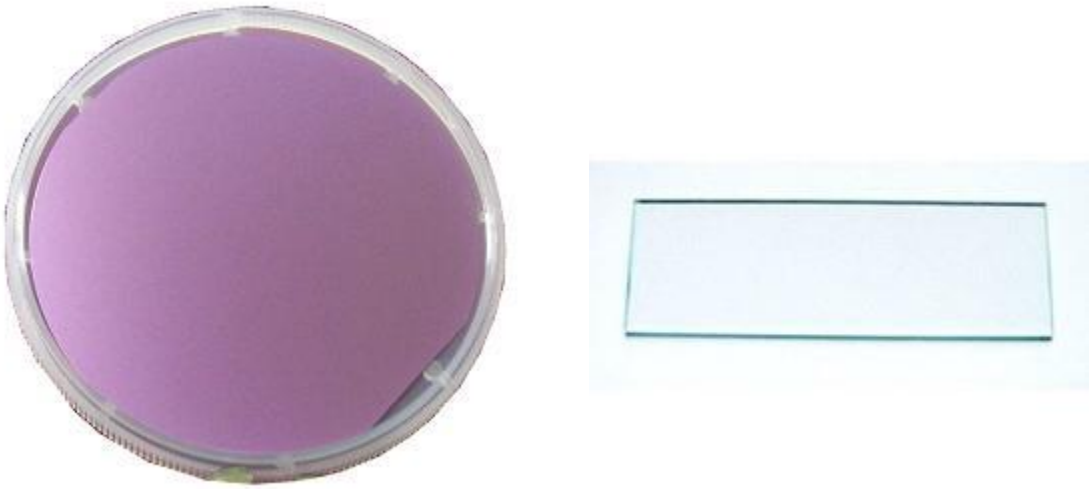

Figure 2-03-(a) Si wafer with 100nm of SiO_2 layer for FET fab(b) Glass substrate used in Memristor fab.

2.1.4 Solvents

Two types of solvents were used in fabrication.

For major parts of the measurements dimethyl formamide (DMF)(Fig 2-04) was used as the solvent.

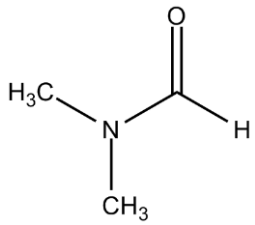

Figure 2-04- Chemical structure of solvent DMF.

For the mixed cation devices, dimethyl sulfoxide(DMSO) as Fig 2-05 was used as a mixture with other solvents due to its dipolarity and higher boiling point which helps in dissolving and mixing compared to DMF solely. Both DMF and DMSO were mixed in relevant ratios to dissolve the mother materials in fabricating the crystal films.

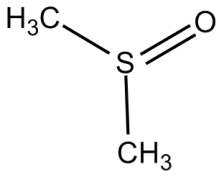

Figure 2-05- Chemical structure of solvent DMSO.

Since their mixture has a higher boiling point, an excess amount of heating at 100^{o}C was needed after the hot casting process. This step was carried out to make sure of removing all the solvents from the film.

2.1.5 Deposition technique

Fabrication of perovskite crystals was done using the two types of techniques. Large grain devices were fabricated using the technique which has been invented by Wanyi et al[64], while small grain devices were fabricated using the standard technique which has a post annealing process after spin coating.

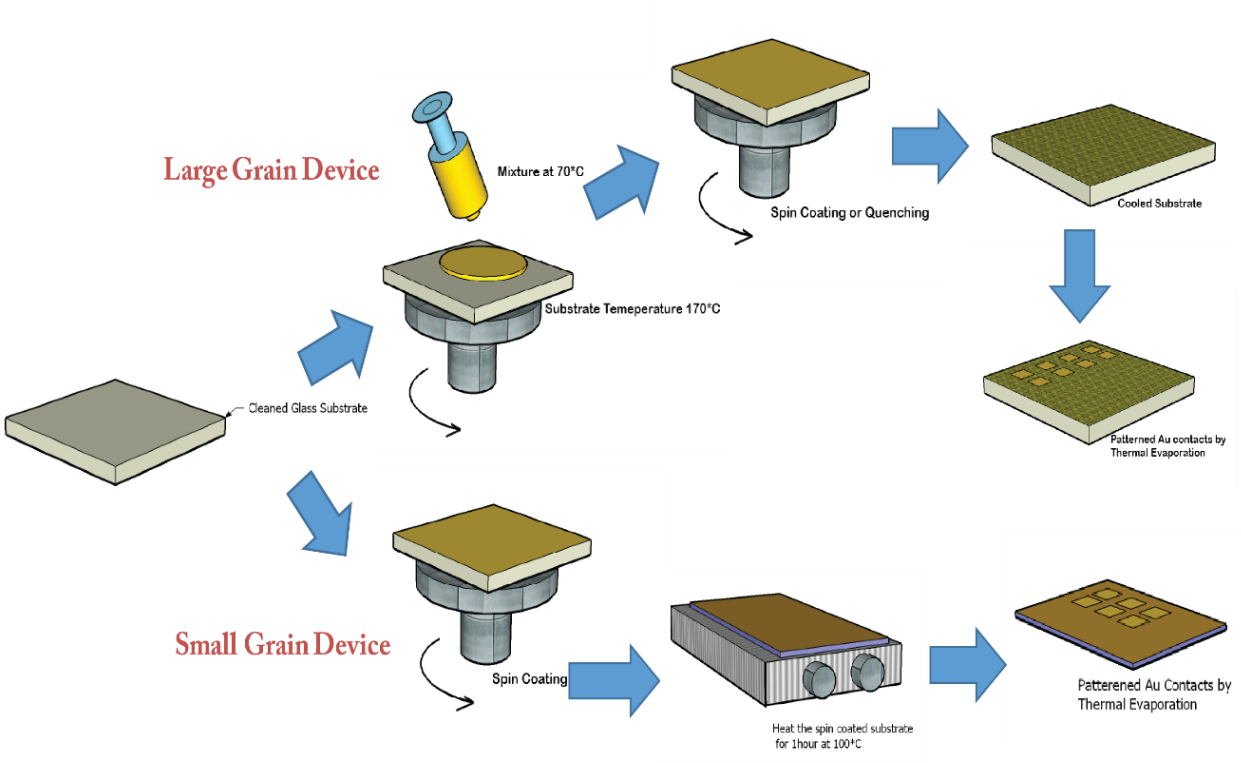

Figure 2-06- Fabrication of small and large grain devices.

Perovskite solution was stirred overnight at 70^{o}C before spin coating. An optimum thickness of 400nm was achieved by spin coating 100µl of solution at 5000rpm for 1minute. As it shows in Fig 2-06 in the hot casting technique, a sudden change in the color from yellowish brown to dark brown was observed, while in the conventional method post annealing was necessary to achieve a better quality thin film.

2.1.6 Electrode deposition

Fabricated films on substrates were transferred to the electron beam chamber after aligning the mask onto the largest crystal (inside single grain). The chamber was pumped down to ultra-high vacuum level (10^{-7} torr) and deposited 100nm of gold using electron beam deposition technique.

Two types of masks were used in FETs, Memristors and Gas sensors. For gas sensors, an interdigitated pattern was used to increase the collection of current, whereas in other instances, a simple two terminal patterns were used as shown in Figure 2-06.

2.1.7 Characterization techniques

Main focus here is to understand the electrical properties of the devices which are being proposed, and which are being interested in. Yet some optical and other characterization techniques described below were used to evaluate the quality of the films and devices which we fabricate and used.

2.1.7.1 X-Ray Diffraction spectroscopy

To understand the quality of the crystal fabricated, a thin film was deposited on each substrate and XRD (X-Ray Diffraction) spectrum was analyzed for each of them.

XRD spectroscopy has been used in crystallography to detect the crystal structure and how it is oriented. X-ray as the beam was used since the wave length of X-ray is in the same order of the atomic radius of most of the material we use. When a high-powered X-ray beam is generated and exposed to the powder or film, the intensity of the diffracted beam could be detected by the detector which moves on the other side of the sample stage where film is placed.

The software will create a plot of intensity of the collected beam versus twice the diffraction angle in which the detector was placed. This would give us an idea about the average symmetry of the film.

Miller indices were used to identify the planes related to the peaks we observed.

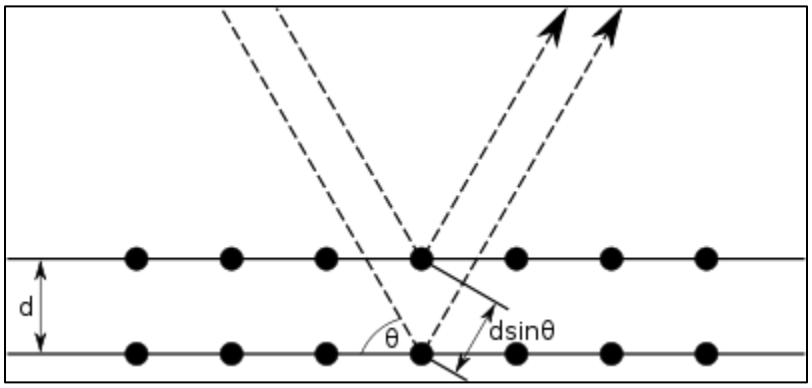

Figure 2-07- Basic diffraction pattern from two planes in crystal structure.

For crystal plane of atom as Fig 2-07 using Bragg's law,

$$2dsin\theta = n\lambda \qquad (2.1)$$

where d is the lattice spacing of the crystal planes and λ is the wave length of the incident beam. n is a positive integer.

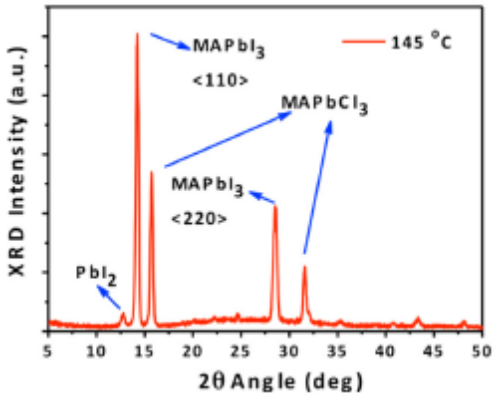

Figure 2-08- Typical diffraction pattern of hot casted perovskite film on glass.[68]

Fig 2-08 shows general XRD peaks associated with hybrid perovskites. Fig2-09 shows XRD peaks by two types of films

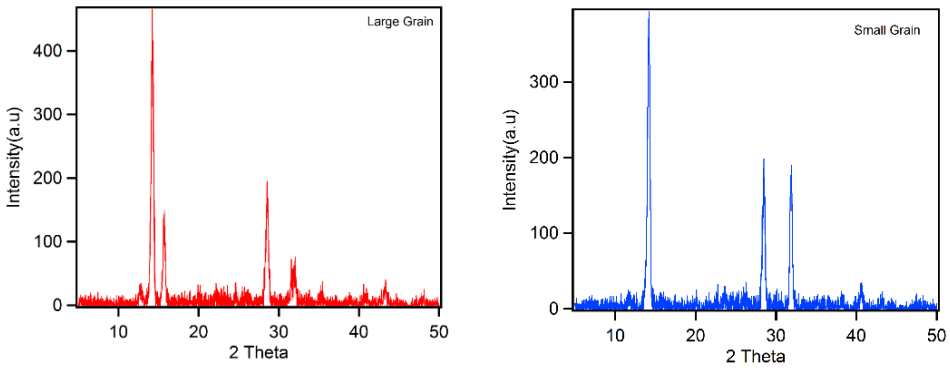

Figure 2-09- XRD spectrums of Large and Small grain devices we used in our measurements.

2.1.7.2 Optical absorption spectroscopy

Optical absorbance spectrum was another measurement that was used in confirming the quality of the crystal we had on glass substrates.

When a photon carrying an energy, E_x falls onto a thin film, it can either be absorbed or transparent depending on the band gap (E_g) of the material. If E_x is larger than the band gap it is known to absorb and where energies are less, the beam will penetrate through. In terms of wavelength,

$$E_g \propto {}^{1}/_{\lambda} \qquad (2.2)$$

it could be said that light with higher wave lengths has more potential to penetrate through compared to lower wave lengths.

The optical absorption coefficient α is an important factor in representing the ability of the film to convert light into current. It will determine the penetration depth which is

related to $1/\alpha$ value. According to Beer Lambert's law the current generated at a depth of y from the surface is defined as

$$I(y) = I_0 \exp(-\alpha y) \qquad (2.3)$$

From the steepness of the band edge we can get an idea of whether the material is a direct or indirect band gap material. It is well known that with the direct band gap material the drop is much steeper.

A thin film was deposited on systematically cleaned glass substrate to confirm the characteristics of the hot cast and conventional post annealed hybrid perovskite samples as Fig 2-10. This certification was done to ensure the quality of the hybrid perovskite film that was used in all instances.

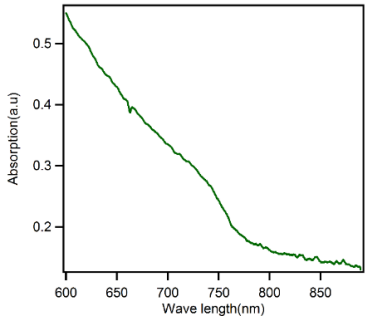

Figure 2-10- Absorbance spectrum of Large grain film.

2.1.7.3 Incident Photon-to-electron Conversion Efficiency (AC & DC)

A thin film with 400nm thickness of hybrid perovskite was deposited on a thoroughly cleaned glass substrate and a 100nm thin gold layer pattern was deposited using a mask.

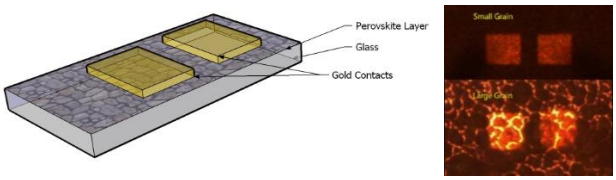

Figure 2-11-(a) Device view (b)Top view of Large and Small grain devices.

Two methods were used to deposit the thin film. One is the more common post annealed film and the other is the hot cast film. Fig 2-11 shows optical images of both films.. Annealed or spin coated films were transferred to the ST500-1-4CXKEL-TR probe station and then a vacuum level of 10^{-7}Torr was achieved inside the chamber using a turbo molecular pump before conducting electrical measurements of the devices on the films.

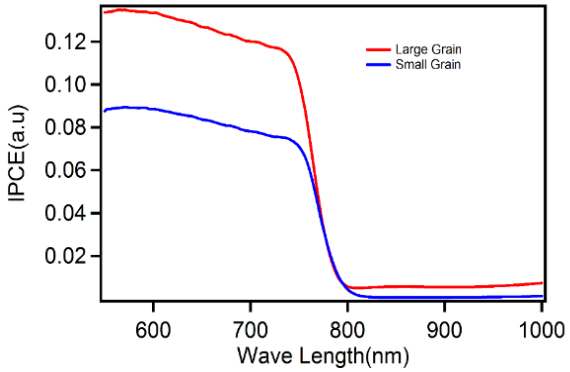

Figure 2-12-Comparison of IPCE of Large and Small grain devices with DC bias.

The calculated quantum yield which represents a quantified value of the conversion efficiency of a device can be defined as,

$$Quantum\ yield = \frac{number\ of\ carriers\ generated}{Number\ of\ photons\ incident}$$

The number of carriers is another representation of current generated and the ratio will determine how efficient the conversion ability of the material which we are interested in is. By calculating the power and current density we could simplify the efficiency in terms of,

$$IPCE = \frac{I(Acm^{-2})}{P(Wcm^{-2})} X \frac{1240}{\lambda(nm)} \qquad (2.4)$$

Initial DC photo current measurements were conducted with a small applied bias in series (0.5V). This is because the device itself has no internal potential to support the collection process. This was mainly due to the same type of electrodes we deposited as contacts on the sample. Fig 2-12 shows the comparison of small and large grain lateral IPCE comparison.

In both AC and DC measurements, IPCE could be used to quantify the quality of the films. Here Delta-Nu DNS-500 diffraction grating monochromator was used with Newport 66885 1000W halogen light as the light source to generate various wavelengths of the light.

For AC measurement, ThorLabs' MC-200B chopper was used with E&G instruments' model 5210 Lock-in Amplifier.13Hz was used as the reference frequency for the lock-in amp.

In the gas sensor study, for sun exposure Newport's 100W light source was used and focused onto the sample area to get the average illumination of 100mWcm^{-2} power.

2.1.7.4 Current Voltage Curves

To understand the dependence of the conductivity of the intrinsic film and its behavior with band bending near the interfaces, an external electrical field was applied, and generated current was collected under the dark condition. To detect the effect of light on the conductivity and transport, a similar kind of IV (current-voltage) sweep was conducted in the presence of an external light source. Fig 2-13 shows typical cyclic curve on positive voltage.

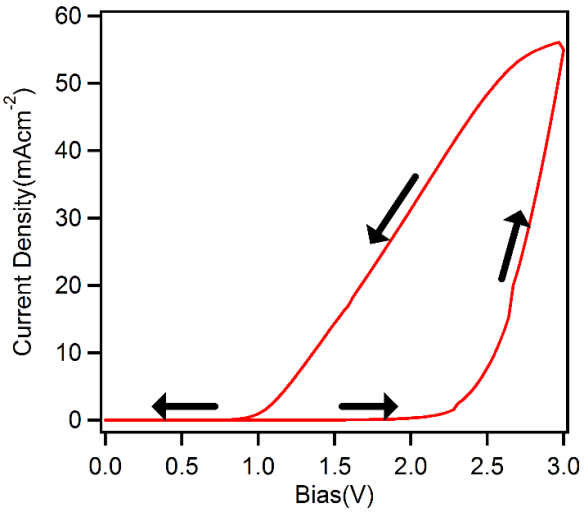

Figure 2-13- DC voltage scan on positive bias with repeating.

An I-V sweep was conducted between the top contacts with a known rate and repeated the sweep under both polarities. For FETs a metal gate was introduced with a separation of 100,300 and 500nm of insulating SiO_2 layer. Then the same I-V sweeps were done with different gate voltages to detect the average polarity of the material.

2.1.7.5 Quartz Crystal Microbalance

Piezoelectrical material is said to form an electric field in the presence of mechanical stress. Vice versa effect can also be achieved using an electric field. It is known as converse piezoelectric effect. Using an AC voltage, it is known that crystal could be made to oscillate. As shown in fig 2-14 by using the appropriate voltage, crystal could be oscillated in its resonance frequency.

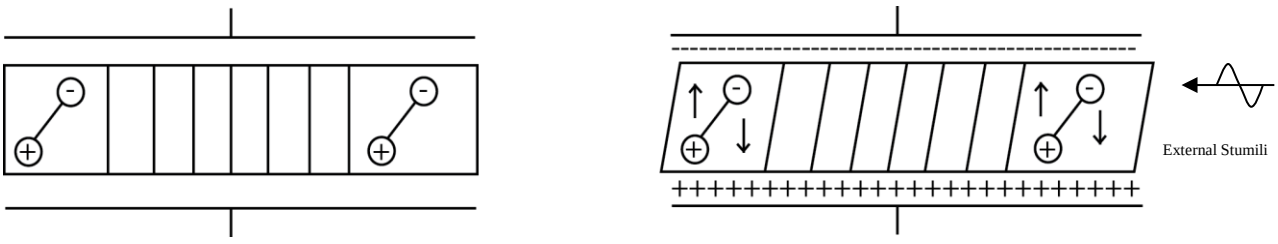

Figure 2-14-(a)Initial status of the Quartz crystal (b)After applying the AC voltage on the crystal

It is known that if some interaction happens on the surface of the crystal, we could determine the effective change by using QCM. The change in the mass is calculated using the Sauerbrey equation by fitting a curve to detect the resonance frequency. It is determined by incorporating the resonant frequency change of the crystal to the mass change.

$$\Delta m = -\frac{A\sqrt{\rho_q \mu_q}}{2f_0^2}\Delta f \qquad (2.5)$$

$\boldsymbol{A}$ active crystal area
$\boldsymbol{f_0}$ intrinsic frequency of quartz crystal
$\boldsymbol{\rho_q}$ density of quartz crystal
μ_q shear modulus of quartz crystal
$\boldsymbol{\Delta f}$ frequency change
$\boldsymbol{\Delta m}$ mass change

3. ELECTRICAL CHARACTERIZING RESULTS

3.1 Two probes results

To understand how the factors affect the dark conductivity of the film, an optical measurement was conducted on the sample to detect the film morphology. This was also conducted because it had been observed that by using the hot cast technique, millimeter sized grains each associated with a grain boundary were achieved. In lateral device structure (specially the top contact devices) quality of the surface could be identified as a candidate that could play a major role when it comes to surface electrical transporting.

3.1.1 Various parameters compared with standard devices

3.1.1.1 Fabrication techniques

As shown in Fig3-02 a set of electrical experiments fabricated from two types of devices(Fig 3-01). One with hot casted and one with standard (as casted).

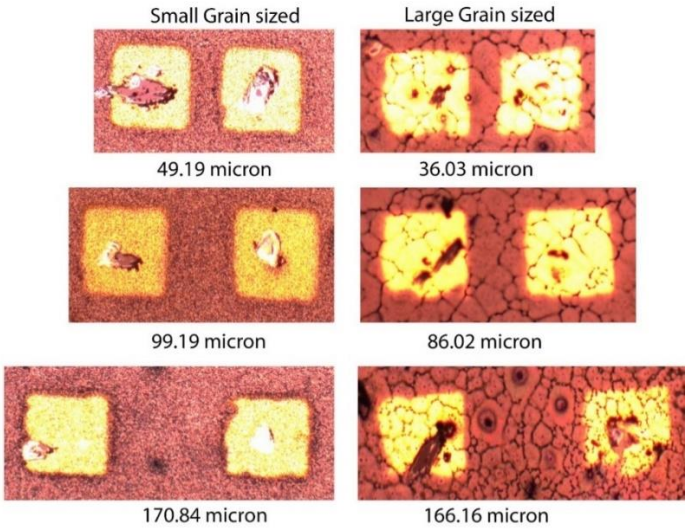

Figure 3-01- Optical images of different channel length with small and large grain devices

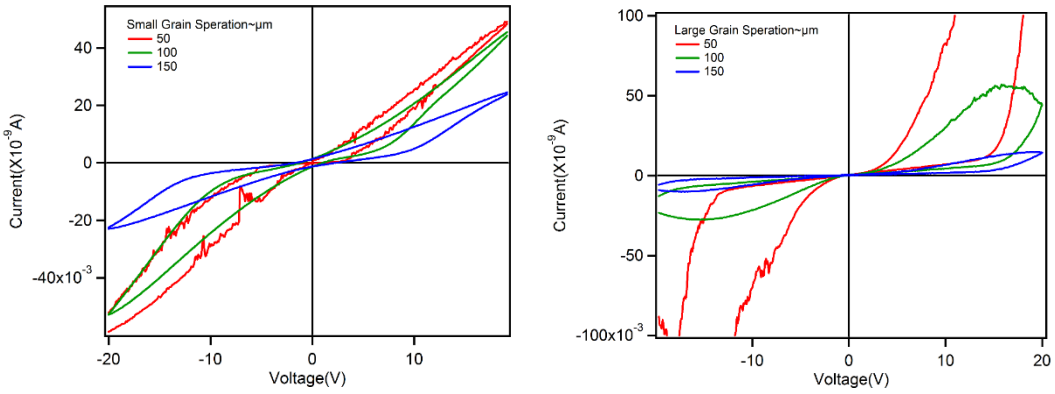

Figure 3-02- Initial current voltage comparison of devices on glass.

A significant difference was observed from device to device in the I-V scans in hot casted films whereas the films fabricated in the conventional method didn't show that much change. For different voltage regions, the current levels were increased in a similar manner in all conventional type devices where it is directly related to the actual field between the two pads. In hot cast films significant differences were observed where rapid increase in current was observed after passing some voltage point.

3.1.1.2 Hysteresis effect comparison

Here our measurements were conducted in a cyclic manner where I-V curves went back and forth a few times until they got stabilized on to the same path. As a result we were able to know about the effect of hysteresis(based on the area under the curve) which is addressed generally in the field of hybrid perovskite[69].We could observe a trend that follows in the normalized area under the curve with the applied bias between the pads as shown in fig 3-03 . Here normalization was done with respect to the maximum area we got.

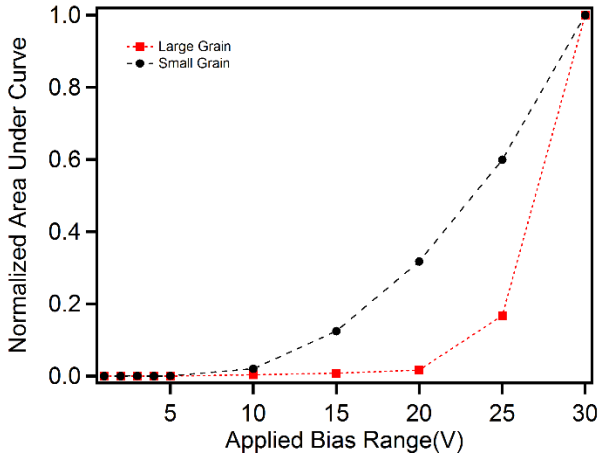

Figure 3-03- Normalized area under the curve Vs applied bias under dark.

3.1.1.3 Temperature effect comparison

In order to understand how the temperature affects current value when voltage changes and how hysteresis changes for each IV curve, a set of I-V scans was conducted on both types of films. Here also for each temperature the 3rd scan was used for curve fitting. The activation energy was calculated by fitting an exponential curve for each IV curves (Fig 3-04).

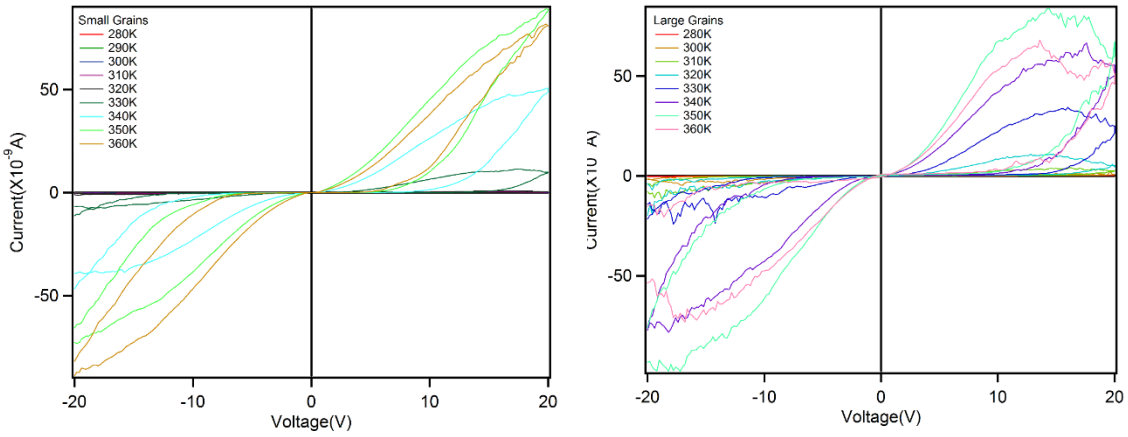

Figure 3-04- Cycled Ids Vs Vds scans under dark for various temperatures.

3.1.1.4 Activation energy comparison

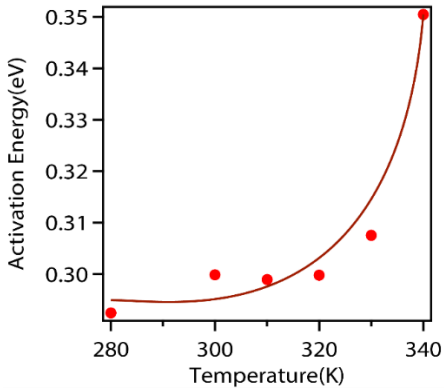

Figure 3-05- Activation energy calculated for large grain device.

In both cases, maximum current value for each curve increased significantly with the temperature. So calculations suggested that overall activation energy increases(Fig 3-05) with increase of temperature of the film regardless of the two fabrication techniques.

3.1.1.5 Dependence of number of grains

In the case of large grain devices significant changes were observed in devices with a shorter channel length. Depending on whether there is a single or multiple grain boundary lying between the contacts pads, IV scans showed a difference in the conductivity.

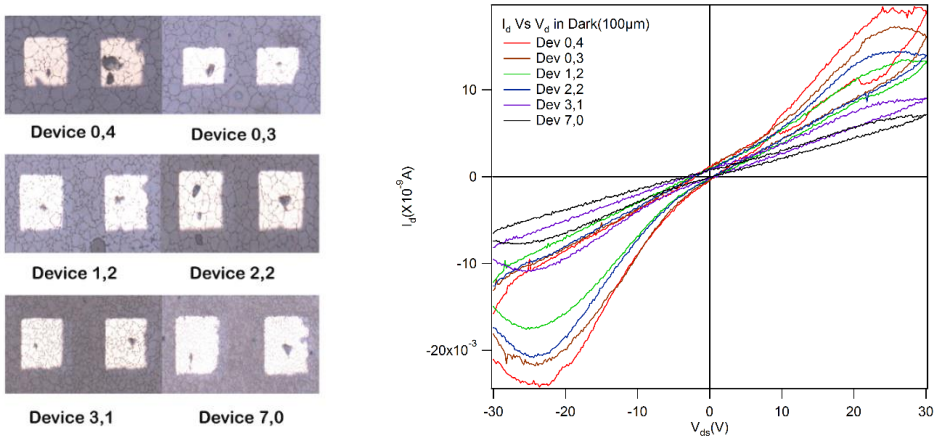

Figure 3-06-(a) Devices of various # of grain boundaries (b) Ids Vs Vds curves under dark of shown devices.

When there is less, or no grain boundary in-between the two contact pads, I-V curves showed a sudden improvement (turned ON effect) in conductivity in each direction.(Fig 3-06) The smaller the number of grain boundaries, a more significant change was observed.

3.1.1.6 Dependence of the field

Initial experiments suggested that there is a dependence of current values on the electric field we applied between the channels. A set of three devices was selected with different channel lengths but with similar surface morphology, and scans were conducted using a similar field range by changing the voltage we applied.

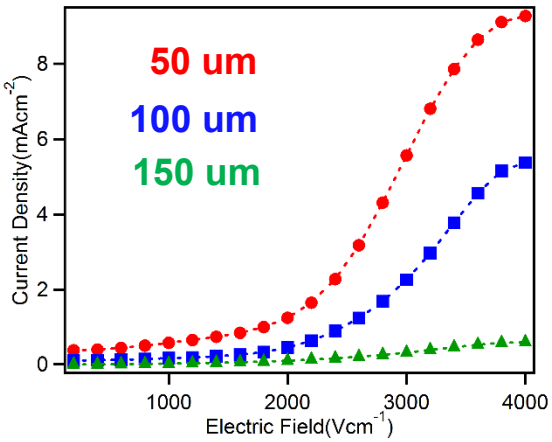

Figure 3-07- Dependence of different electric field under dark condition of 3 channel lengths.

Fig 3-07 suggested that the current change could be either related to the ionic movement as those in the field suggested[70], or due to some localized polarization effect. Even when voltage scan direction is reversed, the current displayed the same effect where if permanent ion diffusion would occur we should have observed less current in one

direction which was not the case in ours. Moreover, by displaying slower current at the longer channel length this experiment also suggests that this could be related to having more atoms between the two contacts. This could be a possible effect due to a localized polarizing effect or a combined effect of the atoms.

As the cyclic I-V curves suggested single grain or one grain devices can retain a state (charge) for some time. These results encouraged us to examine the possibility of using the two-terminal device as memory-based semiconductor using hot casted films.

3.2 Study on the memristive behavior of hot casted films.

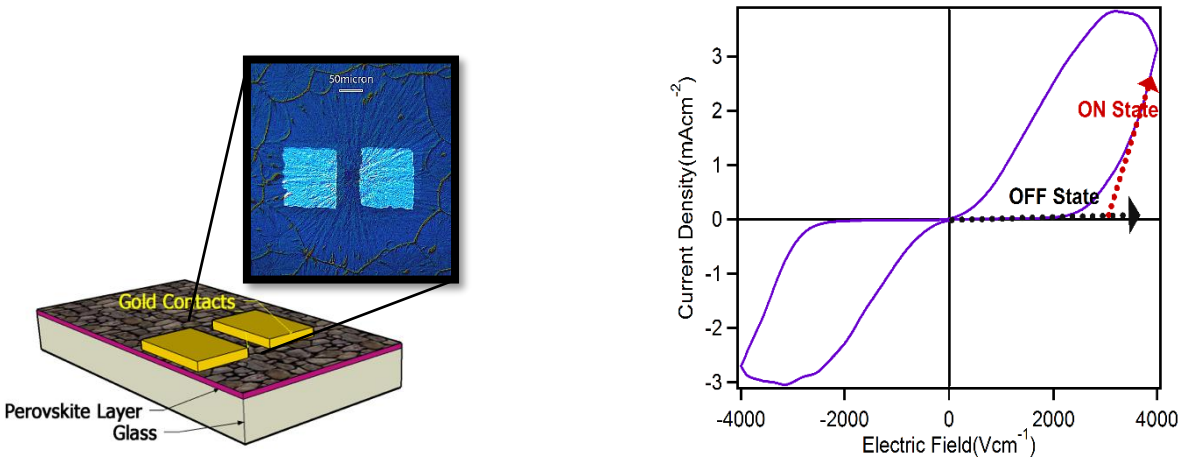

Figure 3-08-(a) Device structure inside one grain boundary (b) Cyclic Ids Vs Vds curve for such device.

To understand the possibility of using a device fabricated by hot casted film with hybrid perovskite thin film as a memristor, a comparison was conducted to verify the main characteristics of a memeristor as suggested by L.O Chua [57].Following describe the detailed results of each experiments conducted on devices as Fig 3-08.

3.2.1 Testing three finger prints of memristor

3.2.1.1 Field dependence on device characteristics

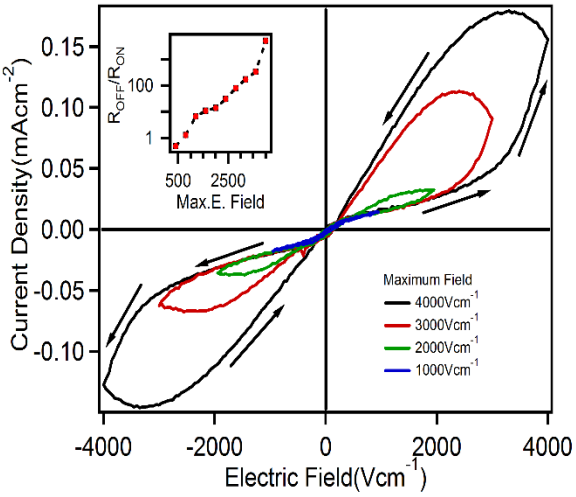

Figure 3-09-Cyclic J_{ds} Vs E_{ds} curve for different ranges. Inset showed R_{off}/R_{on} ratio with max E field.

As Fig3-09 ifferent fields were applied (cyclic) on a 50micron channel length device which was fabricated inside a single grain as shown in fig3-16(a). After the initial forming process (cycling the maximum bias at the same rate) for 3 cycles the current was stabilized as mentioned before. This also suggests that poling does have a significant effect on the conductivity of the film. When the applied field is higher we could observe the higher turning ON point (voltage where the conductivity shows a sudden increase). Also, when reversing, it shows that it reaches zero and then repeats it in the negative direction. It shows more symmetric behavior with the field and current densities.

3.2.1.2 Frequency dependence on device characteristics

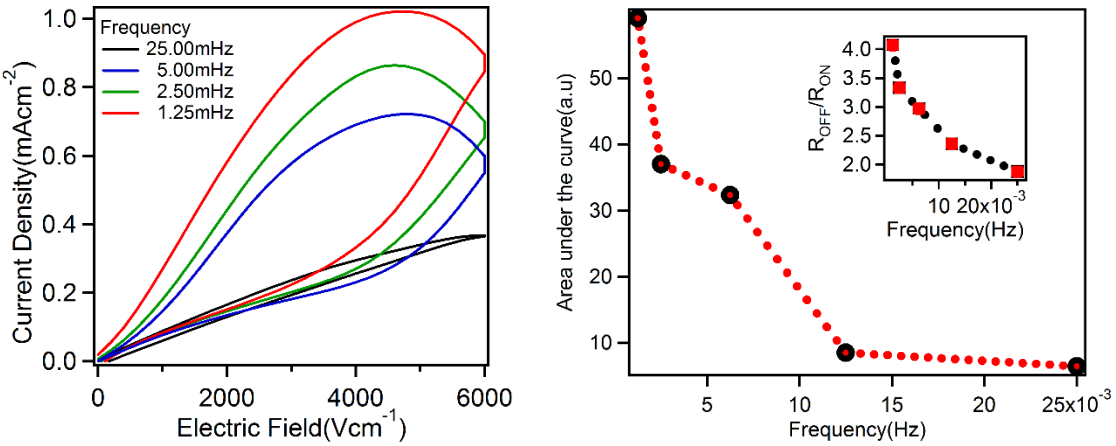

Figure 3-10-(a) Frequency dependence of a device (b) Summary of Area under curve with frequency.

One of the three fingerprints [57]of being able to predict the ability of the film to act as a memristor is the frequency dependence. Fig 3-10 present the dependence of the frequency by varying the voltage sweep speed of the two-terminal device. Analysis of the curves suggests that with the increase of frequency the hysteresis effect lowers down, and more over the effect of memory also comes down as suggested by the inset in the fig 3-18.

3.2.1.3 Poling effect on device characteristics

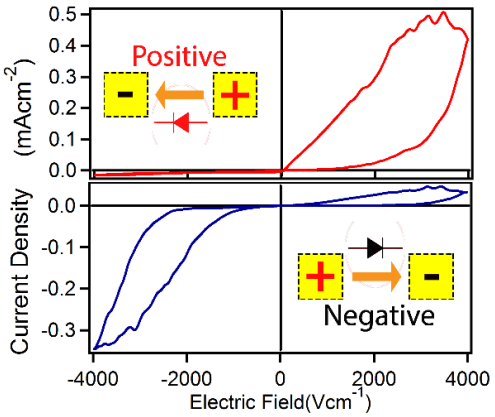

Figure 3-11-Poling effect of cyclic J_{sd} Vs E_{sd} curve.

Since the applied external field is mainly affecting the memristive behavior, we followed an experiment on a more symmetric device and applied the given external bias for 30mins.Then the cyclic I-V measurement was conducted. A significant change was observed in the I-V scans where on the polarity side of the applied field the current density was enhanced. A similar kind of observation was made when applying the opposite polarity as Fig 3-11.

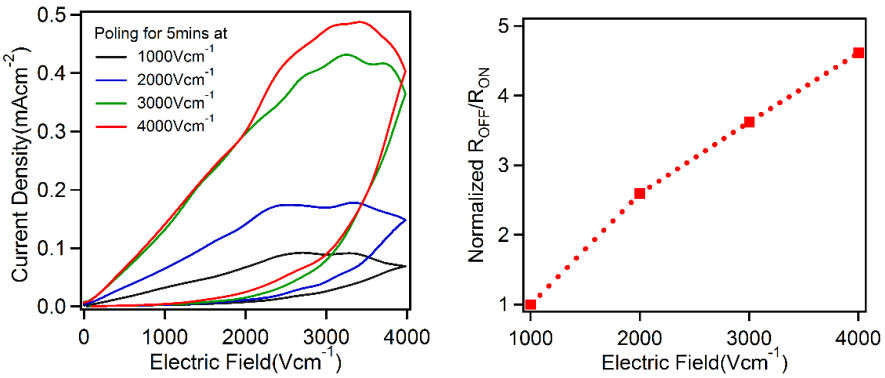

Figure 3-12-(a) Poling effect of various fields (b) Summary of poling effect.

Different external biases were used for 5mins and then the IV scan was conducted. Conductance at higher biases improved significantly, where the quality of the memristor also increased simultaneously as Fig 3-12.

3.2.2 AC photocurrent experiment with DC bias

To understand the effect of poling more deeply an AC photo current measurement was conducted on the samples. A source meter was connected in series with AC photo current setup as shown in Fig 3-13.

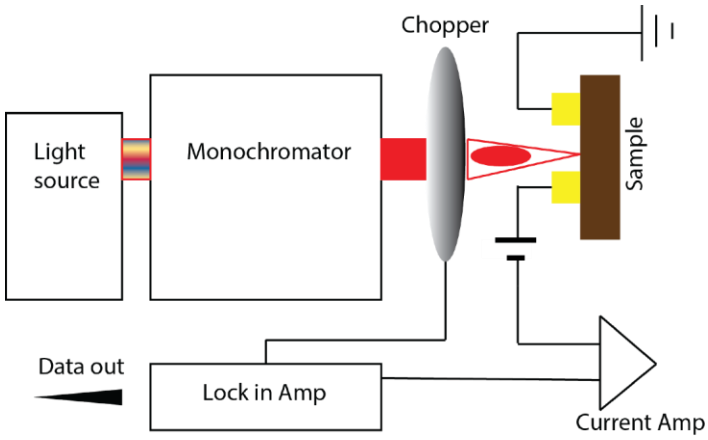

Figure 3-13- AC photo current setup with DC bias.

Since we could measure an AC photo current without applying any external bias our hypothesis was there would be an internal built in potential that exists in a pristine sample to support that. Our aim was to probe an opposite external bias as Fig 3-14, which would result in a current value which goes through a minimum. The minimum could represent as the built-in field reversely.

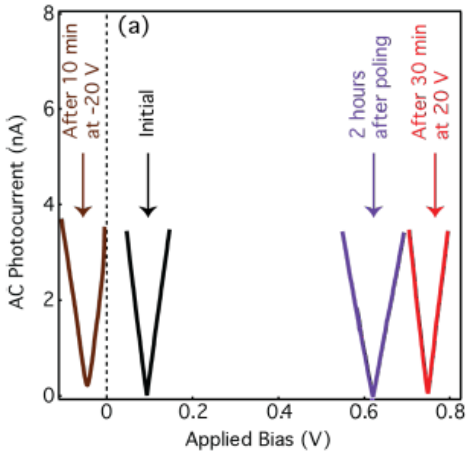

Figure 3-14- Shift of the minimums due to poling.

3.2.3 Temperature dependence on device characteristics

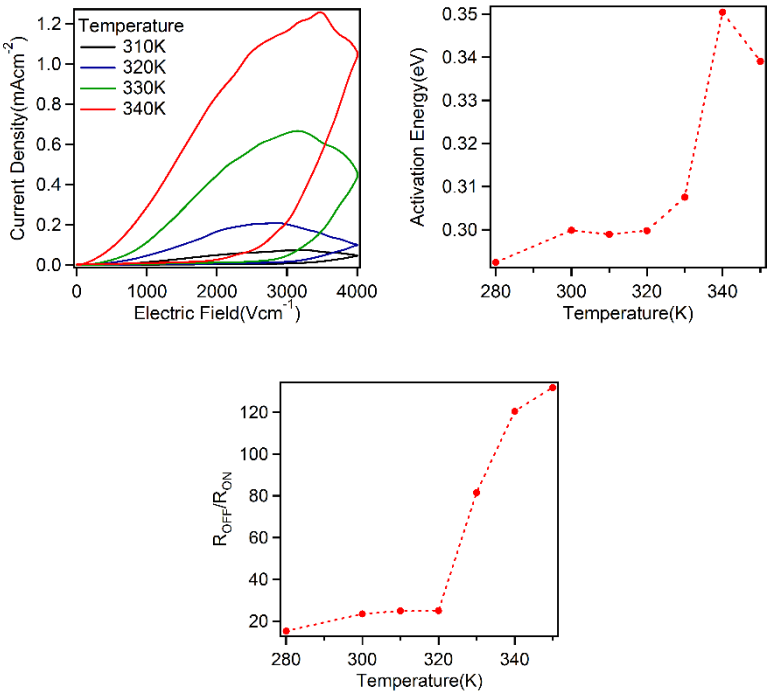

Figure 3-15 -(a) Temperature dependence of a device (b) Summary of activation energy calculated with temperature (c)Summary of R_{off}/R_{on} ratio with temperature.

To understand the activation energy effect of the film, a temperature study was conducted. Fig 3-15 shows the results from room temperature to higher temperature.

Once the temperature increased we could observe the improvement of conductivity at higher external biases. Improving the conductivity at higher biases resulted in better quality memristor.

To understand the contact barrier effect of the devices plot has been made with the natural log of the current values versus the 1/kT values for two states we defined.

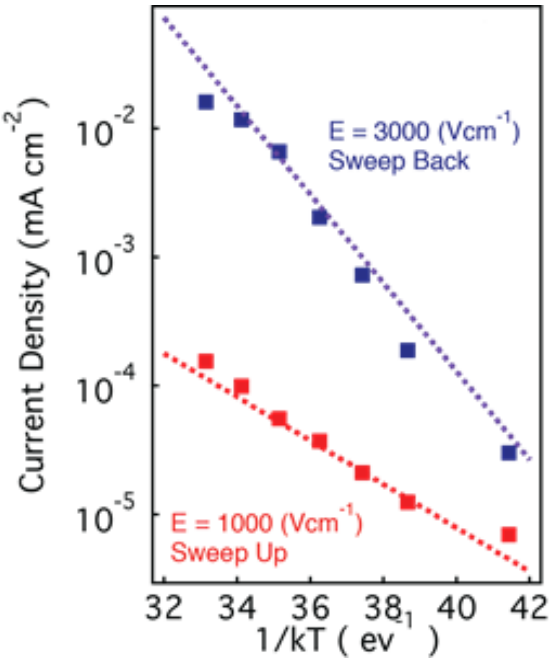

Figure 3-16 -Current density dependence with the calculated (1/kT) values

As shown in Fig 3-16 potential barrier was calculated based on the 3.1 thermal activated equation.

$$I = I_0 e^{-\left(\phi/kT\right)} \qquad (3.1)$$

and for the ON state as OFF states and came up with ON state(0.79eV) it was higher compared to the OFF state(0.39eV). This confirmed the increase is from bulk and not resulted from contact barrier. Combining the effect of the temperature and built in potential we came up with a hypothesis to describe the effect. Due to inbuilt potential

initial current flow occurs and with applied bias ion motion happened and due to the ion motion, it has been known to create carriers[71] and they helps to increase the current generated and when applied biased revered ion motion creates a built-in field with oppose the current flow and it halts the current making the device in OFF state as in Fig 3-17.

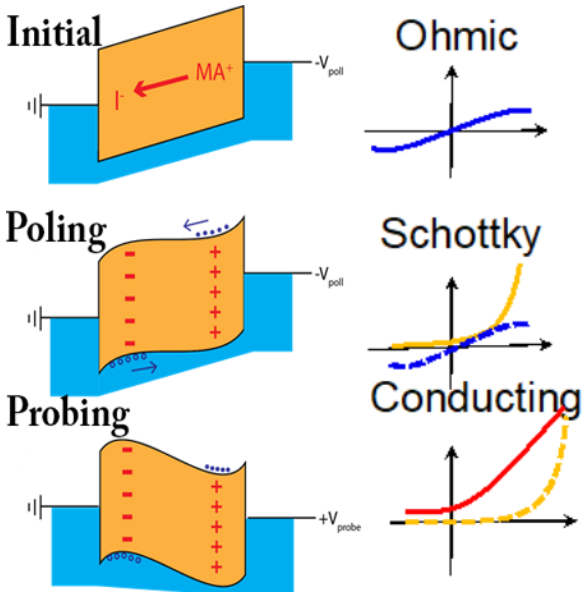

Figure 3-17 -Proposed model for the memristive behavior of hybrid perovskite.

3.2.4 Charge holding ability of the memristor

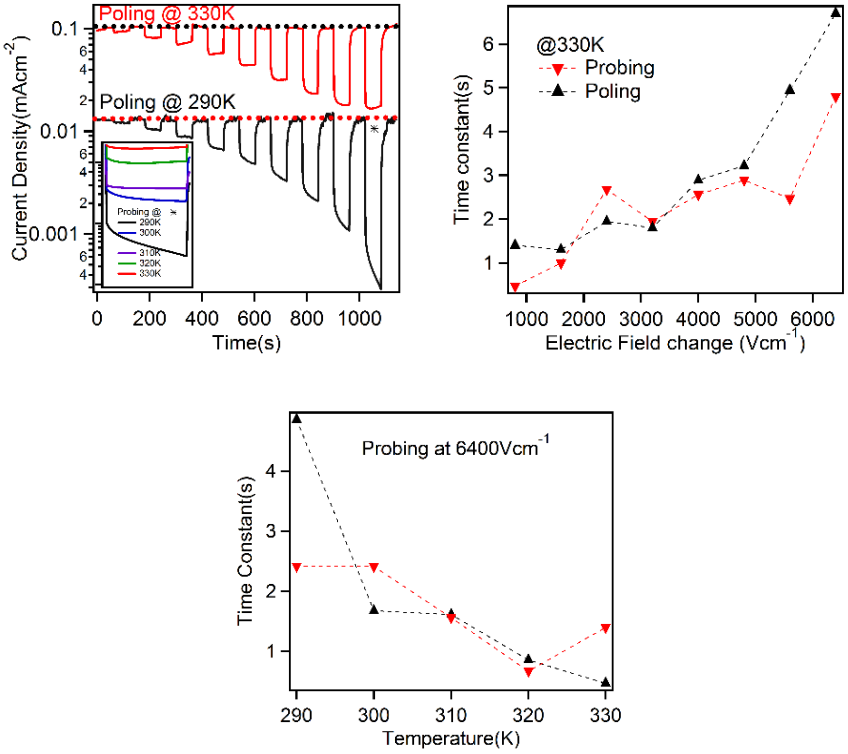

Figure 3-18-(a) Repeatability of poling and probing (b) Summary of time constants for poling and probing. (c)Summary of poling with temperature.

After confirming the possibility of using the film in memristors, a set of experiments was conducted to confirm the ability of holding the charge at a given level. Two states were defined below. A poling state, where the higher bias is applied, and the film is in the conducting state, and the other is the probing state where bias is lower than the poling state. After achieving the poling state different probing states were tested. For each probing state, time constant was calculated by fitting simple exponential fit. As is shown in the fig3-18 the time it can hold the charge also improved. Also, a set of experiments was conducted by changing the surface temperature. As is shown in fig3-18 the tendency of holding the charge gets reduced with the surface temperature. Since it has been proved

that the crystal phase of the lattice sees a change from orthorhombic to cubic at higher temperature, we could suggest that the memory effect we were able to observe tends to get higher when symmetry reduces. That means any distortion made by poling will restore slowly compared to less symmetric devices.

3.2.5 Improving the properties of memristor device

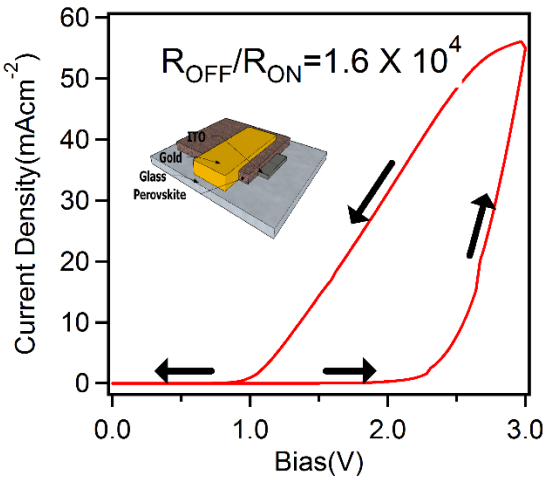

Figure 3-19-Cyclic J Vs V curve for sandwiched device.

Some techniques to improve the quality of the memristor were tested. One is making the sandwiched device structure. Some attempts were made using Au-Au contacts, but short circuiting was significant in all the devices fabricated. Then a few devices were fabricated using the patterned ITO substrate as Fig 3-19. Since adhesion of Perovskite layer on ITO is better compared to glass the device fabrication was a much easier process.100nm of Au layer was deposited on the hybrid perovskite layer for the other contact. Since almost similar kind of work functions were reported[72] for Au and ITO we did expect a similar kind of band structure for this device. Since the thickness of hybrid perovskite layer is around 400nm, we expected it to have lower bias to get the

same effective field as before. Observations did prove the same result. Where the voltage to observe the conducting state reduced significantly, the maximum R_{off}/R_{on} ratio was achieved as shown in the figure.

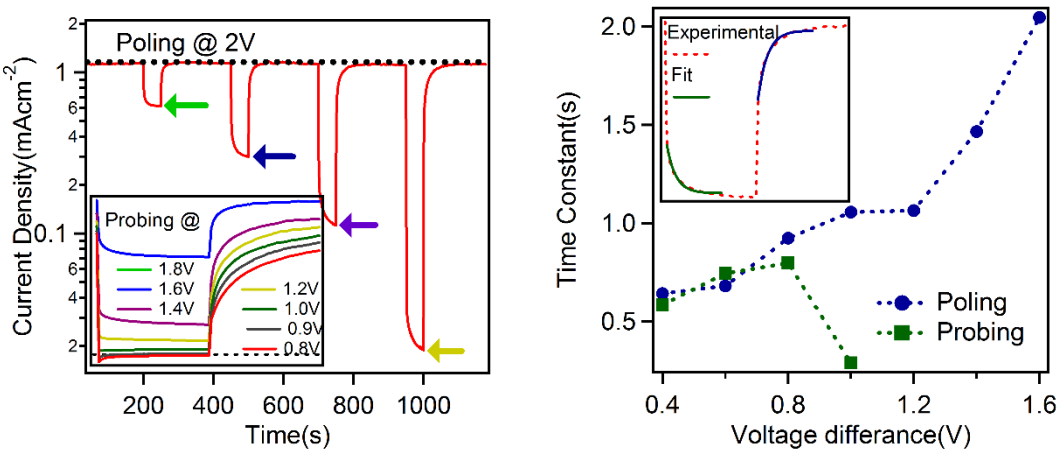

Figure 3-20-(a) Probing from 2V in sandwiched structure (b) Time constant change calculated.

Typical memory ability was tested using poling and probing steps as before. From initial cyclic IV measurements, poling voltage was figured out. This voltage was applied for a constant time and then suddenly moved to the probing voltage and the current value change with time was observed as Fig 3-20. Then similarly an exponential curve was fitted until it reached the current saturation point. As the graph shows the time constant directly relates to the charge holding ability. This increases with larger voltage difference between poling and probing states of the device.

3.2.6 Improvements possible

To understand the origin of the effective polarity that contributes to the memristive behavior we conducted a few experiments. This was done by altering the source materials that could directly affect the final observation based on each individual molecular polarity or size in the crystal lattice cell.

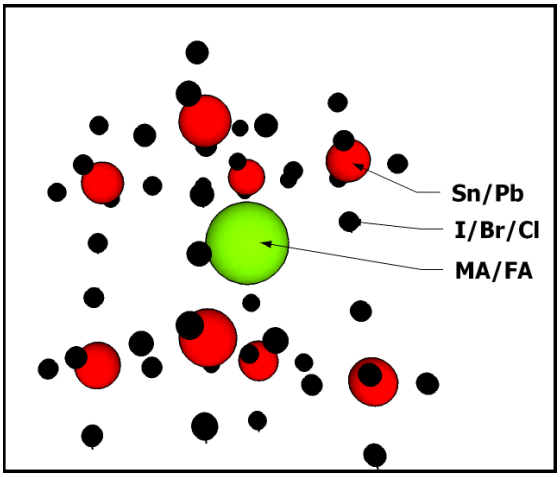

Figure 3-21-Cystal orientation of mixed cation devices.

As is shown in the Fig 3-21 there are a few possibilities that we could change in theory to see the effect. Anions as halides cations as Sn^{2+} or Pb^{2+} and the organic part which is MA^{+} or FA^{+} could alternate so we could observe the effect of each ion.

3.2.7 Mix cation in memristor

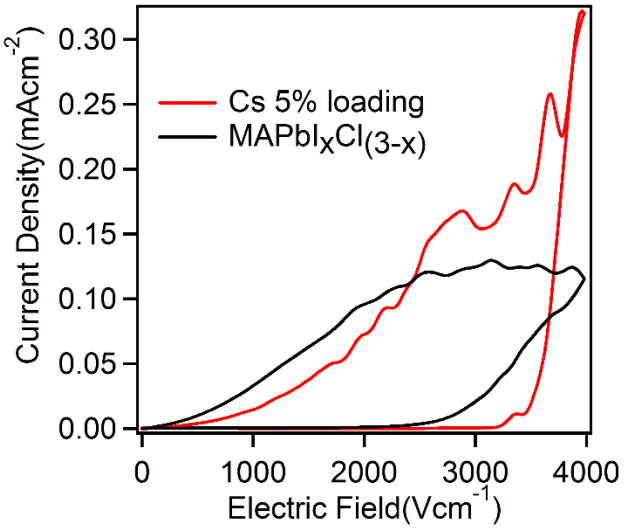

Figure 3-22-Cyclic J_{sd} Vs E_{sd} curve for sandwiched mixed cation device.

By the inclusion of Cs in the structure it has been found that improvement in the current density and ratio between the resistances at higher and lower conducting states could be observable as Fig 3-22. Another interesting observation was the Turning ON field. By the inclusion it has been clearly observed that turn on field value also shifted towards the higher side. It means the field needs to get the deformation of the lattice which becomes larger with the inclusion of Cs.

3.3 Three probe results (FETs)

To understand the basic characteristics of the film initial measurements were conducted on the films with two contacts on top and other below the insulating later using doped silicon layer. Only initial scans and steps were conducted during the stay at LANL was presented here. Currently ongoing experiments are being completed by N D Canicoba et. al. at LANL

As Fig 3-23 showing, top surface the film morphology can observe single or multiple grains using the hot casted technique. As For three terminal devices it is necessary to understand how the grain boundary continued to the surface.

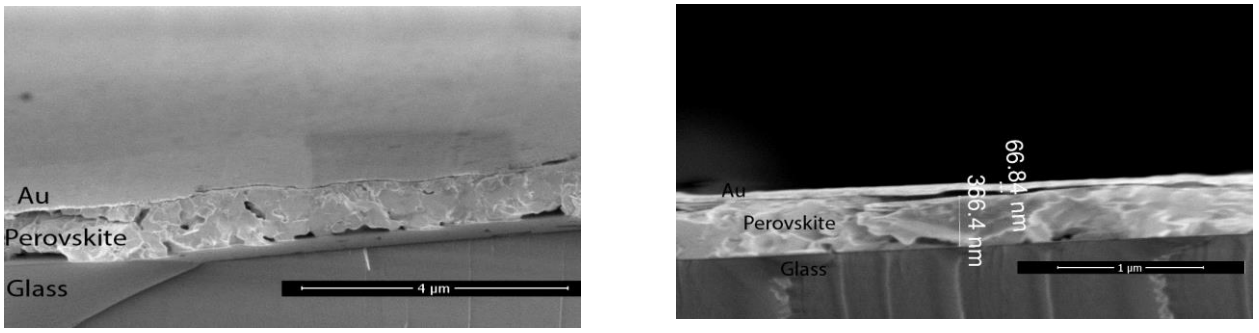

Figure 3-23- Cross sectional SEM images of perovskite device on glass.

The above figures show cross sectional images from a scanning electron microscope (SEM) in a top contact device. In some instances, it revealed that the grain boundary observed from the top doesn't necessarily continue through to the surface of the substrate.

3.3.1 Electrical measurements

A Field Effect Transistor (FET) can be used to understand some basic properties of a semiconducting material which could be used in electronic devices. In organic or hybrid

semiconductor devices, two types of device architectures were discussed. One is the top contact device, where a layer of the relevant material was deposited on top of the insulating layer and metal contacts were fabricated on top of the film. For the bottom contact device structure, a layer of metal contacts was fabricated on the insulating layer and then the relevant thin film was deposited. Various material properties such as mobility and average dopant type[73] of the relevant film could be approximated by conducting I-V scans on these two types of device structures.

A hybrid perovskite film with the thickness of 400nm was fabricated using the hot cast technique which was developed by Wanyi et.al at LANL[64] . To understand and compare the above-mentioned properties of conventional and hot cast films, a set of measurements was conducted. Theorists had predicted the superiority of the properties of hot cast films over those of the conventional type. This led to the recognition of the importance of examining the above-mentioned characteristics through FETs. This would also help to understand whatever defects there are and find ways and means of reducing them and by doing that we can improve our film quality in the field of hybrid perovskite. Electrical measurements were conducted on the samples in both dark and light conditions.

3.3.1.1 In dark

Hot cast film was deposited on 300nm SiO_2 layer after treating the layer with the following standard methods of surface cleaning. First the substrates were cleaned with acetone and isopropyl alcohol (IPA) for 15 mins each, followed by deionized (DI) water treatment. Then substrates were annealed on a hotplate with a surface temperature of $120^{O}C$ for another 15mins. Just before transferring to the glove box, substrate surfaces

were treated with oxygen plasma for 4mins to make a better adhesive surface. Extra caution was taken to avoid the solution seeping over the edges which could result in creating a current leakage path from the film to the gate. Source-Drain voltage was set up to a constant value between -10V to 10V range and the Gate voltage was swept from -40V to 40V. Sweep was done repeatedly until currents showed stable values (normally after 3rd scan the currents were stable). In dark conditions current values were low in the relevant voltage region. Due to this reason we had to use a current amplifier to measure the resultant current.

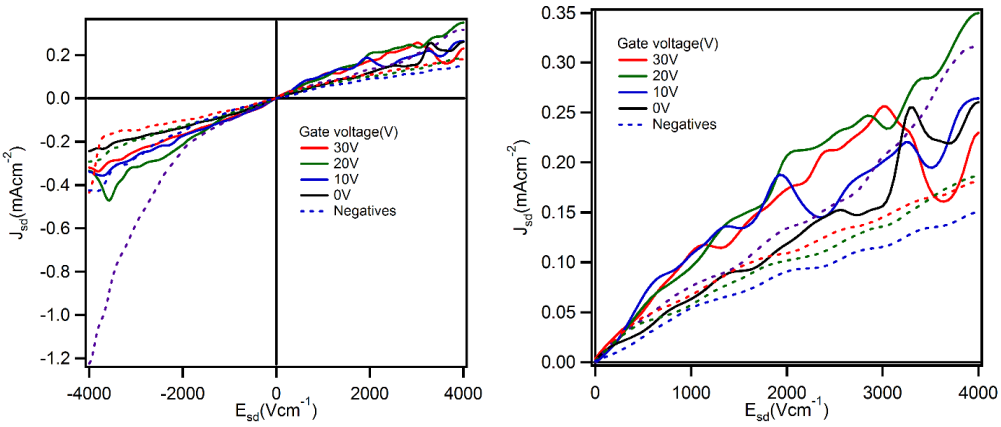

Figure 3-24- (a) J_{sd} Vs E_{sd} scan under dark with different gate voltages. (b) zoomed view

With the application of different gate voltages same measurement was conducted by sweeping the source to drain voltage (or field) as shown in Fig 3-24.

To understand the effect of gate, a single source-drain voltage was selected (15V in following figure) and the current values versus the gate voltage were plotted as Fig 3-25.

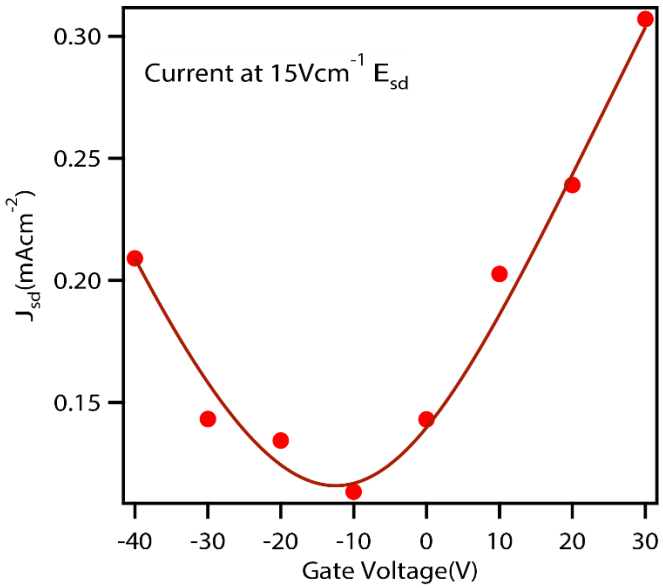

Figure 3-25- Extracted data of J_{sd} Vs E_g from J_{sd} Vs E_{sd} curve.

Since the current level was comparatively small, an interdigitated finger pattern had to be used to fabricate the film to increase the area of interest which would resulted in higher current values. This direction of the measurement contributed to the expansion of application of hybrid perovskite film as gas sensors which we will discuss in next chapter.

3.3.1.2 Increased device area

Fig 3-26 shows the optical image of the finger patterned device and source drain current curves with various gate voltages.

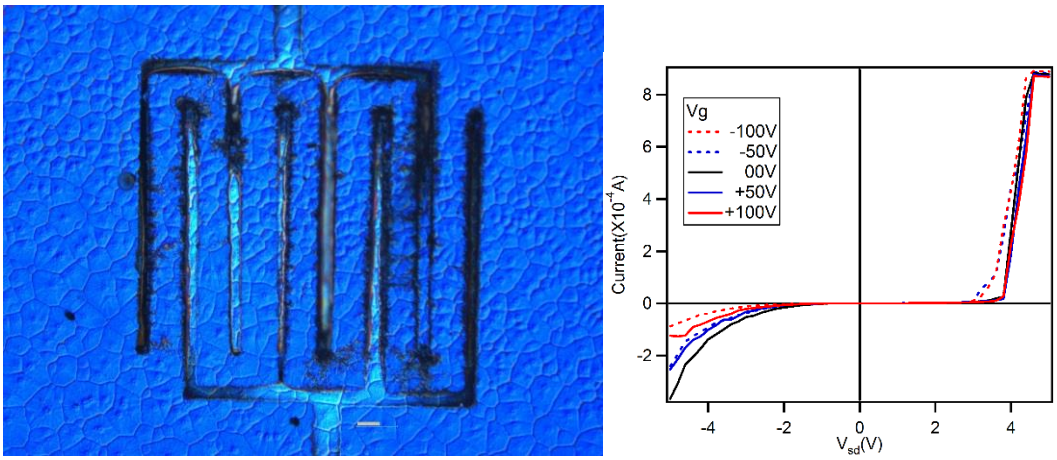

Figure 3-26-(a) Optical image of interdigitated device. (b) I_{sd} Vs V_{sd} scan under dark.

As expected the increase in the area resulted in larger dark currents. Finally, it helped us to observe the magnified effect of the gate. Also, as shown in the above curves we were able to use higher gate voltage dependency as Fig 3-27 by using such a device pattern.

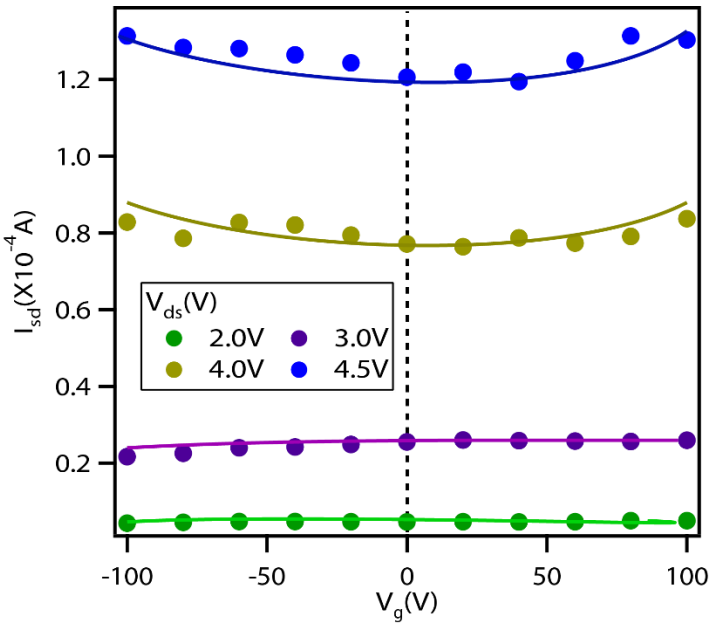

Figure 3-27- Extracted data from I_{sd} Vs V_{sd} curves under dark.

3.3.1.3 In light

Since hybrid perovskite film was more often used as light sensing material, similar kinds of measurements were conducted by exposing the device to low intense light (<1 Sun).

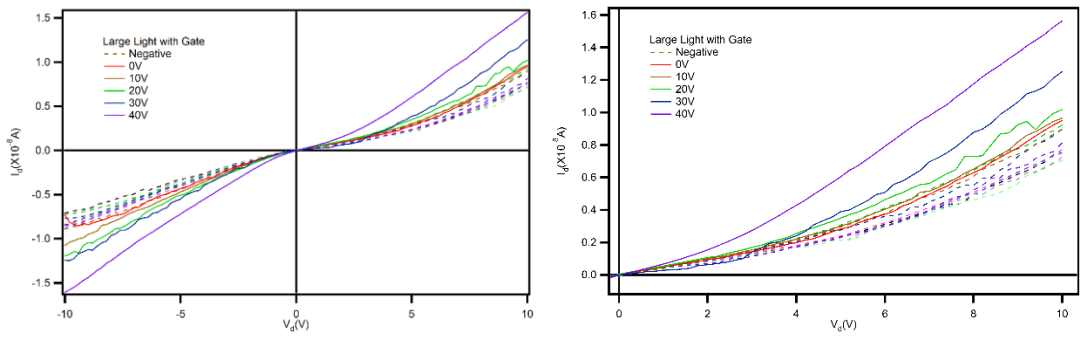

Figure 3-28- (a)I_{ds} Vs V_{ds} scan under light condition. (b) zoomed view

Similarly, by extracting the data from single source-drain voltage (15V) Fig 3-28 was constructed.

These two initial experiments suggested that the large grain films showed more n-type (Fig 3-29) behavior under light compared to bi-polar behavior under dark conditions.

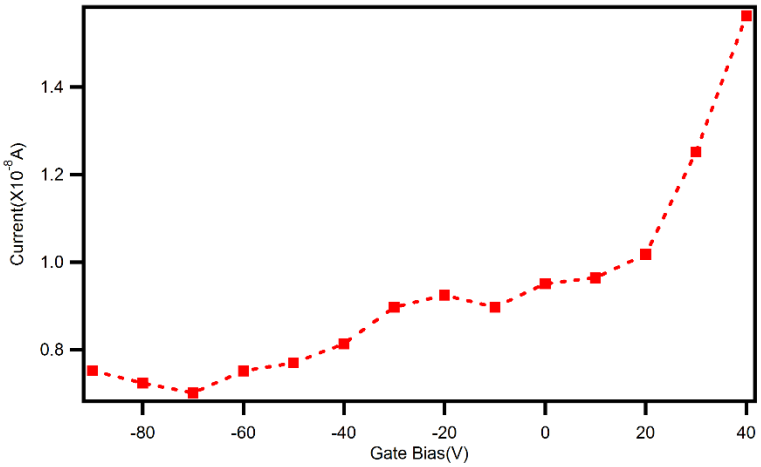

Figure 3-29- Ids Vs Vg scan under light condition.

3.3.1.4 Wave length dependence

To understand the wave lengths of light associated with the n-type behavior, a different set of experiments was conducted with exposure to different wavelengths. As before a low powered light with different wavelengths was focused on to the 50micron channel.

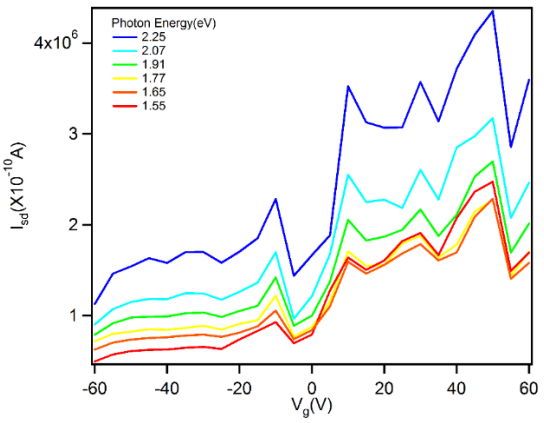

Figure 3-30- I_{ds} Vs V_g scan under different wavelengths of light.

For lower wavelengths higher n-type behavior was observed, where overall current showed an increase as expected when going beyond the band edge as Fig 3-30.

4. PHOTO CONDUCTIVITY RESULTS

4.1 Gas sensor result

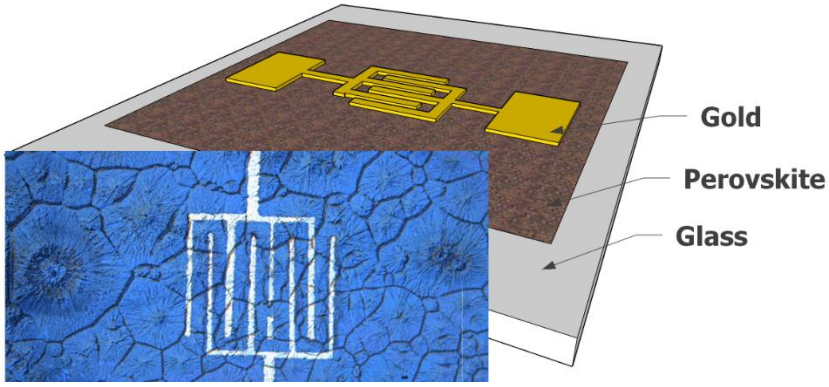

Figure 4-01- Optical view and device structure of the interdigitated finger pattern.

Improving the signal level was achieved by increasing the device area by introducing a finger patterned mask instead of the small square pads as Fig 4-01. Same electron beam deposition technique was used in contact fabrication process. To avoid any air or moisture contamination a Janis Sr-300 cryostat was used to load the sample and a turbo molecular pump was used to pump down chamber pressure to 10^{-7}torr.

4.2 Exposure to different gases

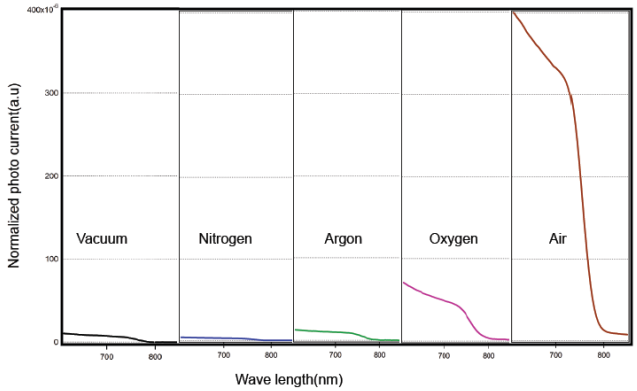

Figure 4-02- IPCE of AC photo current with different environments. (a)Vacuum (b)Nitrogen (c)Argon (d)Oxygen (e)Air

Perovskite oxides have been studied for many years and have been proposed for a variety of gas sensing applications [74, 75]. Recent work has shown that this can be exploited to create hybrid perovskite sensors to detect humidity[76], acetone, nitrogen dioxide[77] and oxygen[78]. There has also been interest in understanding how hybrid perovskites behave under different gas environments, both as a means to improve device efficiency and to limit material degradation. To understand the effect of gas exposure the sample was exposed to continuous flow of different gases for 100minutes.

Initial scans showed different magnitudes of current under exposure to different gas environments. Similar to observations for photoluminescence[79], the photocurrent is found to increase with exposure to humid air and oxygen .Time dependent behavior was also different from gas to gas. Extended time exposure of gases (after 100mins of scanning) affect the current levels for each scan as Fig 4-02. This could be directly associated with the films chemical behavior in which temporary or permanent damages

could occur in the film during the exposure. In another instance a secondary constant solar light was made to shine over the devices under the above mentioned different environments, to detect the amplification effect and reduce the trap effects if there were any on devices as Fig 4-03.

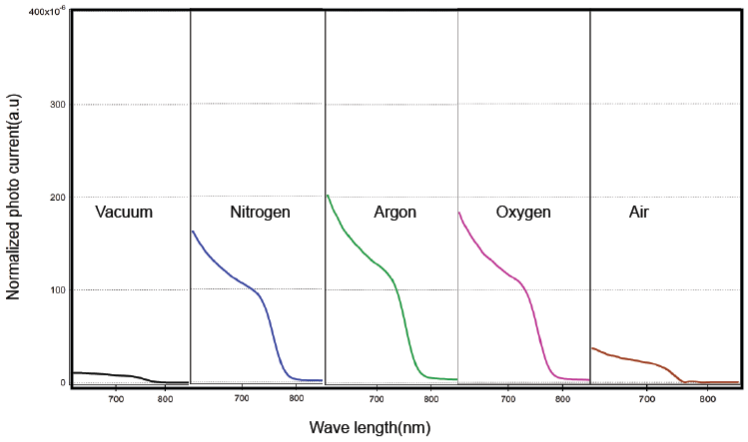

Figure 4-03- IPCE of AC photo current with different environments with extra Sun after 100mins (a)Vacuum (b)Nitrogen (c)Argon (d)Oxygen (e)Air

For different air exposures interesting observations were made, where in some instances initial increase was reduced by introducing the extra light over the spectrometer light. Shift in the band edge was also observed where an extra feature appeared just below the band edge.

4.2 Extended exposure of air & light

To observe the effective changes in the device during the extra amplification process, a measurement was conducted for over 5 hours as Fig 4-04.

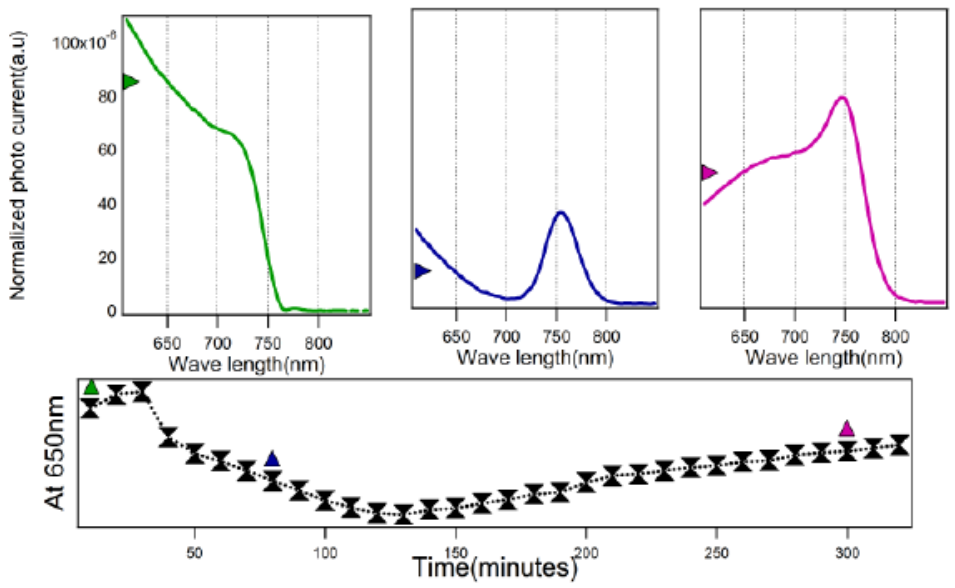

Figure 4-04- Time dependence of IPCE of AC photo current under air. (a)Initial (b)With extra light (c)After recovery

Clear indication of appearance of sub state could be observed during the process of exposing to air and sun together. We could also observe the recovery of band edge with the inclusion of new state which could be hidden inside the active region for a pristine device. The graph below represents the amplitude change of the device at 650nm with time.

Recovery process was also observed after removing the extra sun.

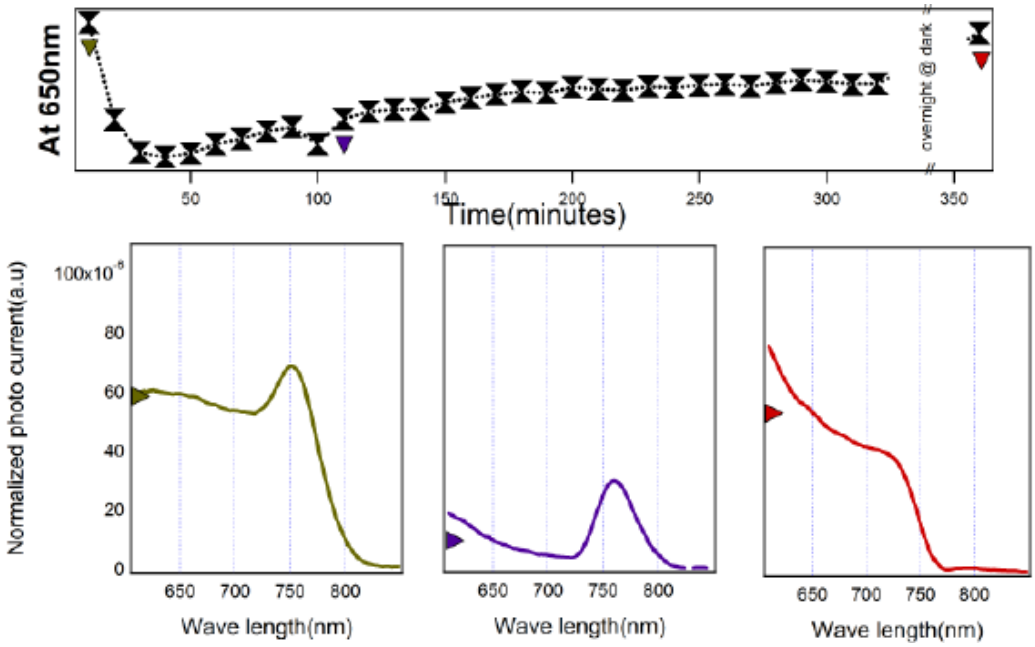

Figure 4-05- Recovery of AC photo current under air with time. (a) Initial (b) with extra light (c) Recover overnight.

Here too the recovery process of returning to the state with shifted band edge was observed as Fig 4-05. Again, the process included the intermediate state that shows a single peak at 750nm.

4.3 Analysis of gas exposure

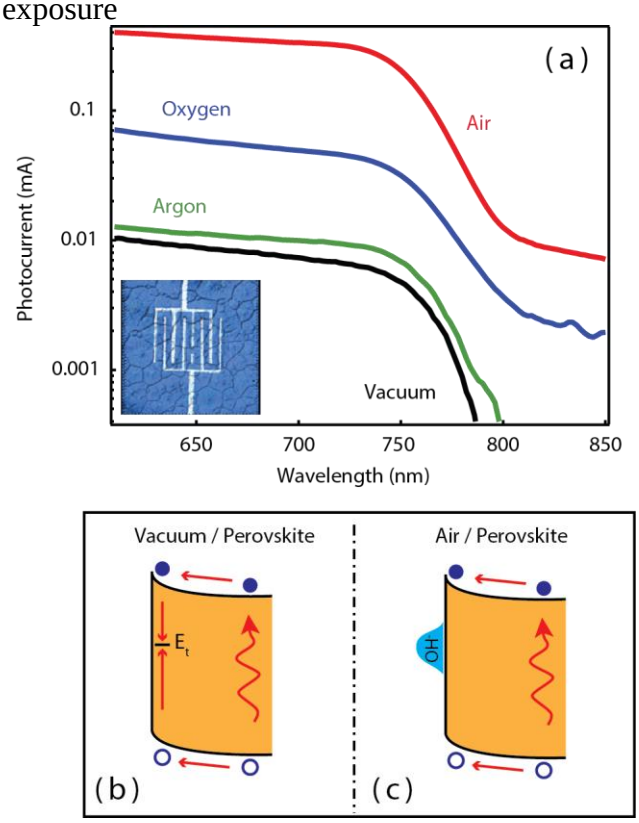

figure 4-09. (a)Photo current response under various environments. Inset shows the device configuration. (b)Possible band diagrams under Vacuum (c) Under Air.

Since it has been known that exposure to air could resulted in fast degradation of sample chemically, a set of experiments were conducted on a sample degraded by exposure to 5 suns under vacuum.

Figure 4-09 shows the AC photocurrent as a function of wavelength with monochromatic chopped light incidence from the top surface. When the electron-hole pairs are photo excited, the photocurrent is generated by collecting the electron travelling towards the bottom electrodes. The sample is first measured in vacuum. The photocurrent turns on as the wavelength reaches the band-edge of the perovskite (at approximately 780 nm[80, 81]) where the photon energy is high enough to excite electron-hole pairs across

the valence / conduction band gap (Fig. 4-09 b). To be detected by the contacts, the electron-hole pairs must spatially separate before recombination occurs. Surface trap states[82] provide recombination pathways and greatly reduce the detected photocurrent. Recent experiments that measure the photoluminescence of hybrid perovskite films have shown that recombination centers can be neutralized by exposing the sample to air or to oxygen[83]. The improvement is thought to be due to the reaction of recombination centers with O_2 or OH^- groups.

To probe the surface recombination using our photocurrent experiments, the sample was exposed to a variety of different gases, and the effect on the photocurrent observed. As shown in Fig. 4-09(a), exposing the sample to oxygen causes a significant increase in the photocurrent, while exposure to air causes an even larger increase. Exposure to Argon (an inert gas) however, results in very little change to the photocurrent. This suggests that the photocurrent increase is due to a chemical absorption of the background gas[84] with recombination centers on the sample surface (see Fig. 4-09(c)). Bonding of the gas molecules neutralizes surface trap states, reducing electron-hole recombination and increasing the photocurrent.

The removal of recombination pathways by exposure to oxygen or air is temporarily beneficial to solar cell efficiency, since reduced recombination leads to a higher percentage of charge being collected by the contacts. However, over time, perovskite solar cells degrade as the air reacts with the perovskite. Degradation due to O_2 presence has been commonly described by generation of super oxide(O_2^-) which could react with

MA components to produce PbI_2, I_2 and $MeNH_2$ [85]. The degradation accelerates in the presence of solar level illumination since the light provides energy to drive chemical reactions[86]. This same effect can be seen in the surface photocurrent measurements. The top row of panels in Figure 4-10 shows a series of photocurrent measurements done to test the influence of air and solar illumination on a pristine perovskite film. The top left panel shows the photocurrent as measured in vacuum. The signal is plotted on a log scale, and the photocurrent is normalized to a value of 1 at a wavelength of 730 nm in vacuum. The next panel to the right shows the photocurrent after the sample is exposed to air. In agreement with the results of Fig. 4-09, the photocurrent increases dramatically with air exposure, in this case by more than a factor of 10. In the next panel to the right, the sample is exposed to one sun illumination from a solar simulator. (The AC photocurrent is measured using the small perturbation of a mW chopped light source on top of the continuous light from the solar simulator). After 5 minutes exposure, the photocurrent has increased by a small amount. However, continued illumination results in a sharp degradation in the photocurrent over time. After 100 minutes exposure, the photocurrent decreases by more than a factor of 100. In addition, a new peak appears in the photocurrent spectrum (at approximately 780 nm). This peak is most likely due to the generation of a new chemical species[87] as the perovskite reacts with the air. After the solar illumination is removed for one hour (shown in the far-right top panel), the degradation of the photocurrent signal remains—it is still extremely low, and the new feature at 780 nm is still observed. This suggests that the film is permanently altered by the light-driven reaction between the air and the perovskite.

4.4 Photo conductivity of degraded sample

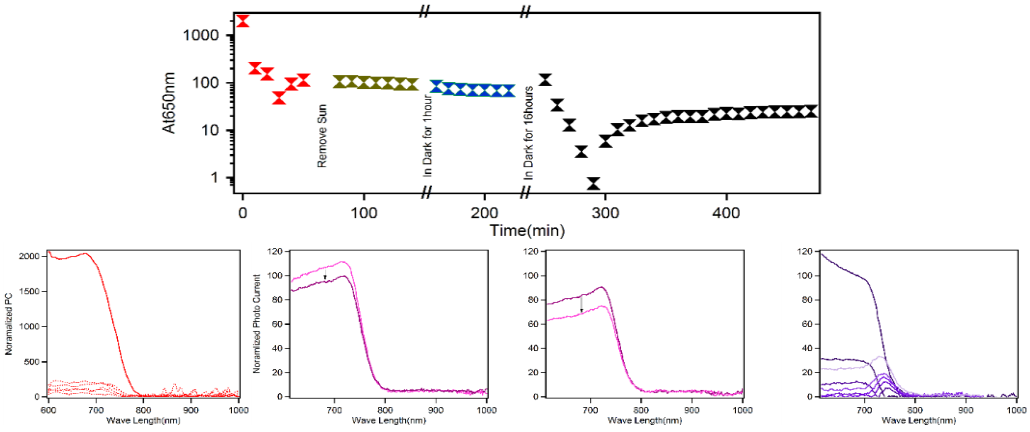

Figure 4-06-Recovery of AC photocurrent after initial light exposure with variation of time. Top graph shows the variation of 650nm value.

Sudden degradation was observed when exposed to extra sun. When zoomed in, as Fig 4-06 shows the effect was still intact while keeping the sample in the dark for 1hour.When sample was kept in dark through overnight for 16hours sample showed some recovery yet decreased signal was observed as extra light is shined. Then even without exposure to the extra sun the device showed the cyclic process which is similar in what we observed before.

These preliminary results suggested to us that these hot cast perovskite films could be used as a gas sensing material.

4.5 Exposure to inert environment

Different gas exposures on the sample resulted in contamination of the film (chem-adsorption) which showed reduction in photoconductivity. This degradation lead to the appearance of the extra feature in the spectra. Non-reactive gases recoverability prompted us to look into the possibility of inert gas sensing ability of hybrid perovskite film.

To understand the effect under different inert gas environments, a pristine sample was exposed only to different inert gases. Similar experiments were conducted to observe the effect while purging the cryostat with He and Ar as Fig 4-07.

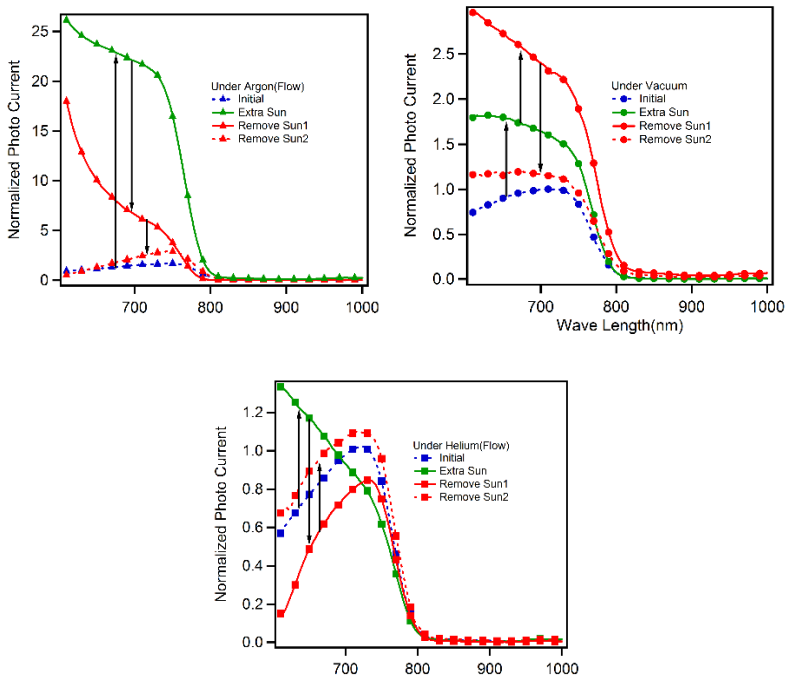

Figure 4-07- Comparison of IPCE of AC photo current with different environments. (a)Argon (b)Vacuum (c)He

Under vacuum or with He gas flow, not much improvement could be observed whereas under Argon gas flow with extra sun, a significant improvement was visible throughout

the absorbed energy regime. Extra feature which was observed in initial experiments under air was not observed under these conditions.

Another set of experiments were also conducted by just purging with inert gases including those of larger molecule sizes as Fig 4-08.

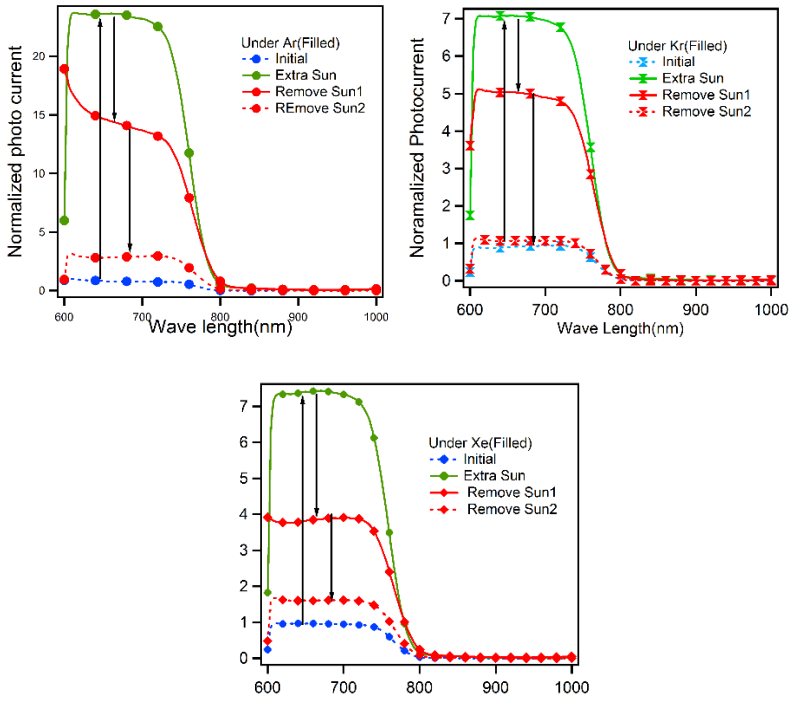

Figure 4-08- Comparison of IPCE of AC photo current with different environments. (a)Argon (b)Krypton (c)Xenon

Similar kind of enhancement was observed when purged with Argon gas. For other two gases such significant enhancement was not observed as for Argon. Yet the passivation of surfaces was observed for the other two gases with larger particle sizes.

4.6 Analysis of inert gas exposure

Chemical surface absorption does not occur with the inert gas, and therefore little change is observed. Similar insensitivity was observed when the sample was exposed to the other noble gases (Helium, Neon, Xenon, and Krypton).

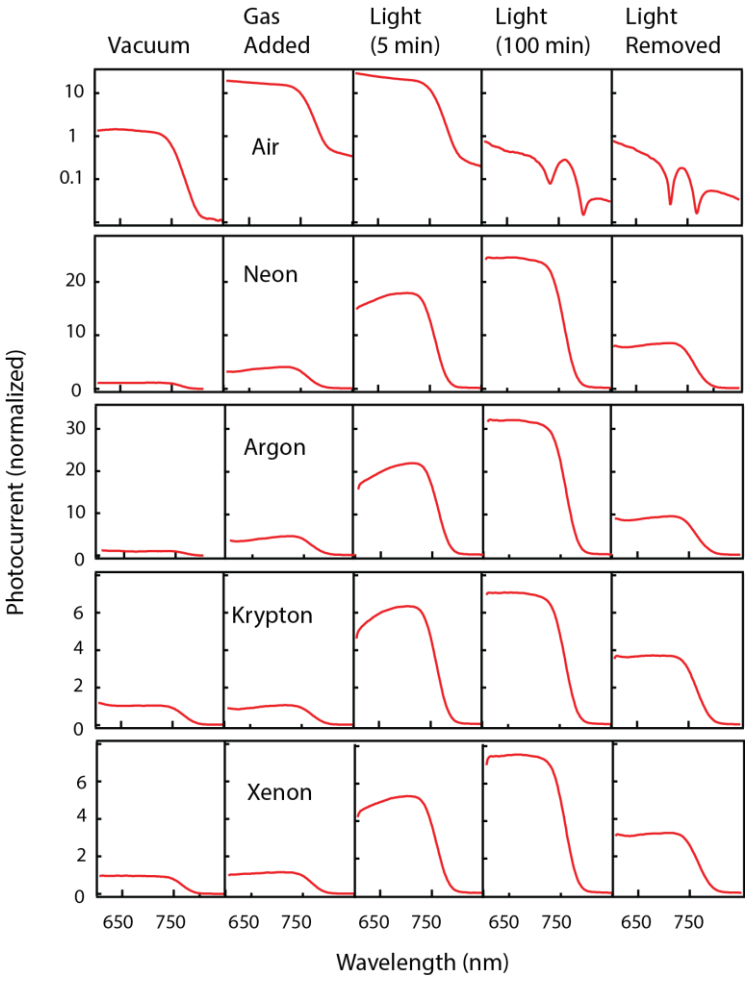

Figure 4-10. Normalized photo current curves under systematic exposure of various environments.

Of interest would be a method to neutralize the recombination pathways and increase solar cell efficiency (as observed with the air exposure) without the accompanying chemical reactions that degrade the perovskite. One possibility is demonstrated in the remaining panels of Fig. 4-10. Here, the influence of solar radiation on the photocurrent spectrum is measured with the sample exposed to different inert noble gases. Each row

shows the spectra in a different noble gas, increasing in atomic number from top to bottom through neon, argon, krypton, and xenon. The photocurrents are plotted on a linear scale. The first column shows the spectrum when the sample is kept in vacuum. There is a small sample-to-sample variation, so that the results are normalized by setting the photocurrent to a value of 1 at a wavelength of 730 nm in vacuum. The second column shows the photocurrent with the addition of the noble gas. In contrast to the results in air, the photocurrent increases by only a small amount with the addition of the noble gas. As described above, the inert gases do not react with the perovskite surface so have little impact on the recombination centers[88].

The third and fourth columns show the photocurrent under exposure to one sun illumination. The photocurrent increases as a function of illumination time for each of the noble gases, until eventually saturating; there is a large increase in the photocurrent after 5 minutes illumination, and an even larger increase after 100 minutes illumination. The time for saturation varies from sample-to-sample, but after 100 minutes exposure (column 4) the increase has saturated for all four gases. The total change also varies depending on the inert gas, with argon showing the largest change, increasing by a factor of 30 compared to the signal in vacuum. The fifth column shows the photocurrent after the solar illumination has been removed for 30 minutes. The photocurrent magnitude slowly returns to its original value, with no permanent changes to the photocurrent spectrum. We note that measurements done with the sample in vacuum show no increase upon illumination, so both the gas and the light are needed to produce the observed change. The increase is observed for all inert gases tested, except for helium, where the change is indistinguishable from having the sample in vacuum.

The combination of inert gas plus solar illumination appears to be effective at neutralizing surface recombination centers without damaging the perovskite film. In fact, it is known from the literature that solar cell efficiency can be improved temporarily by exposure to high intensity light[89]. This is often used as a method to boost efficiencies prior to characterizing solar cells for reporting purposes. Explanations for this effect are that the light soaking neutralizes the surface traps[90], or increases the open circuit voltage due to charge accumulation at interfaces[91]. High quality perovskite solar cells are typically fabricated in an argon environment[92] and then encapsulated, so it is possible that the effect we observe here is due to the same mechanism.

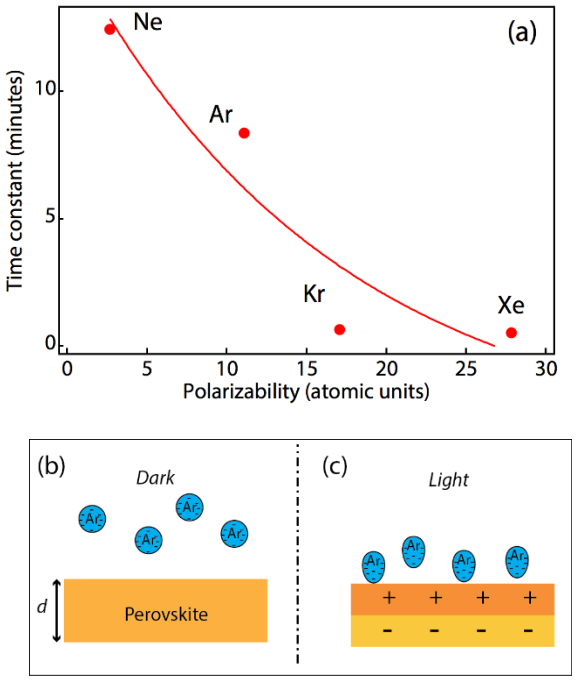

Figure 4-11 (a)Time constants values of the current saturation with extra light and gas. (b) Possible mechanism improves surface conductivity under dark and (c) extra light illumination.

A possible mechanism for the photoinduced enhancement in the photocurrent is shown in Fig. 4-11(b) and 4-11(c). It is known that solar illumination modifies the charging state of a semiconductor surface[93], and this can lead to either enhanced or decreased gas adsorption. In addition to depopulating/populating surface states, band bending at the surface leads to charge separation of photoexcited electron-hole pairs so that solar illumination produces a dipole surface electric field. An inert gas should not readily react with the perovskite surface. however, the surface field can generate a local dipole on inert gas molecules[94]. This will attract the inert gas molecules and lead to phys-adsorption of the gas molecules on the perovskite. Once adsorbed, the inert molecules remain attached with an activation energy that increases with the molecular weight and polarizability of the exposed molecule, as has been determined for noble gas adsorption on a variety of semiconductor surfaces[95].

The photocurrent measurements show that the phys-adsorbed noble gases (while not as effective as the chem-adsorbed OH^-) are able to neutralize the surface recombination centers. The attractive force between the inert gas molecules and the semiconductor surfaces is proportional to the surface electric field multiplied by the polarizability of the gas molecules. The ability of any molecule to neutralize the recombination centers must be dependent on additional factors besides just the electrostatic force between the molecule and the surface. Additional evidence for the model, however, is seen in the rate at which the photocurrent increases with solar illumination. This is plotted in Fig. 4-11(a) as a function of the polarizability of the four noble gases tested in Fig. 4-10. The rate of photo-induced change clearly increases with increasing gas polarizability[96]. This shows that

while the amount of surface trap neutralization depends on the particular molecule, the rate at which the molecules arrive at the surface increases with increasing polarizability, as would be expected by surface field induced dipoles. Finally, we note that no sun induced increase in the photocurrent is observed when helium is used as an inert gas. This is most likely because the binding energy of the helium for phys-adsorption on the perovskite is below the thermal energy. The binding energy for helium on other semiconductor surfaces is reported to be less than 26 meV.

4.7 QCM results on inert gas exposure

In order to understand the adsorption effect on the hybrid perovskite with light and gas exposure we are conducting a set of experiments using the Quartz Crystal Microbalance (QCM). Typical 400nm thin layer of hybrid perovskite was deposited on a 10MHz quartz crystal. Then it was mounted inside a high vacuum chamber, where we could shine light on the perovskite film by using an external light source. Resonance frequency was monitored during the gas purging from a needle valve, while the pressure of the chamber rises up to 1.5e-1torr from 2.4e-5torr (overnight monitoring of the frequency was done to minimize the drift effect of the measurement). Once it reaches 1.5e-1torr pressure systematic light and dark exposure was conducted on the sample as Fig 4-12.

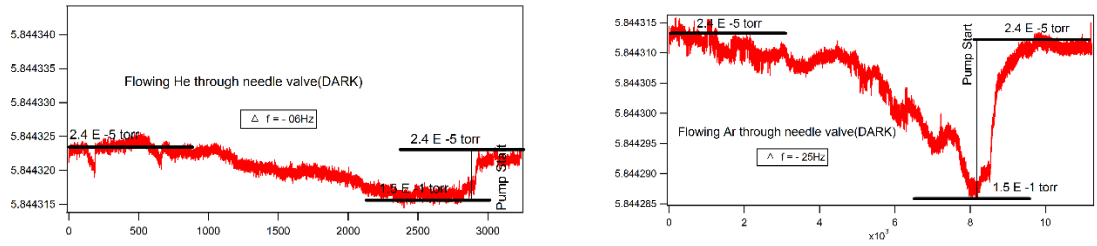

Figure 4-12Resonance frequency measurement in MHz with (a)He (b) Ar environment in dark.

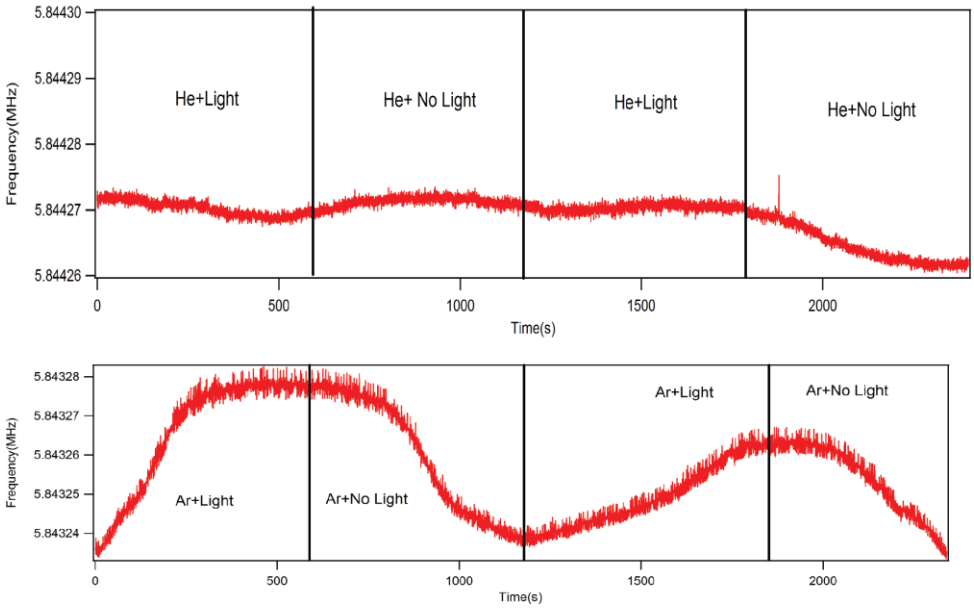

Figure 4-13 Resonance frequency with light and dark under (a)He (b) Ar with 1.5e-1torr pressure.

As decrease in the frequency during the initial gas exposure suggests a small mass increase in the crystal during the process. As a comparison Ar and He exposure also showed the same kind of behavior as a general trend as Fig 4-13. Magnitude wise Ar showed higher effective change. More experiments are needed to be done on this to get a clear idea of the relation of the mass change of the film and the conductivity change in the hybrid perovskites.

In conclusion, it is shown that the combination of an inert gas with one-sun illumination can passivate the surface recombination centers in a hybrid perovskite leading to a stable increase in the photocurrent. QCM data provides that it could be probable that exposure of light could expand the film where the gas interaction with expanded area could be resulted in enhancement in conductivity. This also could be an effective method to improve hybrid perovskite solar cell efficiency and could also function as a hybrid perovskite based inert gas sensor.

5. CONCLUSION

To comprehend and verify advantageous properties peculiar to hot cast hybrid perovskite and their possible applications was the focus of this study. A couple of unique and unrevealed applications fabricated from hybrid perovskite thin films have been presented. Main application mentioned here is a byproduct from the process of exploration of Field Effect Transistors using hot cast technique. Detailed analysis of each device structure is presented. Are they practicable? What are their advantages? What important steps have been taken to improve their particular properties? All these have been discussed. It is granted however that further improvements to these devices and FETs are possible.

Characteristics such as mobility, dopant type… etc. using FETs are the most important findings with regard to any semiconducting material. These characteristics will be useful in predicting and explaining the performances of these materials. Any defects predicted from this could be used to find ways and means to improve the performance of any device using a thin film. Up-to-date not many publications have addressed the subject of FETs using halide perovskite because of its instability in room temperatures . A few attempts have been made to explain the performance of FETs under low temperature. In our study we were successfull in fabricating high quality thin film that produces stable electrical measurement and to prove its ambipolar behavior under dark condition. Initial

scans also revealed n-type behavior under light conditions. More research work on this area is currently going on at LANL.

Application of hybrid perovskite film as a memory application is discussed in detail in this work. Successful attempts were made to fabricate lateral and sandwiched devices using hot casting technique. For the lateral, the best performance was observed from a device which was entirely inside a single grain boundary. We initially proved that the relevant memristors obey the basic fundamental requirements theorized by L.Chua.et al [55]. Explanation for such behavior matched the hypothesis of using the ionic movement of each individual atom in the crystal structure under the presence of the electric field applied. Explanations were mainly based on electrical and structural measurements carried out on the devices which displayed peculiar behavior. Such explanation for two terminal devices are unfamiliar territory for hybrid perovskite. Our explanation does not totally tally with the general explanation of permanent ionic movement which the community used in order to explain the behavior in solar cell structure. Our justification was based on rather localized ionic movement compared to whole in explaining this phenomenon. Also, we presented the results from preliminary attempts done on sandwiched structure that produced better performances compared to lateral. It was also proved that parameters such as the gate voltage and exposed light could alter the electrical performances of the semiconducting film. It is an advantage that these parameters could easily be implemented as controllers that could tune the performances of the device externally.

Application as an inert gas sensor is another area we explored for use of halide perovskite thin film in new devices. Evidence has been presented to prove that the film could be used as an inert gas sensor. Phys-adsorption effect was used to theorize the effect and explain the results. Also, it has been found that chem-adsorption of reactive gases showed non-reversible alteration to the films chemistry. Wide area of study is possible for gas sensor application since the adsorption effect totally depends on the temporary interaction with the surface and gas molecules hovering above. Considering the above-mentioned interaction, flow sensing could be the next best option to explore. Since lower wavelength light penetrates deeper in to the film, further improvement could be achieved by considering higher energy photon interaction with the film.

All device types we have discussed here have a common advantage, where they use the same architecture as in common photo voltaic devices such as solar cells and LED's. Such integration ability could be considered as an advantage over other device applications. A few possibilities of using hybrid perovskite as a semiconductor material (thin film) has been addressed here. We have proved that fabricating high-quality crystal is the initiating point of a vast range of applications. When the fabrication process becomes simpler and consistent, exploration of the sciences behind the devices would become more feasible. [97]

REFERENCES

1. Cavalcante, L.S., et al., *Synthesis, structural refinement and optical behavior of CaTiO3 powders: A comparative study of processing in different furnaces.* Chemical Engineering Journal, 2008. **143**(1): p. 299-307.
2. Chakhmouradian, A.R. and P.M. Woodward, *Celebrating 175 years of perovskite research: a tribute to Roger H. Mitchell.* Physics and Chemistry of Minerals, 2014. **41**(6): p. 387-391.
3. Rose, Valentin, Index entry in: Deutsche Biographie, https://www.deutsche-biographie.de/gnd117594520.html [10.11.2017].
4. https://en.mvd.ru/Ministry/history
5. Mitzi, D.B., et al., *Conducting tin halides with a layered organic-based perovskite structure.* Nature, 1994. **369**: p. 467.
6. Raveau, B., et al., *Crystal Chemistry of High-Tc Superconducting Copper Oxides*. Vol. 15. 2013: Springer Science & Business Media.
7. Li, C., et al., *Formability of ABX3 (X = F, Cl, Br, I) halide perovskites.* Acta Crystallographica Section B, 2008. **64**(6): p. 702-707.
8. Sato, T., et al., *Extending the applicability of the Goldschmidt tolerance factor to arbitrary ionic compounds.* Scientific Reports, 2016. **6**: p. 23592.
9. Shannon, R., *Revised effective ionic radii and systematic studies of interatomic distances in halides and chalcogenides.* Acta Crystallographica Section A, 1976. **32**(5): p. 751-767.
10. Gschneidner, K.A., L. Eyring, and M. Brian Maple, *Preface*, in *Handbook on the Physics and Chemistry of Rare Earths*. 2001, Elsevier. p. v-viii.
11. Bednorz, J.G. and K.A. Müller, *Perovskite-Type Oxides—the New Approach to High-Tc Superconductivity. Nobel Lecture.* Angewandte Chemie International Edition in English, 1988. **27**(5): p. 735-748.
12. Blasse, G., *Luminescence of inorganic solids: From isolated centres to concentrated systems.* Progress in Solid State Chemistry, 1988. **18**(2): p. 79-171.
13. Cherry, M.; Islam, M. S.; Catlow, C. R. A. J. Solid Sate Chem.1995,138, 125
14. Guan, J., et al., Trans*port properties of SrCe0.95Y0.05O3−δ and its application for hydrogen separation. Soli*d State Ionics, 1998. 110(3**):** p. 303-310.
15. Shima, D. and S.M. Haile, The i*nfluence of cation non-stoichiometry on the properties of undoped and gadolinia-doped barium cerate. Soli*d State Ionics, 1997. 97(1)**:** p. 443-455.
16. Weber, D., CH3NH*3PbX3, ein Pb(II)-System mit kubischer Perowskitstruktur / CH3NH3PbX3, a Pb(II)-System with Cubic Perovskite Structure. Vol*. 33. 1978.

17. Knop, O., et al., Alkyl*ammonium lead halides. Part 2. CH3NH3PbX3 (X = Cl, Br, I) perovskites: cuboctahedral halide cages with isotropic cation reorientation. Cana*dian Journal of Chemistry, 1990. 68(3)**:** p. 412-422.
18. Kojima, A., et al., Organ*ometal Halide Perovskites as Visible-Light Sensitizers for Photovoltaic Cells. Jour*nal of the American Chemical Society, 2009. 131(1**7):** p. 6050-6051.
19. Ito, S., et al., High-*conversion-efficiency organic dye-sensitized solar cells with a novel indoline dye. Chem*ical Communications, 2008(41): p. 5194-5196.
20. Grätzel, M., Dye-s*ensitized solar cells. Jour*nal of Photochemistry and Photobiology C: Photochemistry Reviews, 2003. 4(2): p. 145-153.
21. Numerical Simulations on Perovskite Photovoltaic DevicesBy Bernabé Marí Soucase, Inmaculada Guaita Pradas and Krishna R. Adhikari DOI: 10.5772/61751
22. Lee, M.M., et al., Efficien*t Hybrid Solar Cells Based on Meso-Superstructured Organometal Halide Perovskites. Science,* 2012. 338(6107**):** p. 643-647.
23. Yin, W.-J., T. Shi, and Y. Yan, Unique P*roperties of Halide Perovskites as Possible Origins of the Superior Solar Cell Performance. Advance*d Materials, 2014. 26(27): **p.** 4653-4658.
24. Yin, W.-J., T. Shi, and Y. Yan, Unusual *defect physics in CH3NH3PbI3 perovskite solar cell absorber. Applied* Physics Letters, 2014. 104(6): **p.** 063903.
25. Giorgi, G., et al., Small Pho*tocarrier Effective Masses Featuring Ambipolar Transport in Methylammonium Lead Iodide Perovskite: A Density Functional Analysis. The Jou*rnal of Physical Chemistry Letters, 2013. 4(24): p**.** 4213-4216.
26. Stranks, S.D., et al., Electron-*Hole Diffusion Lengths Exceeding 1 Micrometer in an Organometal Trihalide Perovskite Absorber. Science*, 2013. 342(6156**):** p. 341-344.
27. Grinberg, I., et al., Perovski*te oxides for visible-light-absorbing ferroelectric and photovoltaic materials. Nature,* 2013. 503: p. **509**.
28. Frost, J.M., et al., Atomistic *Origins of High-Performance in Hybrid Halide Perovskite Solar Cells. Nano Le*tters, 2014. 14(5): p**.** 2584-2590.
29. Chen, Q., et al., Planar H*eterojunction Perovskite Solar Cells via Vapor-Assisted Solution Process. Journal* of the American Chemical Society, 2014. 136(2): **p.** 622-625.
30. Zhou, H., et al., Interfac*e engineering of highly efficient perovskite solar cells. Science*, 2014. 345(6196**):** p. 542-546.
31. Zhao, C., et al., Revealin*g Underlying Processes Involved in Light Soaking Effects and Hysteresis Phenomena in Perovskite Solar Cells. Advance*d Energy Materials, 2015. 5(14): p**.** 1500279-n/a.
32. Noh, J.H., et al., Chemical *Management for Colorful, Efficient, and Stable Inorganic–Organic Hybrid Nanostructured Solar Cells. Nano Le*tters, 2013. 13(4): p**.** 1764-1769.
33. Lee, J.-W., et al., Formamid*inium and Cesium Hybridization for Photo- and Moisture-Stable Perovskite Solar Cell. Advance*d Energy Materials, 2015. 5(20): p**.** 1501310-n/a.
34. Green, M.A., et al., Solar ce*ll efficiency tables (version 36). Progres*s in Photovoltaics: Research and Applications, 2010. 18(5): p**.** 346-352.

35. Green, M.A., et al., Solar cell *efficiency tables (version 47). Progress* in Photovoltaics: Research and Applications, 2016. 24(1): p**.** 3-11.
36. Green, M.A., et al., Solar cell *efficiency tables (Version 45). Progress* in Photovoltaics: Research and Applications, 2015. 23(1): p**.** 1-9.
37. Green, M.A., et al., Solar cell *efficiency tables (version 49). Progress* in Photovoltaics: Research and Applications, 2017. 25(1): p**.** 3-13.
38. Green, M.A., et al., Solar cell *efficiency tables (version 51). Progress* in Photovoltaics: Research and Applications, 2018. 26(1): p**.** 3-12.
39. Chiarella, F., et al., Combined *experimental and theoretical investigation of optical, structural, and electronic properties of thin films(X=Cl,Br). Physica*l Review B, 2008. 77(4): p**.** 045129.
40. Chung, I., et al., All-solid*-state dye-sensitized solar cells with high efficiency. Nature*, 2012. 485: p. **486**.
41. Tsai, H., et al., High-eff*iciency two-dimensional Ruddlesden–Popper perovskite solar cells. Nature*, 2016. 536: p. **312**.
42. Chiang, C.-H. and C.-G. Wu, Bulk het*erojunction perovskite–PCBM solar cells with high fill factor. Nature* Photonics, 2016. 10: p. 1**96**.
43. Hao, F., et al., Lead-free *solid-state organic–inorganic halide perovskite solar cells. Nature* Photonics, 2014. 8: p. 48**9**.
44. Volonakis, G., et al., Lead-Free *Halide Double Perovskites via Heterovalent Substitution of Noble Metals. The Jou*rnal of Physical Chemistry Letters, 2016. 7(7): p. 1254-1259.
45. Yangyang, D., et al., Formation *of Hybrid Perovskite Tin Iodide Single Crystals by Top-Seeded Solution Growth. Angewan*dte Chemie, 2016. 128(10): **p.** 3508-3511.
46. http://www.computerhistory.org/siliconengine/field-effect-semiconductor-device-concepts-patented/
47. https://web.stanford.edu/dept/news/pr/02/shockley1023.html
48. Dimitrakopoulos, C.D. and D.J. Mascaro, Organic *thin-film transistors: A review of recent advances. IBM Jou*rnal of Research and Development, 2001. 45(1): p**.** 11-27.
49. https://electronics.stackexchange.com/questions/18885/mosfet-as-a-switch-when-is-it-in-saturation
50. Pesavento, P.V., et al., Gated fo*ur-probe measurements on pentacene thin-film transistors: Contact resistance as a function of gate voltage and temperature. Journal* of Applied Physics, 2004. 96(12): **p.** 7312-7324.
51. Senanayak, S.P., et al., Understa*nding charge transport in lead iodide perovskite thin-film field-effect transistors. Science* Advances, 2017. 3(1).
52**.** Mitzi, D.B., C.D. Dimitrakopoulos, and L.L. Kosbar, Structur*ally Tailored Organic−Inorganic Perovskites: Optical Properties and Solution-Processed Channel Materials for Thin-Film Transistors. Chemis*try of Materials, 2001. 13(10): **p.** 3728-3740.
53. He, Y. and G. Galli, Perovski*tes for Solar Thermoelectric Applications: A First Principle Study of CH3NH3AI3 (A = Pb and Sn). Chemis*try of Materials, 2014. 26(18): **p.** 5394-5400.

54. Chin, X.Y., et al., Lead iod*ide perovskite light-emitting field-effect transistor. Nature* Communications, 2015. 6: p. 73**8**3.
55. Chua, L., Memristo*r-The missing circuit element. IEEE Tr*ansactions on Circuit Theory, 1971. 18(5): p**.** 507-519.
56. Kavehei, O., et al., The four*th element: characteristics, modelling and electromagnetic theory of the memristor. Proceed*ings of the Royal Society A: Mathematical, Physical and Engineering Science, 2010.
57. Adhikari, S.P., et al., Three Fi*ngerprints of Memristor. IEEE Tr*ansactions on Circuits and Systems I: Regular Papers, 2013. 60(11): **p.** 3008-3021.
58. Amrani, E., A. Drori, and S. Kvatinsky. Logic de*sign with unipolar memristors. in 201*6 IFI*P/IEEE International Conference on Very Large Scale Integration (VLSI-SoC). 2016.*
59. Yanagida, T., et al., Scaling *Effect on Unipolar and Bipolar Resistive Switching of Metal Oxides. Scienti*fic Reports, 2013. 3: p. 16**5**7.
60. Lin, G., et al., An organ*ic-inorganic hybrid perovskite logic gate for better computing. Journal* of Materials Chemistry C, 2015. 3(41): p**.** 10793-10798.
61. Gu, C. and J.-S. Lee, Flexible *Hybrid Organic–Inorganic Perovskite Memory. ACS Nan*o, 2016. 10(5): p**.** 5413-5418.
62. Brattain, W.H. and J. Bardeen, Surface *Properties of Germanium. Bell Sy*stem Technical Journal, 1953. 32(1): p**.** 1-41.
63. Langmuir, I., THE CONS*TITUTION AND FUNDAMENTAL PROPERTIES OF SOLIDS AND LIQUIDS. PART I. SOLIDS. Journal* of the American Chemical Society, 1916. 38(11): **p.** 2221-2295.
64. Nie, W., et al., High-eff*iciency solution-processed perovskite solar cells with millimeter-scale grains. Science*, 2015. 347(6221**):** p. 522-525.
65. Neukirch, A.J., et al., Polaron *Stabilization by Cooperative Lattice Distortion and Cation Rotations in Hybrid Perovskite Materials. Nano Le*tters, 2016. 16(6): p**.** 3809-3816.
66. Nie, W., et al., Light-ac*tivated photocurrent degradation and self-healing in perovskite solar cells. Nature* Communications, 2016. 7: p. 11**5**74.
67. Tsai, H., et al., Light-in*duced lattice expansion leads to high-efficiency perovskite solar cells. Science*, 2018. 360(6384**):** p. 67-70.
68. Mallajosyula, A.T., et al., Large-ar*ea hysteresis-free perovskite solar cells via temperature controlled doctor blading under ambient environment. Applied* Materials Today, 2016. 3: p. 96-102.
69. Shao, Y., et al., Origin a*nd elimination of photocurrent hysteresis by fullerene passivation in CH3NH3PbI3 planar heterojunction solar cells. Nat Com*mun, 2014. 5: p. 57**8**4.
70. Xiao, Z., et al., Giant sw*itchable photovoltaic effect in organometal trihalide perovskite devices. Nat Mat*er, 2015. 14(2): p**.** 193-198.
71. Frolova, L.A., N.N. Dremova, and P.A. Troshin, The chem*ical origin of the p-type and n-type doping effects in the hybrid methylammonium–lead iodide (MAPbI3) perovskite solar cells. Chemica*l Communications, 2015. 51(80): **p.** 14917-14920.

72. Hölzl, J. and F.K. Schulte, Work fun*ction of metals, in Sol*id Su*rface Physics, J. Höl*zl, F.K. Schulte, and H. Wagner, Editors. 1979, Springer Berlin Heidelberg: Berlin, Heidelberg. p. 1-150.
73. Bao, Z., A. Dodabalapur, and A.J. Lovinger, Soluble *and processable regioregular poly(3-hexylthiophene) for thin film field-effect transistor applications with high mobility. Applied* Physics Letters, 1996. 69(26): **p.** 4108-4110.
74. Toan, N.N., S. Saukko, and V. Lantto, Gas sens*ing with semiconducting perovskite oxide LaFeO3. Physica* B: Condensed Matter, 2003. 327(2): **p.** 279-282.
75. Martinelli, G., et al., Screen-p*rinted perovskite-type thick films as gas sensors for environmental monitoring. Sensors* and Actuators B: Chemical, 1999. 55(2): p**.** 99-110.
76. Ren, K., et al., Turning *a disadvantage into an advantage: synthesizing high-quality organometallic halide perovskite nanosheet arrays for humidity sensors. Journal* of Materials Chemistry C, 2017. 5(10): p**.** 2504-2508.
77. Zhuang, Y., et al., High-per*formance gas sensors based on a thiocyanate ion-doped organometal halide perovskite. Physica*l Chemistry Chemical Physics, 2017. 19(20): **p.** 12876-12881.
78. Stoeckel, M.-A., et al., Reversib*le, Fast, and Wide-Range Oxygen Sensor Based on Nanostructured Organometal Halide Perovskite. Advance*d Materials, 2017. 29(38): **p.** 1702469.
79. Fang, H.-H., et al., Ultrahig*h sensitivity of methylammonium lead tribromide perovskite single crystals to environmental gases. Science* Advances, 2016. 2(7).
80**.** Sadhanala, A., et al., Blue-Gre*en Color Tunable Solution Processable Organolead Chloride–Bromide Mixed Halide Perovskites for Optoelectronic Applications. Nano Le*tters, 2015. 15(9): p**.** 6095-6101.
81. Hao, F., et al., Anomalous *Band Gap Behavior in Mixed Sn and Pb Perovskites Enables Broadening of Absorption Spectrum in Solar Cells. Journal* of the American Chemical Society, 2014. 136(22): **p.** 8094-8099.
82. Wu, X., et al., Trap Sta*tes in Lead Iodide Perovskites. Journal* of the American Chemical Society, 2015. 137(5): **p.** 2089-2096.
83. Galisteo-López, J.F., et al., Environm*ental Effects on the Photophysics of Organic–Inorganic Halide Perovskites. The Jou*rnal of Physical Chemistry Letters, 2015. 6(12): p**.** 2200-2205.
84. Horgan, A.M. and I. Dalins, A study *of the adsorption of oxygen on Ni(111) using auger electron spectroscopy: Chemical shifts and valence spectra. Surface* Science, 1973. 36(2): p**.** 526-543.
85. Bryant, D., et al., Light an*d oxygen induced degradation limits the operational stability of methylammonium lead triiodide perovskite solar cells. Energy* & Environmental Science, 2016. 9(5): p. 1655-1660.
86. Christopher, P., H. Xin, and S. Linic, Visible-*light-enhanced catalytic oxidation reactions on plasmonic silver nanostructures. Nature* Chemistry, 2011. 3: p. 46**7**.
87. Yu, H., et al., The Role *of Chlorine in the Formation Process of "CH3NH3PbI3-xClx" Perovskite. Advance*d Functional Materials, 2014. 24(45): **p.** 7102-7108.

88. Krebs, F.C. and K. Norrman, Analysis *of the failure mechanism for a stable organic photovoltaic during 10 000 h of testing. Progres*s in Photovoltaics: Research and Applications, 2007. 15(8): p**.** 697-712.
89. Snaith, H.J., et al., Anomalous *Hysteresis in Perovskite Solar Cells. The Jou*rnal of Physical Chemistry Letters, 2014. 5(9): p. 1511-1515.
90. Wetzelaer, G.-J.A.H., et al., Trap-Ass*isted Non-Radiative Recombination in Organic–Inorganic Perovskite Solar Cells. Advance*d Materials, 2015. 27(11): **p.** 1837-1841.
91. Hu, J., et al., Photovol*tage Behavior in Perovskite Solar Cells under Light-Soaking Showing Photoinduced Interfacial Changes. ACS Ene*rgy Letters, 2017. 2(5): p. 950-956.
92. Christians, J.A., R.C.M. Fung, and P.V. Kamat, An Inorg*anic Hole Conductor for Organo-Lead Halide Perovskite Solar Cells. Improved Hole Conductivity with Copper Iodide. Journal* of the American Chemical Society, 2014. 136(2): **p.** 758-764.
93. Anothainart, K., et al., Light en*hanced NO2 gas sensing with tin oxide at room temperature: conductance and work function measurements. Sensor*s and Actuators B: Chemical, 2003. 93(1): p**.** 580-584.
94. Dalton, L.R., A.W. Harper, and B.H. Robinson, The role *of London forces in defining noncentrosymmetric order of high dipole moment–high hyperpolarizability chromophores in electrically poled polymeric thin films. Proceed*ings of the National Academy of Sciences, 1997. 94(10): **p.** 4842-4847.
95. Da Silva, J.L.F. and C. Stampfl, Trends i*n adsorption of noble gases He, Ne, Ar, Kr, and Xe on All-electron density-functional calculations. Physica*l Review B, 2008. 77(4): p**.** 045401.
96. Schwerdtfeger, P., ATOMIC S*TATIC DIPOLE POLARIZABILITIES, in At*oms, M*olecules and Clusters in Electric Fields. 2011,* PUBLISHED BY IMPERIAL COLLEGE PRESS AND DISTRIBUTED BY WORLD SCIENTIFIC PUBLISHING CO. p. 1-32.
97. Blancon, J.-C., et al., The Effe*cts of Electronic Impurities and Electron–Hole Recombination Dynamics on Large-Grain Organic–Inorganic Perovskite Photovoltaic Efficiencies. Advance*d Functional Materials, 2016. 26(24): **p.** 4283-4292.

CURRICULUM VITAE

Kasun Fernando
shrikasun@gmail.com

782 Frederick Stamm Ct,Apt 3
Louisville, KY 40217.

Home -(502) 365 5757
Mobile-(502) 510 6787
Skype -shrikasun

SUMMARY OF QUALIFICATIONS

Accomplished and enthusiastic electrical engineer with more than 7+ years of experience in nano-electronics, micro/nano-fabrication, synthesis and characterization (electrical, magnetic and optical) of nano-materials such as Graphene, ITO, MoS_2 and Halide Perovskites. One+ years full time research experience at Los Alamos National Laboratory, the foremost national laboratory in the United States of America. Member of a research group ranked among the top 5 groups specialized in Halide Perovskite as an Energy Harvesting material. Actively involved in renewable energy research with emphasis on photo-voltaic devices in Organic, Dye-Sensitized and Perovskite technology.

SUMMARY OF SKILLS

Synthesis of novel and known materials.
Initial point of new findings:

- Optimization of single and multi-layered Graphene growth using low pressure Chemical Vapor Deposition (CVD).
- Epitaxial growth of Graphene on patterned SiC.
- Active layer growth of organic solar cells (OSC) by spin casting techniques.
- Fabrication of anode and cathodes for dye sensitized solar cells (DSSC).
- Active layer growth of Halide Perovskite using the hot casting technique.
- Improvement of process efficiency of synthesis of nano materials (single and multi-layered graphene on various substrates) and photo voltaic devices (OSC and DSSC with implementation of novel materials).

Characterization of the materials.

- Use of Raman spectroscopy, scanning electron microscopy (SEM) and scanning tunneling microscopy (STM) to characterize the single and multi-layered graphene.
- Used UV-Vis NIR microscopy to understand the band alignments and absorption properties of the active layer in OSC and DSSC.
- Used atomic force microscopy to measure the roughness of anode and Perovskite layers.
- Used X Ray diffraction microscopy (XRD), high resolute optical microscopy, SEM to confirm the high quality of Perovskite films.
- Used EQCM for micro scale mass measurements.

Fabrication of the devices.

- Used single layered graphene as a replacement for Transparent Conducting Oxide (TCO) in various photo voltaic devices.
- Fabricated organic and dye sensitized solar cells as photo voltaic devices.
- Fabricated solar cells and field effect transistors (FETs) under inert atmospheric condition by Halide Perovskites films to improve and characterize the performance of the thin film.

Characterization of Devices.

Various techniques were used to characterize the devices fabricated.

- Four probe conductivity measurement was to determine the conductivity of the Graphene on glass substrate.
- Use of white light and optical parametric amplified (OPA) laser to determine hidden states in the materials using the capacitive photo current technique.
- Use of incident photon to charge carrier efficiency (IPCE) and Current Voltage curves to determine the efficiency of the devices.
- Two and Four Probe Current Voltage measurements to characterize the gated and non-gated FET devices under dark and illuminated conditions.

EDUCATION

Ph.D. Electrical Engineering (August 2011– August 2018**)**
University of Louisville, Louisville, KY under Prof. Bruce W. Alphenaar

M.S. Physics (Aug 2009 – May 2011**)**
University of Louisville, Louisville, KY under Prof. Gamini U. Sumanasekera

B.Sc. Physics (Hons.) (Nov 2001 – April 2006**)**
University of Sri Jayewardenepura, Sri Lanka

PROFESSIONAL PROFILE

Graduate Teaching Assistant, University of Louisville, Department of Electrical and Computer Engineering Jan 2018-July2018

- Conducting lab classes for ECE 211 and grading work for ECE 473.Completing the thesis work.

Graduate Fellow under Graduate school, University of Louisville, Department of Electrical and Computer Engineering Aug 2017-Jan 2018

- Completing the thesis and work conducted during the PhD.

Student Affiliate, Los Alamos National Laboratory May 2017-Aug 2017

Projects:

- Application of Halide perovskite films in Memory devices.
- Understanding and optimizing the effect by varying different cations and anions to improve the performance of the Memory based device.

Graduate Research Assistant, University of Louisville, Department of Electrical and Computer Engineering Jan 2016-May2017

- Concluding studies, I started at Los Alamos National Laboratory and disseminating the knowledge to my school group in Louisville.

Student Affiliate, Los Alamos National Laboratory **Jan 2015-Dec 2015**

Projects:

- Electrical characterization of field effect transistors for Perovskite material fabricated by hot casting technique.
- Fabrication of thin film of halide perovskite on substrates such as glass and SiO_2 using hot casting technique (invented by the group).
- Fabrication of complete solar cells or FETs by thermal and electron beam evaporated metal contacts.
- Characterization of thin films by IPCE and XRD and various electrical measurements on the devices using a probe station under normal and liquid helium temperatures.

Graduate Student, University of Louisville, Department of Electrical and Computer Engineering **Aug 2011-Dec 2014**

Project 1:

Application of rare earth metal in organic solar cells.

- Fabricated thin film solar cells using PCBM, P3HT with Nd nanoparticles in active layer to improve the quality of the film.
- Improvement was verified by absorption, IPCE and IV characteristics.
- Other characterization techniques such as pump probe measurement supported the improvement of the quality of the film.

Project 2:

Application of rare earth metal in dye sensitized solar cells.

- Fabricated DSSC photo anode using mixture of TiO_2 and Nd nanoparticles by the doctor blade technique resulting in improvement of solar cell.
- Improvement was verified by absorption, IPCE, IV and CV measurements.

Graduate Student, University of Louisville, Department of Physics and Astronomy **Aug 2010-Aug 2011**

Project:

Building and optimizing single layer graphene growth by Chemical Vapor Deposition (CVD).

- Build a CVD system that can produce various CVD grown materials with pressure of 10^{-7} torr and fully automated temperature control.
- Was able to grow single and multi-layered graphene and transfer them in to various substrates using different transfer techniques.

- Characterizing was done by mainly using Raman spectroscopy and Scanning Electron Microscopy (SEM) imaging.
- Application of synthesized graphene to replace Transparent Conducting Oxides such as FTO and ITO in various photo voltaic fabrications.

Graduate Teaching Assistant, University of Louisville, Department of Physics and Astronomy Aug 2009-Aug 2011

- Had been a graduate teaching assistant for Introduction to Mechanics, Thermodynamics and few other undergrad level courses (PHYS 111, PHYS 223, PHYS 224, PHYS 295, PHYS 298).
- Conducted Laboratory classes, graded Lab reports and tutored Undergraduate students.
- Maintained instruments, lab protocols and safety.

Teaching Assistant, University of Moratuwa, Sri Lanka. Department of Electrical Engineering May 2006-Aug 2009

- Had been a teaching assistant for various undergraduate level courses (EE 101, EE 109, EE 219, EE 227,EE 218 ,EE 223 ,EE 219 ,EE 304 ,EE 318).

Teaching Assistant, University of Sri Jayewardenepura, Sri Lanka. Department of Physics May 2005-May 2006

- Acted as a coordinator for introductory level courses to 1st year undergraduates (PHY 154).
- Conducted laboratory classes, graded Lab reports and tutored Undergraduate students.
- Maintained instruments, lab protocols and safety.

Internship, Industrial Training Institute (ITI), Sri Lanka.
January 2005-May 2005

- Worked with two research engineers in building a custom humidity detector for Gliricidia fuelwood for energy production.

OTHER SKILLS

Laboratory Proficiency

- Went through the mandatory training (lab safety, chemical, gas, electrical, Handling of hazardous material …etc) that a research scientist had to go through to get the access to the Los Alamos National Laboratory.

- Involved with maintaining lab safety and supply (chemicals, Gas cylinders…etc).

- Instrumental expertise

  Design of custom programs using Lab-View for electrical, optical and magnetic measuring instruments

  Optical Instruments-Handling and troubleshooting Class 4 Laser systems (high power OPA), white light systems (IPCE, UV-Vis spectroscopy). Spatial optical characterizing instruments, solar simulator testing solar cells.

  Characterizing Instruments-Scanning Electron Microscopy (SEM), X-Ray Powder Diffraction spectroscopy (XRD), Raman Spectroscopy, Atomic Force Microscopy (AFM), Surface profilometers, Xray Photo Electron Spectroscopy (XPS), Quartz Crystal Microbalance (QCM)

  High class glove box handling, maintenance of Ultra-High vacuum CVD systems, Handling of plasma systems.

  Fabrication- Novel nano-materials such as single layer and multi layered graphene. High efficient Silicon, Organic, Dye Sensitized and Mix Halide Solar cells starting from scratch.

  Metal Dispositioning Technique- Electron Beam (EBeam) Lithography (Use and troubleshooting), Thermal Evaporation, Sputtering, and Spray Coating.

  High magnetic field instrument handling with liquid Nitrogen (100K) and Liquid Helium (2K) Cryogenics and Certified class 100/1000 clean room user in MNTC at University of Louisville.

Novel Ideas from the research-Able to produce novel types of photo voltaic devices by understanding the physics behind them and able to characterize new materials in a way to understand the usability of that material.

Software Proficiency

- Software Packages for Data analysis: LabView, Matlab, Mathematica, L-edit, IGOR, Peakfit, Origin, Endnote, Microsoft Office

AWARDS

- Teaching Assistantship, August 2007-August 2009. (Department of Physics, University of Louisville)
- Research Assistantship under Conn Center for Renewable Energy Research. August 2009-December 2014. (Department of Electrical and Computer Science Engineering, University of Louisville).
- Graduate completion Award (School of Interdisciplinary and Graduate Studies)

PUBLICATIONS

- Optical Generation and Detection of Polaronic States in PCBM 2013 H Shah, A Carver, **K Fernando**, S Kolli, B Abeyweera, S Lisenkov, M Menon, B W Alphenaar The Journal of Physical Chemistry C 117 (50), 26538-26542
- Charge transfer in rare earth oxide hybrid solar cells 2014 **K Fernando**, B Pandit, J Liu, BW Alphenaar Chemical Physics Letters 592, 155-159
- Increased efficiency of dye-sensitized solar cells by addition of rare earth oxide microparticles into a titania acceptor T Luitel; **K Fernando**; B Tatum; B Alphenaar; F Zamborini Electrochimica Acta 211, 918-925
- Large-area hysteresis-free perovskite solar cells via temperature controlled doctor blading under ambient environment A Mallajosyula, **K Fernando**, S Bhatt, A Singh, B Alphenaar, W Nie, G Gupta, A. Mohite Applied Materials Today 3, 96-102
- Effect of Rare-Earth Metal Oxide Nanoparticles on the Conductivity of Nanocrystalline Titanium Dioxide: An Electrical and Electrochemical Approach, P.Kharel, P.Cuillier, **K.Fernando**, F. Zamborini, BW.Alphenaar, The Journal of Physical Chemistry C,2018
- Unique Unipolar Memristor with Ultra-Low Turn-on Voltage Using Hybrid Halide Perovskite **K. Fernando**, Devesa Canicoba Noelia, Hsinhan Tsai, Jacky Even, Mercouri G. Kanatzidis, Jean Christophe Blancon, Wanyi Nie, Bruce W Alphenaar and Aditya D. Mohite In progress

- Ambipolar hybrid perovskite field-effect transistors at room temperature Noelia Devesa Canicoba, **Kasun Fernando**, Fangze Liu, Jean-Christophe Blancon, Hsinhan Tsai Jacky Even, Mercouri G. Kanatzidis, Muhammad A. Alam, Regis Rogel, Laurent Le Brizoual, Bruce W. Alphenaar, Wanyi Nie and Aditya D. Mohite In progree
- Hybrid perovskites for inert gas detection **K. Fernando**, W. Nie, A.D. Mohite, and B.W. Alphenaar In progress